Recent Progress in Electrode Materials for Sodium-Ion Batteries

*Hyungsub Kim, Haegyeom Kim, Zhang Ding, Myeong Hwan Lee, Kyungmi Lim, Gabin Yoon, and Kisuk Kang**

Grid-scale energy storage systems (ESSs) that can connect to sustainable energy resources have received great attention in an effort to satisfy ever-growing energy demands. Although recent advances in Li-ion battery (LIB) technology have increased the energy density to a level applicable to grid-scale ESSs, the high cost of Li and transition metals have led to a search for lower-cost battery system alternatives. Based on the abundance and accessibility of Na and its similar electrochemistry to the well-established LIB technology, Na-ion batteries (NIBs) have attracted significant attention as an ideal candidate for grid-scale ESSs. Since research on NIB chemistry resurged in 2010, various positive and negative electrode materials have been synthesized and evaluated for NIBs. Nonetheless, studies on NIB chemistry are still in their infancy compared with LIB technology, and further improvements are required in terms of energy, power density, and electrochemical stability for commercialization. Most recent progress on electrode materials for NIBs, including the discovery of new electrode materials and their Na storage mechanisms, is briefly reviewed. In addition, efforts to enhance the electrochemical properties of NIB electrode materials as well as the challenges and perspectives involving these materials are discussed.

1. Introduction

Ever-growing populations and energy demands have led to a global increase in the use of fossil fuels, and the resulting high levels of CO_2 emissions are expected to cause various environmental issues such as global warming and desertification.[1,2] Although the price of oil has continuously decreased since 2010,[3] for the greener and more sustainable-energy-focused generation, energy harvesting from renewable energy resources (i.e., solar, wind, hydro, tidal, and geothermal energies) has become a critical issue in recent years. To store and use these energy resources efficiently, the development of large-scale ESSs has also become an important research area, and various technologies including pumped-hydroelectric storage, compressed-air energy storage, flywheels, capacitors, and batteries have been evaluated as grid-scale ESSs.[4–7] To date, approximately 98% of the energy (≈177 GW) in the world is stored using pumped-hydroelectric storage.[8] However, because the generation of sustainable energies is generally intermittent and has geological limits relative to current large-scale energy generation facilities, the electrochemical way of energy storage is regarded as an optimal choice based on its low capital cost with compactness, high energy density, high round-trip efficiency, and long cycle life.[5,6]

Among various electrochemical grid-scale ESSs, LIBs have been considered the most promising ESSs because of their high gravimetric and volumetric energy densities.[9,10] Since the success of LIBs in portable devices in the early 1990s,[9–11] LIB technology has experienced rapid advances and commercialization in mid-size applications such as hybrid electric vehicles (HEVs) and electric vehicles (EVs). In addition, many prototypes of grid-scale LIBs (approximately tens of megawatt-hours) that are connected to renewable energy sources such as solar and wind power have appeared on the market.[12–14] However, there are several significant challenges facing LIBs for their application in grid-scale ESSs. One of the greatest issues to date is the cost with respect to not only the processing/fabrication but also the raw materials. Significant reduction of the cost of LIBs is still not a trivial matter even for mid-sized applications such as EVs. Moreover, there exists a growing concern whether the conventional LIB technology is sustainable. The global Li resources are estimated to be 30–40 Mt, which is insufficient to satisfy the increased demands on energy storage by LIB technology.[15,16] Although recent reports have forecasted that the supply of Li resources is expected to partly meet the demand for Li for EVs based on scenarios from the International Energy Agency (IEA)

Dr. H. Kim, Dr. H. Kim, Dr. Z. Ding,
M. H. Lee, K. Lim, G. Yoon, Prof. K. Kang
Department of Materials Science and Engineering
Research Institute of Advanced Materials
Seoul National University
Seoul 08826, Republic of Korea
E-mail: matlgen1@snu.ac.kr

Dr. H. Kim, G. Yoon, Prof. K. Kang
Center for Nanoparticle Research Institute for Basic Science (IBS)
Seoul National University
Seoul 08826, Republic of Korea

Dr. H. Kim
Lawrence Berkeley National Laboratory
1 Cyclotron Rd., Berkeley, CA 94720, USA

Dr. Z. Ding
College of Chemistry and Chemical Engineering
Taiyuan University of Technology
Shanxi, Taiyuan 030024, P. R. China

DOI: 10.1002/aenm.201600943

consistent with 50% reduction in CO_2 emissions by 2050,[1] there are still doubts about its availability for grid-scale ESSs. Almost a quarter of Li reserves are expected to be depleted by EV applications by 2050.[15,16] Several reports have indicated that Li recycling can support the supply of Li by 2050 with a recycling rate of 50–100%; however, currently, the recycling rate is less than 1%, and there is a lack of advanced techniques and facilities as well as economic incentives for Li recycling.[15] While more than 60% of Li reserves are located in a specific area in the form of mineral and brine, and the production of Li is strongly dependent on countries in the area,[15,16] the price of Li_2CO_3 has continued to increase since 2000 and is anticipated to dramatically increase when the EV market starts to blossom.[15–17]

Rechargeable battery systems utilizing Na as a guest ion have been extensively studied to develop less expensive and sustainable ESSs based on the abundance and easy accessibility of Na.[18–21] Na is the sixth most abundant element in the Earth's crust (≈2.6%), and virtually unlimited Na resources are available from sea water. Early research has focused on high-temperature Na rechargeable battery systems such as Na/$NiCl_2$ and Na–S batteries.[6,22–24] These batteries are now commercialized as grid-scale ESSs; however, the high operating temperature (≈300 °C) and significant corrosion issues must be addressed. Since Na intercalation compounds were first explored in the 1980s,[25–27] room-temperature NIBs have also gained attention for large-scale ESSs.[18–21] Nevertheless, only a limited number of studies were conducted until 2010 shaded by the success of LIBs in small- and mid-size energy storage applications. The large ionic size of Na (1.02 Å) and its low standard electrochemical potential (≈ 2.71 V vs Na^+/Na) compared with those of Li (0.76 Å and 3.04 V vs Li^+/Li, respectively) resulted in low power and energy densities, holding back further developments of NIBs. As the demands for and sizes of batteries have increased, the interest in NIBs has resurged particularly for grid-scale ESSs. As shown in **Figure 1**a, a remarkable number of new materials have been introduced and evaluated as electrode materials for NIBs in the last few years. Similar to LIB chemistry, layered and polyanionic compounds have been extensively investigated as cathode materials, and carbon-based materials, metal oxide compounds, and metals have been studied as anode materials (see Figure 1b,c). Prussian blue and organic materials have also been recently examined as electrode materials for NIBs. As displayed in Figure 1b,c, electrode materials with various redox potentials and their capacities were discovered in only a few years of research, and some of these materials already rival those used in LIBs with respect to their energy densities.

In this review, we will present the most recent progress in NIBs, with a focus on positive and negative electrode materials. This article covers the discovery of new promising positive and negative electrode materials for NIBs and their Na storage mechanisms as well as the many efforts to enhance the electrochemical properties. It would include the latest approaches to enhance the cycle stability of layered materials along with the recent discovery and design strategy of open-framework polyanionic and Prussian blue cathodes. For anode materials, we have focused on the recent mechanistic studies of non-graphitic carbon materials and investigations on utilizing graphite as an anode material with Na–solvent co-intercalation. In addition, electrochemical mechanism studies of new metal (i.e., Na–metal alloying reaction) and metal oxide materials (i.e., conversion and intercalation reactions) are covered, and organic materials for positive and negative electrodes are discussed. Finally, we examine the major challenges facing NIB electrode materials for large-scale ESSs and provide perspectives on the outlook of these materials.

Hyungsub Kim received a B.Sc. degree in materials science and engineering from Hanyang University and a M.Sc. degree from the Korea Advanced Institute of Science and Technology (KAIST). He completed his Ph.D. (2016) at the Seoul National University and is currently a postdoctoral researcher in Chimie du Solide et Energie at Collège de France. His research interest lies in the design of new open framework cathodes for Li/Na rechargeable batteries.

Haegyeom Kim received a B.Sc. degree (2009) from the department of materials science and engineering in Hanyang University, a M.Sc. degree (2011) at graduate school of EEWS from the Korea Advanced Institute of Science and Technology (KAIST), and a Ph.D. degree (2015) on graphite derivatives for Li and Na rechargeable batteries at Seoul National University. Currently, he is a postdoctoral researcher at the Lawrence Berkeley National Laboratory (LBNL) where he works on graphite-based electrode materials for Na rechargeable batteries.

Kisuk Kang is a professor of materials science and engineering at Seoul National University (SNU), where he also received his B.Sc. He did Ph.D. and postdoctoral studies at the Massachusetts Institute of Technology. Since 2013 he has been a tenured professor at SNU. His research laboratory focuses on developing new materials for Li ion batteries and post-Li battery chemistries—such as Na, Mg, and metal–air batteries—using combined experiments and ab initio calculations.

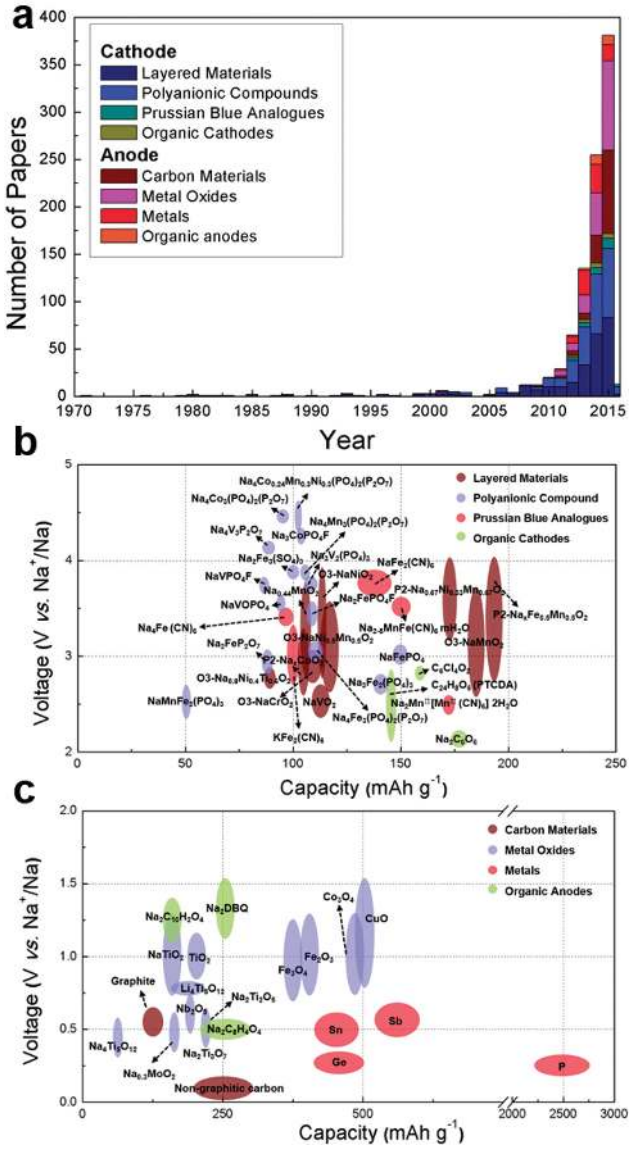

Figure 1. a) The number of publications on NIB electrode materials over time. Voltage–capacity plots of representative b) positive and c) negative electrode materials for NIBs.

2. Cathode Materials

2.1. Layered Transition Metal Oxide Compounds

Na-containing layered transition metal oxides (TMOs) have attracted great interest as cathode materials for NIBs because of their high theoretical capacity (e.g., 243.8 mA h g^{-1} for O3-$NaMnO_2$) and relatively simple synthetic process.[28] Although the electrochemical activity of Na layered TMOs in Na-ion cells was already reported around 1980,[26,27,29,30] with the need to investigate post-LIB systems with low cost and high energy density, the investigation of layered TMO cathodes has recaptured the enthusiasm of the scientific community in the past five years (see Figure 1). Following the notation developed by Delmas et al., all layered Na TMOs, which make up the majority of TMO cathodes for NIBs, can be classified as O3-, P2-, and P3-types depending on the stacking sequence of oxygen layers (O3: ABCABC stacking; P2: ABBA stacking; P3: ABBCCA stacking). Mobile Na cations adopt either prismatic (P) or octahedral (O) sites.[26] In this section, we review the most recent progress on layered TMOs for NIB cathodes.

2.1.1. P2-Type Layered TMOs

Among the various P2-type Na TMOs, Na_xCoO_2 and Na_xMnO_2 have mainly been studied. The P2 phase Na_xCoO_2 preferably forms in the Na composition (x) range from 0.68 to 0.76, whereas O3-Na_xCoO_2 tends to be formed between 0.87 to 1.00 (see **Figure 2**a,b).[31] Early works on electrochemical cycling of P2-Na_xCoO_2 electrode by Delmas et al. and Shacklette et al. demonstrated that the P2 phase remains stable over the composition range of $0.46 < x < 0.83$ with typical multiple plateau discharge curves along with small polarization for the charge–discharge profiles, indicating superior structural reversibility over various single-phase domains for different Na concentrations.[25,32,33] Na diffusion rates in P2-Na_xCoO_2 were observed to be higher than those of $LiCoO_2$ (approximately 0.5–1.5 × 10^{-10} cm^2 s^{-1} vs 1 × 10^{-11} cm^2 s^{-1}), and the diffusion kinetics of Na in O3-$NaCoO_2$ were even superior to those of the P2 phase, as demonstrated in Figure 2c,d.[34] The fast Na ion diffusion was also confirmed by theoretical work performed by Mo et al.[35] These authors revealed that the P2 phase outperforms the O3 phase except at high Na concentrations, and Na ions migrate in a honeycomb sublattice in P2 phase with a lower energy barrier. P2-$Na_{0.74}CoO_2$ prepared using a solid state method delivers a reversible discharge capacity of 107 mA h g^{-1} at 0.1 *C*-rate between 2 to 3.8 V vs Na^+/Na.[36] To enhance the cyclic performance, Han et al. adopted a small amount of Ca in the Na layer of the P2-Na_xCoO_2 structure and observed that the rate capability of $Na_{0.60}Ca_{0.07}CoO_2$ exceeds that of $Na_{0.73}CoO_2$ because of the enhanced Na diffusion coefficient (D) in the former, as demonstrated in Figure 2e,f.[37]

Similar to the case of P2-Na_xCoO_2, P2-Na_xMnO_2 exhibits an electrochemical activity in the Na composition (x) range of 0.45 to 0.85. However, the electrode operation revealed a low Na diffusion rate and poor structural reversibility resulting from the strong Jahn–Teller effect of Mn^{3+} within the structure.[38] Consistent with the findings of Paulsen et al., which indicated that heavily substituted structures and water-exposed cathodes result in the ideal P2-structure with minimum structural distortion, the cation substitution was observed to be an effective method to enhance the structural stability of P2-Na_xMnO_2, as verified by its stable capacity varying from 150 to 220 mA h g^{-1} in recent investigations of $Na_{0.83}[Li_{0.25}Mn_{0.75}]O_2$, $Na_{0.67}Mg_{0.2}Mn_{0.8}O_2$, $Na_{0.67}[Mg_{0.28}Mn_{0.72}]O_2$, $Na_{0.67}Ni_{0.25}Mg_{0.1}Mn_{0.65}O_2$, and $Na_{0.67}Cu_{0.14}Mn_{0.86}O_2$.[39–44]

Mixed layered metal oxides, such as Ni/Mn and Fe/Mn compounds, were adopted to suppress the multiple phase transition and improve the reversibility of P2-Na_xMnO_2 upon galvanostatic cycling. Lu et al. performed an in situ X-ray diffraction (XRD) study on Na extraction and insertion for the P2-$Na_{0.67}Ni_{0.33}Mn_{0.67}O_2$ cathode and claimed that all the original Na (≈0.67) could be extracted from and reversibly inserted into P2-$Na_{0.67}Ni_{0.33}Mn_{0.67}O_2$ with a theoretical capacity of 170.7 mA h g^{-1}.[45] Further structural investigation revealed

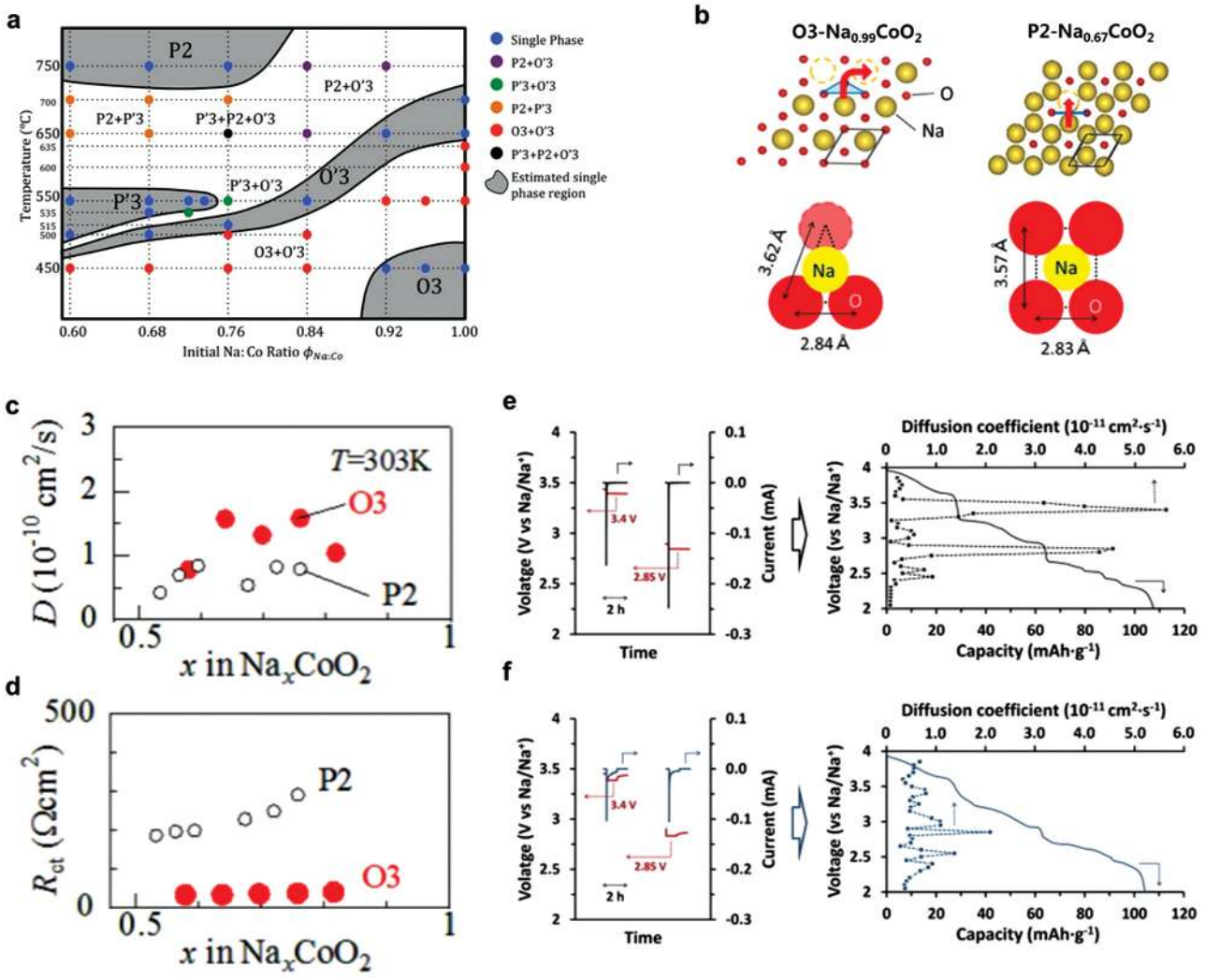

Figure 2. a) Synthesis phase diagram of Na_xCoO_2 as a function of the initial precursor Na:Co ratio and sintering temperature. Reproduced with permission.[31] Copyright 2014, American Chemical Society. b) Na ion diffusion path of O3-type $Na_{0.99}CoO_2$ and P2-type $Na_{0.67}CoO_2$. The red arrows and blue marks represent the Na ion diffusion path and oxygen window, respectively. c) Na-ion diffusion constant (D) of O3- (Red) and P2- (black) type Na_xCoO_2, as a function of the Na content x. d) Ionic charge transfer resistance (R_{ct}) of O3- (Red) and P2- (black) type Na_xCoO_2 as a function of x. Reproduced with permission.[34] Copyright 2015, Nature Publishing Group. Potentiostatic intermittent titration technique (PITT) plot (left) and evolution of diffusion coefficient (D) with depths of discharge (right) of e) $Na_{0.73}CoO_2$ and f) $Na_{0.60}Ca_{0.07}CoO_2$, respectively. Reproduced with permission.[37] Copyright 2015, Elsevier.

that the compound remained in the P2 structure if more than 0.33 Na was occupied in the unit cell, whereas the co-existence of a P2 phase with minor O2-type stacking faults and an O2 phase $Ni_{0.33}Mn_{0.67}O_2$ with stacking faults was observed when less than 0.33 Na was occupied.[45–47] The stable capacity retention was only achieved when the P2–O2 phase transformation was suppressed by limiting the operating voltage to 2.3–4.1 V vs Na^+/Na. To further reduce the multiple phase transitions in the Ni/Mn binary P2 cathode and achieve better structural reversibility, the substitution of Li or other transition metal elements such as Fe, Co, and Ti has been performed by many research groups.[48–53] Kim et al. reported that P2-$Na_{0.85}Li_{0.17}Ni_{0.21}Mn_{0.64}O_2$ can deliver a discharge capacity of 95–100 mA h g^{-1} between 2.0 and 4.2 V with an average voltage of 3.4 V vs Na^+/Na and exhibits only 2% capacity fading after 50 cycles.[48] The Ni^{2+}/Ni^{4+} redox reaction was mainly responsible for the capacity, in which most Li remained fixed in the transition metal layers.[48,54] A more recent investigation conducted by Xu et al. revealed that Li ions in the transition metal layers allow more Na ions to reside in the prismatic sites in the high-voltage region, stabilizing the overall charge balance and retaining the P2 structure for the initial P2-$Na_x[Li_yNi_zMn_{1-y-z}]O_2$ ($0 < x, y, z < 1$).[51] Yuan et al. proposed Co-doped P2-$Na_{0.67}[Mn_{0.65}Co_{0.2}Ni_{0.15}]O_2$ as a promising cathode for NIBs.[53] This electrode delivers an initial capacity of 141 mA h g^{-1} with a slow capacity decay to 125 mA h g^{-1} after 50 cycles at 0.15 C between 2.0 to 4.4 V vs Na^+/Na. The cycle stability was further enhanced by a partial replacement of Co with Al. Fe-doped P2-$Na_{0.5}[Ni_{0.23}Fe_{0.13}Mn_{0.63}]O_2$ also delivered high discharge capacities of 180 mA h g^{-1} at 0.1 C and 60 mA h g^{-1} at 5 C with a relatively stable cycle performance.[50]

The electrochemical activity of α-$NaFeO_2$ in Na-ion cells was recently revisited by Yabuuchi et al.[55] A low reversible capacity of 90 mA h g^{-1} was delivered from the electrode in the voltage range of 3.0 to 3.6 V vs Na^+/Na due to instability of Fe^{4+} at high voltage in the oxide framework. Recently, Lee et al. discussed the chemical instability of Fe^{4+} in the oxygen framework of Na_xFeO_2.[56] More than 20% of Fe^{4+} spontaneously reduced back to Fe^{3+} states in the charged cell, and a concurrent asymmetric phase transition to a new O″3 phase was observed. On the other hand, partial substitution of Mn in this framework led to the discovery of a new high energy cathode, P2-$Na_xFe_{0.5}Mn_{0.5}O_2$, which delivers a discharge capacity of 190 mA h g^{-1} at 0.05 *C* in the voltage range of 1.5 to 4.3 V vs Na^+/Na, as shown in **Figure 3**a,b.[57] Approximately 70% of the discharge capacity can be achieved at 1 *C*. The charge compensation is achieved by the oxidization of Mn^{3+} (below 3.8 V) and subsequent oxidization of Fe^{3+} (above 3.8 V) during the charge process. A reversible electrode operation was observed in the Na composition range of $0.13 < x < 0.86$, and a reversible P2-OP4 phase transition in this region was confirmed. Pang et al. demonstrated that the phase transition from *P63/mmc* (P2-type at the open-circuit voltage) to *P63* (OP4-type when fully charged) occurs during the charge process, and the reverse transition from *P63* to *P63/mmc* was observed upon subsequent discharge to 2.0 V.[58] Additional sodiation to 1.5 V vs Na^+/Na leads to a phase transition from *P63/mmc* to *Cmcm*. A more recent structural study by Talaie et al. revealed that the migration of Fe^{3+} into tetrahedral sites in the interlayer space occurred above 4.0 V, which caused a short range ordering between two adjacent layers, resulting in large cell polarization.[59]

In a continuous effort of transition metal doping, Jung et al. synthesized P2-$Na_{0.7}[(Fe_{0.5}Mn_{0.5})_{1-x}Co_x]O_2$ (x = 0, 0.05, 0.10, and 0.20).[60] The structural evolution during the electrochemical reaction was investigated using in situ synchrotron XRD analysis, which identified a phase transformation from P2 to O2 above 4.1 V vs Na^+/Na for P2-$Na_{0.7}Fe_{0.4}Mn_{0.4}Co_{0.2}O_2$. Although the original P2 structure was restored during the following sodiation processes, the corresponding P2–O2 transition was accompanied by a large lattice volumetric contraction, resulting in poor electrochemical properties. In contrast, P2-$Na_{2/3}(Mn_{1/2}Fe_{1/4}Co_{1/4})O_2$ exhibited a superior rate performance of 130 mA h g^{-1} at 30 C, while the reversibility of the phase transition above 4.2 V requires further improvement.[61] Partial substitution of Fe by Ni yields better energy density, especially in the voltage region between 2.0 and 4.1 V, by avoiding the aforementioned unfavorable phase transition,

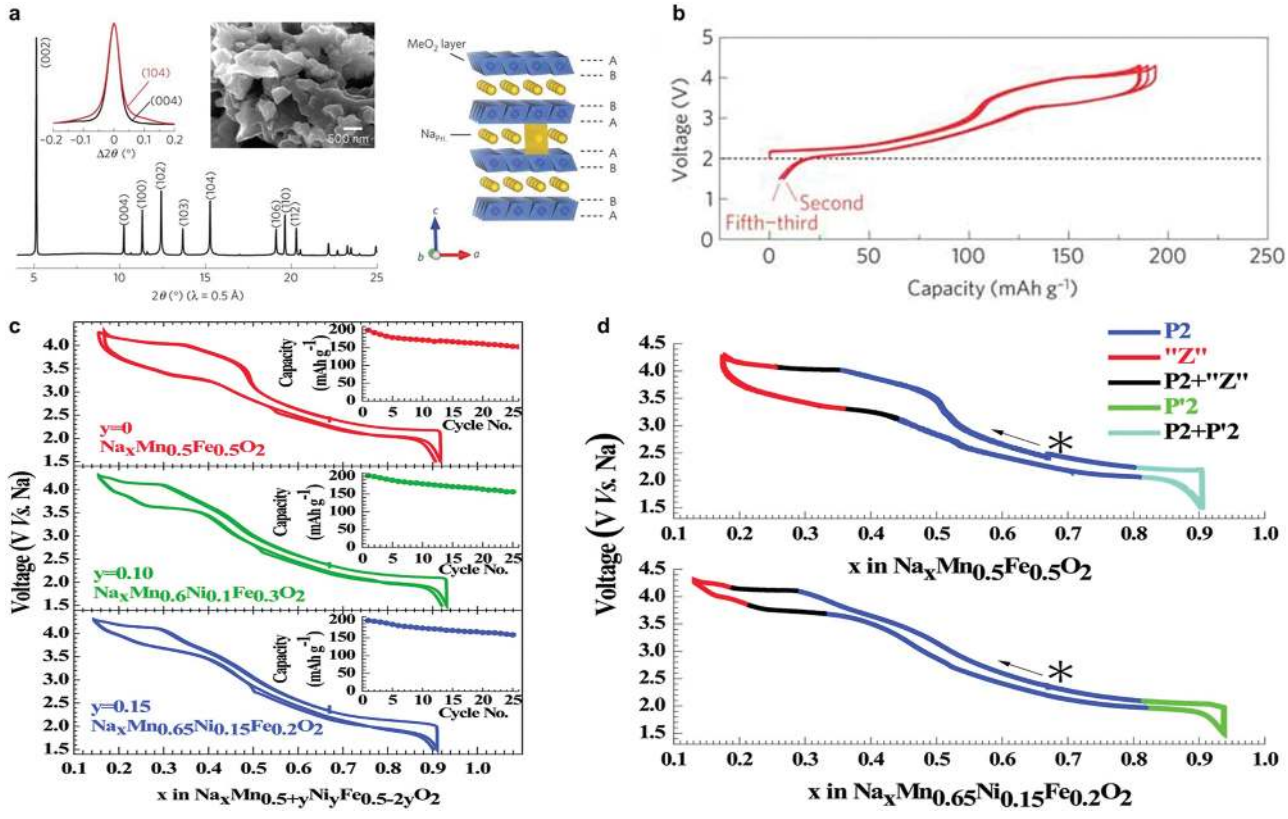

Figure 3. a) Structural characterization of P2-type $Na_{2/3}[Fe_{1/2}Mn_{1/2}]O_2$ based on synchrotron XRD patterns and SEM images. A and B in the schematic illustrations of $Na_{2/3}[Fe_{1/2}Mn_{1/2}]O_2$ indicate the different oxygen layers. b) Galvanostatic charge/discharge profiles of Na/$Na_{2/3}[Fe_{1/2}Mn_{1/2}]O_2$ cell at a current rate of 12 mA g^{-1}. Reproduced with permission.[57] Copyright 2012, Nature Publishing Group. c) Galvanostatic charge/discharge profiles of P2-$Na_{0.67}[Mn_{0.5+y}Ni_yFe_{0.5-2y}]O_2$ (y = 0, 0.1, 0.15) during first two cycles; the specific capacities of this electrode over 25 cycles at 13 mA h g^{-1} (C/20) are also shown in the insets. d) Phase evolution curves within $Na_{0.67}[Mn_{0.5}Fe_{0.5}]O_2$ and $Na_{0.67}[Mn_{0.65}Ni_{0.15}Fe_{0.2}]O_2$ as a function of the Na content x and voltage profiles. P2 represents the initial structure of the electrode, and "Z" and P'2 represent an uncharacterized high potential phase and a distorted phase, respectively. The asterisk (*) represents the starting point of the electrochemical cycling. Reproduced with permission.[59] Copyright 2015, Royal Society of Chemistry.

as illustrated in Figure 3c,d. This strategy was also applied to the P2-$Na_{2/3}Mn_{1/3}Fe_{1/3}Co_{1/3}O_2$ cathode, for which stable cyclic behavior was achieved by limiting the upper voltage to 4.1 V vs Na^+/Na.[62]

Designing a P2–O3 composite was also introduced as an effective way to obtain a high-performance cathode for NIBs. Such an effort was first demonstrated by Lee et al., and their $Na_{1-x}Li_xNi_{0.5}Mn_{0.5}O_{2+d}$ composed of multiple phases including O3, O'3, and P2 enabled fast Na diffusion, resulting in improved rate performances.[63] More recently, Guo et al. proposed a P2–O3 composite of $Na_{0.66}Li_{0.18}Mn_{0.71}Ni_{0.21}Co_{0.08}O_{2+d}$, which exhibited a reversible capacity of 185 mA h g^{-1} at a 0.2 *C*-rate and 134 mA h g^{-1} at 1C.[64] In addition to the Ni/Mn and Fe/Mn mixed TMOs, other interesting combinations have emerged, including $Na_{0.6}Cr_{0.6}Ti_{0.4}O_2Na_{0.67}$, $Ni_{0.33}Ti_{0.67}O_2$, $Na_{0.67}Co_{0.5}Mn_{0.5}O_2$, and $Na_{0.67}Ni_{0.67}Sb_{0.33}O_2$.[63,65–67]

2.1.2. O3-Type TMOs

Compared with Na-deficient P2-type layered cathodes, O3-type compounds are capable of providing high Na contents and are thus practically more useful for commercial rechargeable cells. Among the various O3-type single TMOs, the O3-$NaTMO_2$ (TM = Mn, Cr, Fe, and Ni) system has been extensively studied by many research groups. Parant et al. first reported two polymorphs of O3-Na_xMnO_2 ($x = 0.2$, 0.40, 0.44, 0.70, and 1), a low-temperature phase (α-$NaMnO_2$) with a distorted monoclinic structure and a high-temperature phase (β-$NaMnO_2$) with an orthorhombic structure.[29] Although a report by Mendiboure et al. revealed that only ≈0.2 Na can reversibly de/intercalate into the structure of α- and β-$NaMnO_2$,[38] the α-phase recently proposed by Ma et al. is capable of delivering a discharge capacity of 185 mA h g^{-1} at 0.1 C.[68] Approximately 132 mA h g^{-1} of capacity is maintained after 20 cycles between 2.0 and 3.8 V vs Na^+/Na, which was explained in terms of improvement of nonaqueous electrolytes, i.e., the qualified low water concentration.

O3-$NaCrO_2$ is capable of delivering a high reversible Na capacity of approximately 120 mA h g^{-1} between 2.0 to 3.6 V vs Na^+/Na, although the iso-structural O3-$LiCrO_2$ has been known to be electrochemically inactive in Li-ion cells.[69–71] When the ionic liquid electrolyte NaFSA-KFSA (FSA represents the anion bis(fluorosulfonyl)amide) was adopted as a thermally stable electrolyte, the $NaCrO_2$ electrode exhibited a stable discharge capacity of 113 mA h g^{-1} at a current density of 125 mA h g^{-1} and 90 °C with a 98.5% capacity retention.[69] A recent report by Yu et al. showed that carbon-coated $NaCrO_2$ exhibits excellent capacity retention over 50 cycles with a reversible capacity of 120 mA h g^{-1} at a current density of 20 mA g^{-1}.[72] In addition, the high rate capability was confirmed for the electrode, in which approximately 99 mA h g^{-1} of the discharge capacity was delivered at 150 C. These authors claimed that the surface-conducting carbon layer not only promoted the electrochemical performance but also enhanced the structural integrity in the thermal environment.

Recently, Han et al. showed that O3-$NaNiO_2$ could deliver a reversible capacity of 114.6 mA h g^{-1} with multiple phase transitions within the voltage range of 4.0–1.5 V vs Na^+/Na at 0.1 C (see **Figure 4**a).[73] The substitution of other transition metals in O3-$NaNiO_2$ could lead to better electrochemical performance. Komaba et al. demonstrated that O3-$NaNi_{0.5}Mn_{0.5}O_2$ electrodes could deliver a capacity of 105–125 mA h g^{-1} at current densities of 240–4.8 mA g^{-1} in the voltage range of 2.2–3.8 V vs Na^+/Na.[74,75] When the cathode operation was performed in the expanded voltage range of 2.2–4.5 V, a higher reversible capacity of 185 mA h g^{-1} was achieved. However, the low cycle stability was confirmed in this region due to a multiple phase transition from the original O3 to O'3, P3, P'3, and P3″ phases, as illustrated in Figure 4b. An improved capacity retention was achieved by incorporating a small amount of Fe in the structure. Yuan et al. demonstrated that O3-$NaFe_{0.2}Mn_{0.4}Ni_{0.4}O_2$ exhibits a phase transformation from the P3 to OP2 phase, which has a smaller interslab distance than the P3″ phase in the high-voltage region, resulting in stable cycle performance.[76] Partial replacement of Fe with Ni leads to a high reversible capacity from the large contribution of the Ni^{3+}/Ni^{4+} redox couple as well as suppression of the formation of unstable Fe^{4+}. O3-$NaFe_{0.3}Ni_{0.7}O_2$ also delivers a high discharge capacity of 135 mA h g^{-1} with enhanced cycle stability.[77]

$NaNi_{0.33}Mn_{0.33}Co_{0.33}O_2$ synthesized by Sathiya et al. exhibited a reversible capacity of 120 mA h g^{-1}, which corresponds to the utilization of ≈0.5 Na in the voltage range of 2–3.75 V vs Na^+/Na.[78] A reversible structural evolution occurs during electrochemical cycling in the sequence of O3→O1→P3→P1, as illustrated in Figure 4c. Recently, Hwang et al. proposed a O3 cathode with a composition gradient from the inner end ($Na[Ni_{0.75}Co_{0.02}Mn_{0.23}]O_2$) to the outer end ($Na[Ni_{0.58}Co_{0.06}Mn_{0.36}]O_2$), for which the total electrochemical reaction was based on $Ni^{2+}/Ni^{3+}/Ni^{4+}$ redox couples.[81] This core–shell-like structure is beneficial against the electrolyte corrosion, delivering a high discharge capacity of 157 mA h g^{-1} at a current rate of 15 mA g^{-1}. A high capacity retention of 80% after 300 cycles was observed in a full-cell configuration with a hard carbon anode. Li-doped electrode materials such as $Na_{0.95}Li_{0.15}(Ni_{0.15}Mn_{0.55}Co_{0.1})O_2$ and $Na_{0.78}Li_{0.18}Ni_{0.25}Mn_{0.583}O_2$ were also introduced as high-energy cathodes for NIBs, delivering discharge capacities of ≈200 mA h g^{-1} in Na-ion cells.[82–84] Further works expanded the scope of transition metal compositions, such as $Na(Fe_{0.33}Co_{0.33}Ni_{0.33})O_2$ and a quaternary cathode $Na(Mn_{0.25}Fe_{0.25}Co_{0.25}Ni_{0.25})O_2$. These electrodes exhibited increased reversible capacities compared with $NaNi_{0.33}Mn_{0.33}Co_{0.33}O_2$, which was attributed to the more reversible structure evolution of O3-P3-O3′-O3″, as indicated in Figure 4d.[79,85,86]

In contrast to the general view that O3-structures are only synthesized in Na-rich environments, recent works have reported the discovery of Na-deficient O3-type cathodes (i.e., $Na_{0.8}Ni_{0.4}Ti_{0.6}O_2$ and $Na_{0.67}Fe_{0.67}Mn_{0.33}O_2$) for NIBs, and such works could possibly broaden the strategy for O3 cathode development.[31,80,87,88] The O3-$Na_{0.8}Ni_{0.4}Ti_{0.6}O_2$ electrode delivered a reversible capacity of 85 mA h g^{-1} at 2.8 V vs Na^+/Na with a redox reaction of Ni^{4+}/Ni^{2+} and Ti^{4+}/Ti^{3+}.[87] Approximately 75% of the capacity was maintained after 150 cycles, and a good rate capability was observed. Sharma et al. synthesized a O3-$Na_{0.67}Fe_{0.67}Mn_{0.33}O_2$ electrode, which delivers promising electrochemical properties in Na-ion cells.[88] These authors claimed that this behavior results from the electrode maintaining the O3 structure during electrochemical cycling, where

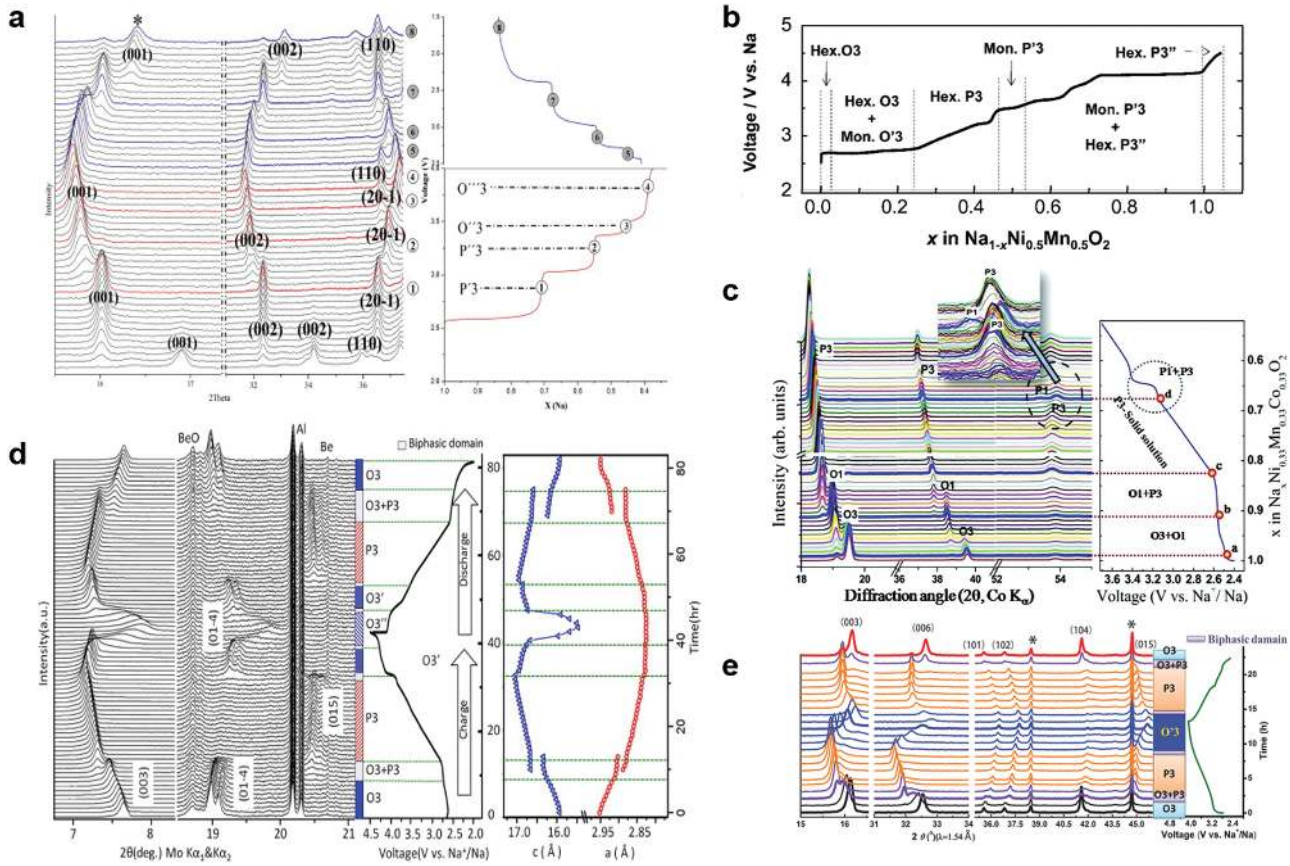

Figure 4. a) In situ XRD patterns of $NaNiO_2$ during the first charge/discharge and voltage curve. Reproduced with permission.[73] Copyright 2014, Elsevier. b) Phase evolution of $Na_{1-x}Ni_{0.5}Mn_{0.5}O_2$ during the first charge. Reproduced with permission.[74] Copyright 2012, American Chemical Society. c) In situ XRD patterns during the first charge of $NaNi_{1/3}Mn_{1/3}Co_{1/3}O_2$. The corresponding voltage profile is presented on the right side. Reproduced with permission.[78] Copyright 2012, American Chemical Society. d) In situ XRD patterns of O3-type $Na(Mn_{0.25}Fe_{0.25}Co_{0.25}Ni_{0.25})O_2$ (left) and the corresponding charge/discharge profiles (middle). The lattice parameters (right) were calculated from refinement of the in situ XRD patterns. Reproduced with permission.[79] Copyright 2014, Elsevier. e) In situ XRD patterns during the first charge/discharge of the O3-$Na_{0.9}[Cu_{0.22}Fe_{0.30}Mn_{0.48}]O_2$. The black asterisks represent peaks from Al. Reproduced with permission.[80] Copyright 2015, Wiley-VCH.

the electrode undergoes a series of two-phase and solid-solution transitions.

Layered Na TMOs have shown promising electrochemical behavior; however, their sensitivity to water and CO_2 still require further improvement for practical mass production. Sathiya et al. demonstrated that as-prepared rhombohedral O3-$NaNi_{1/3}Mn_{1/3}Co_{1/3}O_2$ experienced phase transitions to the monoclinic O1-phase and finally to the rhombohedral P3 phases upon aging in open air conditions for over 300 days mainly because of the absorption of water.[78] Buchholz et al. investigated the correlation between the intercalation of water and the Na content in a mixed P2/P3 structure of $Na_xNi_{0.22}Co_{0.11}Mn_{0.66}O_2$ and observed that a significant amount of water was intercalated until the Na content decreased to below 0.33 per formula unit.[89] More recently, Duffort et al. proposed that the insertion of carbonate ions occurred for the P2-$Na_{0.67}[Mn_{0.5}Fe_{0.5}]O_2$ upon exposure to CO_2 with the assistance of H_2O absorption, which was accompanied by the oxidation of Mn^{3+} to Mn^{4+}, leading to the decreased reversibility and large overpotential.[90] These authors revealed that Ni-substituted P2-$Na_{0.67}[Ni_xMn_{0.5+x}Fe_{0.5-2x}]O_2$ exhibited suppressed reactivity to CO_2. In addition, a recent report introduced a waterproof cathode, O3-$Na_{0.9}[Cu_{0.22}Fe_{0.30}Mn_{0.48}]O_2$, which displays superior structural stability in water. The enhanced stability was demonstrated by the small change in the XRD patterns; however, the mechanism is not yet clear.[80] The electrode operates mainly via redox couples of Cu^{2+}/Cu^{3+} and Fe^{3+}/Fe^{4+}, and its phase transition was similar to that of O3-$Na(Mn_{0.25}Fe_{0.25}Co_{0.25}Ni_{0.25})O_2$, as indicated in Figure 4e.

2.1.3. Other TMOs

$Na_{0.44}MnO_2$, which is isostructural to tunnel-type $Na_4Mn_4Ti_5O_{18}$ with space group *Pbam*, has been extensively studied for both aqueous and non-aqueous NIBs.[91,92] A reversible electrochemical process occurs in the Na composition range of $0.25 < x < 0.65$ for Na_xMnO_2, corresponding to a discharge capacity of 110 mA h g^{-1}. The electrode undergoes a six biphasic transition in the potential range of 2.0 to 3.8 V vs Na^+/Na in non-aqueous electrolyte, and later theoretical work by Kim et al. proposed seven intermediate phases with a series of two-phase reactions based on density functional theory (DFT) calculations.[92,93] Because of the flexible synthesis processes, there

have been many efforts to synthesize morphology-controlled $Na_{0.44}MnO_2$. A nanowire or rod structure of $Na_{0.44}MnO_2$ provides a large surface area and enables fast Na ion diffusion, resulting in high rate performances in Na-ion cells.[92,94–99] To overcome the asymmetric lattice evolution caused by Jahn–Teller distortion of Mn^{3+} upon electrochemical cycling, Ti- and Fe-substituted $Na_{0.44}MnO_2$ were investigated by Zhan et al. $Na_{0.61}[Mn_{0.61-x}Fe_xTi_{0.39}]O_2$ yielded a high operating voltage of 3.56 V vs Na^+/Na and a reversible capacity of 90 mA h g^{-1}.[100,101]

Vanadium oxides (VO_x) have been considered attractive cathodes for rechargeable batteries because of their open framework structure and multivalent character with various metastable phases such as VO_2(B), V_6O_{13}, V_2O_5-y, V_2O_5, and LiV_3O_8. In an effort to use vanadium oxides as cathodes for NIBs, the layered structure of Na_xVO_2 was evaluated as a Na intercalation host and exhibited a reversible capacity of ≈120 mA h g^{-1}.[102,103] Recent work introduced graphene-coated VO_2, which delivered a reversible capacity of 306 mA h g^{-1} at a current density of 100 mA g^{-1}. The electrode displayed a high cycle stability, where a capacity above 110 mA h g^{-1} was retained after 1500 cycles at a current density of 18 A g^{-1}.[104] Hydrated vanadium pentoxide, $V_2O_5 \cdot nH_2O$, with a nanowire-interconnected structure, also exhibited high capacities of 338 mA h g^{-1} at 0.05 A g^{-1} and 96 mA h g^{-1} at 1.0 A g^{-1}.[105] The open structure of VO_x provides an opportunity to ensure a large reversible capacity for alkaline metal cations including Li^+, Na^+, and K^+ and is worthy of further exploration.

2.2. Polyanionic Compounds

Extensive research has been also focused on polyanionic compounds as cathode materials for NIBs because of their structural diversity and stability (see Figure 1a).[18,21,106] Although the presence of heavy polyanion groups reduces the gravimetric capacity of electrode materials in general, the diverse pool of polyanion species (e.g., $(PO_4)^{3-}$, $(SO_4)^{2-}$, $(SiO_4)^{4-}$, and $(P_2O_7)^{4-}$) in nature offers many opportunities to identify new open-framework crystal structures with promising electrochemical properties. In addition, the strong covalent bonding of X–O (X = P, S, Si, and B) in the crystal structure provides structural robustness during electrochemical cycling, and the inductive effect of polyanion groups ensures a high operating potential vs Na^+/Na.[107,108] To date, phosphate-, fluorophosphate-, pyrophosphate, sulfate-, and mixed polyanion-based materials have been studied as important groups of potential electrodes, as illustrated in Figure 1b. In this section, we review recent progress on various polyanionic cathodes for NIBs.

2.2.1. Phosphates

$NaFePO_4$: Olivine $NaFePO_4$, a structural analogue of $LiFePO_4$, has been investigated as a possible cathode material for NIBs because of its high theoretical capacity (≈154 mA h g^{-1}).[109–114] Although the most thermodynamically stable structure of $NaFePO_4$ is a maricite phase, which has no Na diffusion path in the structure, the electrochemically active olivine $NaFePO_4$ can be obtained by delithiation and subsequent sodiation of $LiFePO_4$ (see **Figure 5**a).[109] Figure 5b presents an electrochemical profile of olivine $NaFePO_4$ in a Na-ion cell. The charge curve exhibits two clear plateaus separated by a voltage drop at the Na content of 0.67, which corresponds to the formation of the intermediate phase $Na_{2/3}FePO_4$, whereas one plateau is observed during the first sodiation process. The phase reaction

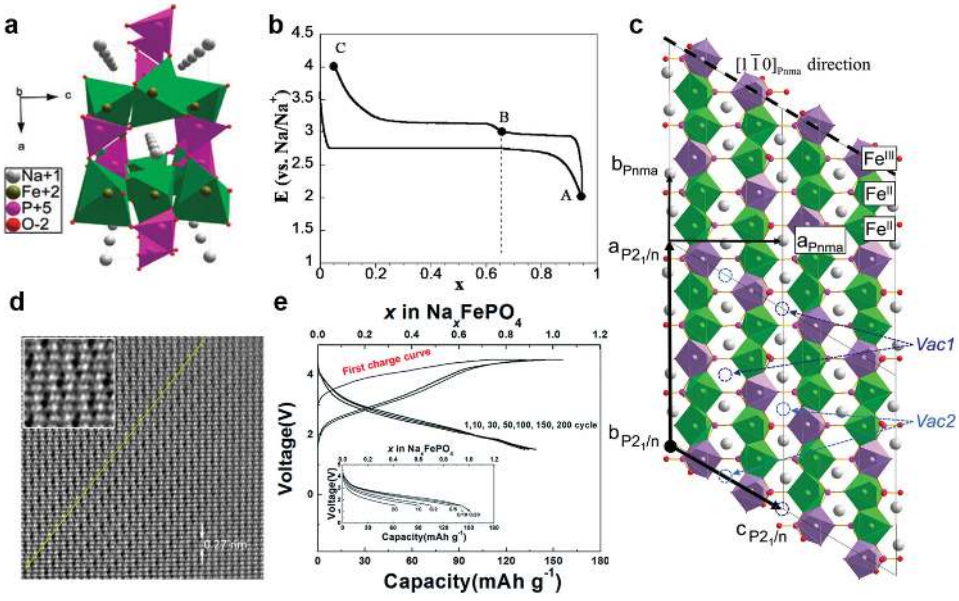

Figure 5. a) Structure schematics and b) galvanostatic charge/discharge profiles of olivine $NaFePO_4$. Reproduced with permission.[109] Copyright 2010, American Chemical Society. c) Structure representation of $Na_{2/3}FePO_4$ along c_{pnma} axis, which corresponds to $b_{P21/n}$ axis. The Na and P atoms are represented by light gray and red spheres, respectively. The FeO_6 octahedra are shown in light green (Fe^{2+}) and purple (Fe^{3+}). Reproduced with permission.[112] Copyright 2014, American Chemical Society. d) STEM image of $Na_{2/3}FePO_4$. The green arrow indicates the orientation of Na vacancies. Reproduced with permission.[113] Copyright 2014, American Chemical Society. e) Charge/discharge profiles of nanosized maricite $NaFePO_4$ in a Na-ion cell. The inset presents discharge profiles at various current rates (C/20, C/10, C/5, C/2, 1C, and 2C). Reproduced with permission.[115] Copyright 2015, Royal Society of Chemistry.

and structure of intermediate states of Na_xFePO_4 ($0 \le x \le 1$) were investigated by Lu et al. and Galceran et al.[111,114] The composition–temperature diagram of olivine Na_xFePO_4 proposed by Lu et al. revealed that the solid-solution phase is favorable for $x > 2/3$ at room temperature, whereas phase separation into $FePO_4/Na_{2/3}FePO_4$ occurs for $x < 2/3$.[111] More recently, Galceran et al. reported a similar phase reaction upon the charge process using in situ XRD analysis, where the solid-solution reaction occurs until the formation of the intermediate phase of $Na_{2/3}FePO_4$, and further Na extraction induces a phase separation into $Na_{2/3}FePO_4$ and $FePO_4$.[114] These authors explained that the phase separation in the region of $0 < x < 2/3$ originates from the large lattice mismatch between $Na_{2/3}FePO_4$ and $FePO_4$ (≈13%) compared with that between $NaFePO_4$ and $Na_{2/3}FePO_4$ (≈3.5%). On the other hand, during the discharge process, they observed a multi-phase reaction (i.e., $Na_{1-x}FePO_4$, $Na_{2/3-x}FePO_4$, Na_xFePO_4, where $x \approx 0.1$), which results in the apparently different discharge profile compared to the charge profile. It was attributed to diffuse interfaces between different phases.[114]

The crystal structure of the intermediate phase of $Na_{2/3}FePO_4$ was investigated by Boucher et al. using transmission electron microscopy (TEM), synchrotron XRD, DFT calculations, and Mössbauer spectroscopy.[112] They revealed that the structure of $Na_{2/3}FePO_4$ can be defined with a monoclinic $P2_1/n$ supercell that results from Na-vacancy and Fe^{2+}/Fe^{3+} charge ordering, as demonstrated in Figure 5c. The ordering of the vacancies along the $[1\text{-}10]_{pnma}$ direction, which corresponds to $[001]_{P21/n}$, was observed based on TEM electron diffraction patterns and Rietveld refinement of synchrotron XRD data. In addition, the charge ordering of Fe^{2+} and Fe^{3+} was confirmed from calculated bond valence sums and Mössbauer spectroscopy analysis. Recently, Galceran et al. directly visualized the Na-vacancy ordering in $Na_{2/3}FePO_4$ using high-angle annular dark field-scanning transmission electron spectroscopy (HAADF-STEM) analysis, as shown in Figure 5d.[113,116] Clear Na-vacancy ordering along the $[1\text{-}10]_{pnma}$ (green arrow line) direction was observed. Despite the interesting findings on olivine $NaMePO_4$ (Me = Fe and Mn), particularly in a comparative study with the olivine $LiMePO_4$, the electrochemical properties in Na-ion cells are not impressive, and the synthesis of the phase is not suitable for large-scale uses, which thus limits its further application in NIBs.[110,117,118]

Recently, Kim et al. demonstrated that the maricite $NaFePO_4$ phase, which is a thermodynamically stable phase based on its stoichiometry but had been believed to be electrochemically inactive because of the absence of apparent Na diffusion paths in the structure, can become electrochemically active when prepared as nano-sized particles.[115] It was reported that a reversible capacity of ≈142 mA h g^{-1} can be achieved with promising rate performances and negligible capacity decay up to 200 cycles (95% retention), as observed in Figure 5e. They found the origin of the electrochemical activity comes from a rapid phase transformation from the maricite $FePO_4$ into amorphous $FePO_4$ occurring during the first Na deintercalation process. During the subsequent cycles, the amorphous $FePO_4$ phase becomes the main contributor of the electrochemical activity. Indeed, the amorphous $FePO_4$ phase is electrochemically active in NIB because of the large number of vacant sites with highly percolated Na pathways, which could ensure facile transfer of Na ions.[119,120] The early reports on amorphous $FePO_4$ revealed comparably poor electrochemical properties in Na-ion cells; however, recent reports indicated that a $FePO_4$/C nanocomposite could deliver a high capacity, stable cycle, and high rate capability.[119–121] Considering the low element cost of Fe and high theoretical capacity of the nanocomposite (≈178 mA h g^{-1}), it could be a promising cathode for NIBs. Nevertheless, the absence of Na in the amorphous $FePO_4$ requires the use of Na-containing anodes, which can limit its combination with conventional anode materials (i.e., hard carbon, P, Sn, and Sb).[122–124] Maricite $NaFePO_4$ can successfully overcome the demerits of amorphous $FePO_4$ while taking advantage of its electrochemical activity. Additionally, Li et al. synthesized Na-containing hollow amorphous $NaFePO_4$ nanospheres that exhibit a Na storage capacity of 148 mA h g^{-1} and stable cycle performance of ≈300 cycles.[120]

NASICON $Na_3V_2(PO_4)_3$: NASICON (NA Super Ionic CONductor) compounds have been intensively investigated as promising cathodes for NIBs because of their open framework structure enabling the fast Na ionic conduction.[106,125–128] The general formula of a NASICON is $A_xMM'(XO_4)_3$, which is composed of corner-sharing MO_6 and XO_4 polyhedra with a three-dimensional (3D) network that allows Na conduction (see **Figure 6**a).[129] Early studies introduced NASICON-type compounds as Na-ion conducting solid electrolytes (e.g., $Na_{1+x}ZrP_{3-x}Si_xO_{12}$);[125] however, more recently, various V-based intercalation compounds were reported as high-energy cathodes based on the multi-electron redox reaction of V^{2+}/V^{3+}, V^{3+}/V^{4+}, and V^{4+}/V^{5+}.[106,126–128] Tremendous efforts have been focused on improving the electrochemical properties of $Na_3V_2(PO_4)_3$ electrodes since the Na de/intercalation behavior of a $Na_3V_2(PO_4)_3$ electrode was reported by Uebou et al.[130] Approximately two Na ions (117 mA h g^{-1}) can be extracted and reinserted into the electrode at ≈3.6 V with a redox reaction of V^{3+}/V^{4+}, and the biphasic reaction between $Na_3V_2(PO_4)_3$ and $NaV_2(PO_4)_3$ with a small volume change of 8.26% was confirmed by Jian et al.[127,130] The electrochemical activity was also observed in the low-voltage region at approximately 1.6 V with a redox reaction of V^{2+}/V^{3+}.

The electrochemical properties of $Na_3V_2(PO_4)_3$ were significantly improved by carbon coating and nanostructuring. Saravanan et al. synthesized porous $Na_3V_2(PO_4)_3$/C using a solution-based approach, and the electrode exhibited an energy density of ≈400 Wh kg^{-1} vs Na^+/Na and stable cycle performances (50% after 30,000 cycles at 40C).[131] Recently, Fang et al. reported hierarchical-carbon-framework-wrapped $Na_3V_2(PO_4)_3$ with a high rate capability (38 mA h g^{-1} at 500C) and cycle stability (54% after 20,000 cycles at 30C), as shown in Figure 6b,c.[128] The carbon-coated $Na_3V_2(PO_4)_3$ in a porous graphene network could also provide a high electrical conductivity of ≈110 S m^{-1}, resulting in a high rate capability (86 mA h g^{-1} at 100C) and cycle stability (64% after 10,000 cycles at 100C).[132] As many research groups reported, the electrochemical properties of $Na_3V_2(PO_4)_3$ electrode appear to be promising, however, the concerns on the use of toxic and costly vanadium and the low specific capacity (≈100 mA h g^{-1}) must be addressed for further application.

Other Phosphate Compounds: Various other phosphate compounds have been proposed and evaluated as electrode materials for NIBs.[130,133–136] Uebou et al. showed that NASICON-$Na_3Fe_2(PO_4)_3$ is capable of reversible de/intercalation by about

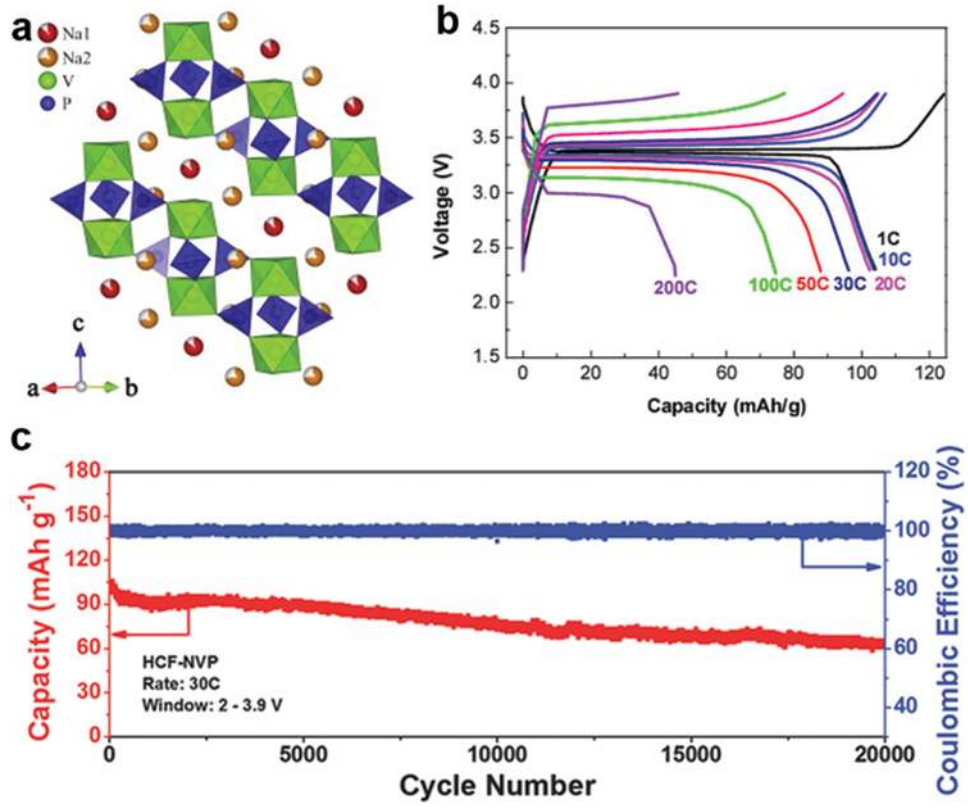

Figure 6. a) Schematic structure of $Na_3V_2(PO_4)_3$. Reproduced with permission.[129] Copyright 2012, Elsevier. b) Galvanostatic charge/discharge curves at various current rates (1C, 10C, 20C, 30C, 50C, 100C, 200C). c) Cycle performance of hierarchical-carbon-framework-wrapped $Na_3V_2(PO_4)_3$ at 30C. Reproduced with permission.[128] Copyright 2015, Wiley-VCH.

0.4 Na per formula unit,[130] and Trad et al. reported that alluaudite $NaMnFe_2(PO_4)_3$ exhibits an electrochemical activity in the voltage range of 1.5–4.3 V (vs Na/Na^+) in Na-ion cells.[133] A poor reversible capacity of 50 mA h g^{-1} was confirmed for $NaMnFe_2(PO_4)_3$; however, Huang et al. recently reported that a $Na_2Fe_3(PO4)_3$/carbon nanotube nanocomposite delivers a discharge capacity of 143 mA h g^{-1} with a stable cycle retention up to 50 cycles.[137] A layered-type phosphate compound, $Na_3Fe_3(PO_4)_4$, was also introduced as a cathode for NIBs.[134] Approximately 1.8 Na ions, which corresponds to a specific capacity of 80 mA h g^{-1}, could be reversibly de/intercalated in the $Na_3Fe_3(PO_4)_4$ with a Fe^{2+}/Fe^{3+} redox reaction.

Song et al. investigated monoclinic $NaVOPO_4$ as a high-voltage cathode for NIBs.[136] The electrode delivers a reversible capacity of 90 mA h g^{-1} with an average voltage of 3.6 V vs Na^+/Na at a current rate of 1/15C. Later work by Chen et al. revealed that the electrode operation involves a single-phase reaction with a negligible volume change (≈1.2%), resulting in a high rate and cycle performances.[138] Although various phosphate compounds have been introduced as new low-cost electrode materials for NIBs, they exhibit generally low energy densities below 400 Wh kg^{-1} and limited cycle stabilities.

2.2.2. Fluorophosphates

The introduction of highly electronegative fluorine ions in phosphate-based structures provides opportunities to find new high-voltage electrodes for NIBs. Fluorophosphate with a general formula of Na_2MePO_4F (Me = Fe, Mn, Co, and Ni) adopts two different polymorph structures, which are a layered-type structure with a space group of orthorhombic *Pbcn* and a 3D framework with monoclinic $P2_1/c$, as illustrated in **Figure 7**a,b.[139,140] Since the initial report on the electrochemical activity of orthorhombic Na_2FePO_4F electrode at high voltage (≈3.5 V vs Li^+/Li) by Ellis et al.,[141] intensive investigations have been focused on various fluorophosphate compounds for NIBs.[117,142–147] Recham et al. prepared nanosized powder of Na_2FePO_4F using ionothermal synthesis routes and demonstrated that ≈0.8 Na can reversibly de/intercalate in Na-ion cells.[142] Kawabe et al. also revealed that carbon-coated Na_2FePO_4F/C could deliver approximately 110 mA h g^{-1} of reversible capacity, which corresponds to 90% of the theoretical capacity at a current rate of 6.2 mA g^{-1}, and 75% of the initial capacity was retained after 20 cycles, as shown in Figure 7c.[144] Along with Na_2FePO_4F, orthorhombic Na_2CoPO_4F, which utilizes a redox couple of Co^{2+}/Co^{3+}, was reported as a high-voltage cathode for NIBs.[143,148,149] Although earlier works displayed poor electrochemical activity in Na-ion cells,[143] Zou et al. recently demonstrated that Na_2CoPO_4F/C synthesized by the spray drying method can deliver a discharge capacity of 107 mA h g^{-1} with a voltage plateau at 4.3 V.[148]

Monoclinic $P2_1/c$ Na_2MnPO_4F was also investigated as a cathode for NIBs.[142,146,147,153] The successful demonstration of the electrochemical activity of Na_2MnPO_4F electrode was firstly

reported by Kim et al., with a discharge capacity of 120 mA h g^{-1} at a current rate of 10 mA g^{-1}.[146] The following study by Lin et al. reported that C/Na_2MnPO_4F nanocomposite materials synthesized via the spray drying method displayed enhanced electronic conductivity, resulting in impressive electrochemical properties (140 and 178 mA h g^{-1} at 30 and 55 °C, respectively).[153] More recently, Zhong et al. revealed that carbon-coated C/Na_2MnPO_4F synthesized by wet ball milling delivers a discharge capacity of 120 mA h g^{-1} with a cycle retention of 70% after 30 cycles.[147] Binary metal compounds, $Na_2Fe_{1-x}Mn_xPO_4F$ ($0 < x < 1$), were also synthesized; the crystal structure remained orthorhombic *Pbcn* until $x \approx 0.2$ and changed to the monoclinic $P2_1/c$ phase at $x \geq 0.25$.[142] Although previous reports indicated that an increase in the Mn content in $Na_2Fe_{1-x}Mn_xPO_4F$ ($0 < x < 1$) results in a dramatic decrease of reversible capacity, Kawabe et al. reported that nanosized C/$Na_2Fe_{0.5}Mn_{0.5}PO_4F$ delivers 110 mA h g^{-1} at C/20 with a clear redox activity of Mn^{2+}/Mn^{3+} at 3.53 V.[154] However, poor power capabilities and cycle performances of the monoclinic $Na_2Fe_{1-x}Mn_xPO_4F$ ($0.25 \leq x \leq 1$) electrodes were not sufficiently high in Na-ion cells.[145,154] The low ionic and electronic conductivities of monoclinic $P2_1/c$ $Na_2Fe_{1-x}Mn_xPO_4F$ phases ($0.25 \leq x \leq 1$) remain great challenges.

V-based fluorophosphate compounds have attracted much attention due to the high operating voltage and stable cycle property.[150,152,155–157] The simplest form of Na-containing V-based fluorophosphates, $NaVPO_4F$, exists in two different polymorphs; one with monoclinic *C2/c* and the other with tetragonal *I4/mmm* structures.[157] Barker et al. first proposed tetragonal $NaVPO_4F$ as a cathode for NIBs.[155] They showed that the $NaVPO_4F$ electrode delivers a discharge capacity of 82 mA h g^{-1} with an average voltage of 3.7 V. The monoclinic $NaVPO_4F$ electrode also exhibits electrochemical activity in Na-ion cells.[158] A discharge capacity of approximately 80 mA h g^{-1} was delivered with an average voltage of 3.7 V. There have been many efforts to enhance the electrochemical properties of $NaVPO_4F$ through doping or carbon coating; however, only limited enhancement of the cell performances was reported.[158–160]

Two other important fluorophosphates compounds, $Na_3(VO_x)_2(PO_4)_2F_{3-2x}$ ($x = 0, 1$), were introduced as cathode materials for NIBs. Le Meins et al. first synthesized $Na_3V_2(PO_4)_2F_3$ and reported the crystal structure with a space group of $P4_2/mnm$.[161] The structure can be described with $[V_2O_8F_3]$ bi-octahedron and $[PO_4]$ tetrahedron units, and the bi-octahedra are connected by a fluorine atom along the *c*-axis, forming large Na diffusion channels along the *a* and *b* directions (see Figure 7d). Although earlier works evaluated the electrochemical properties of $Na_3V_2(PO_4)_2F_3$ in Li-ion

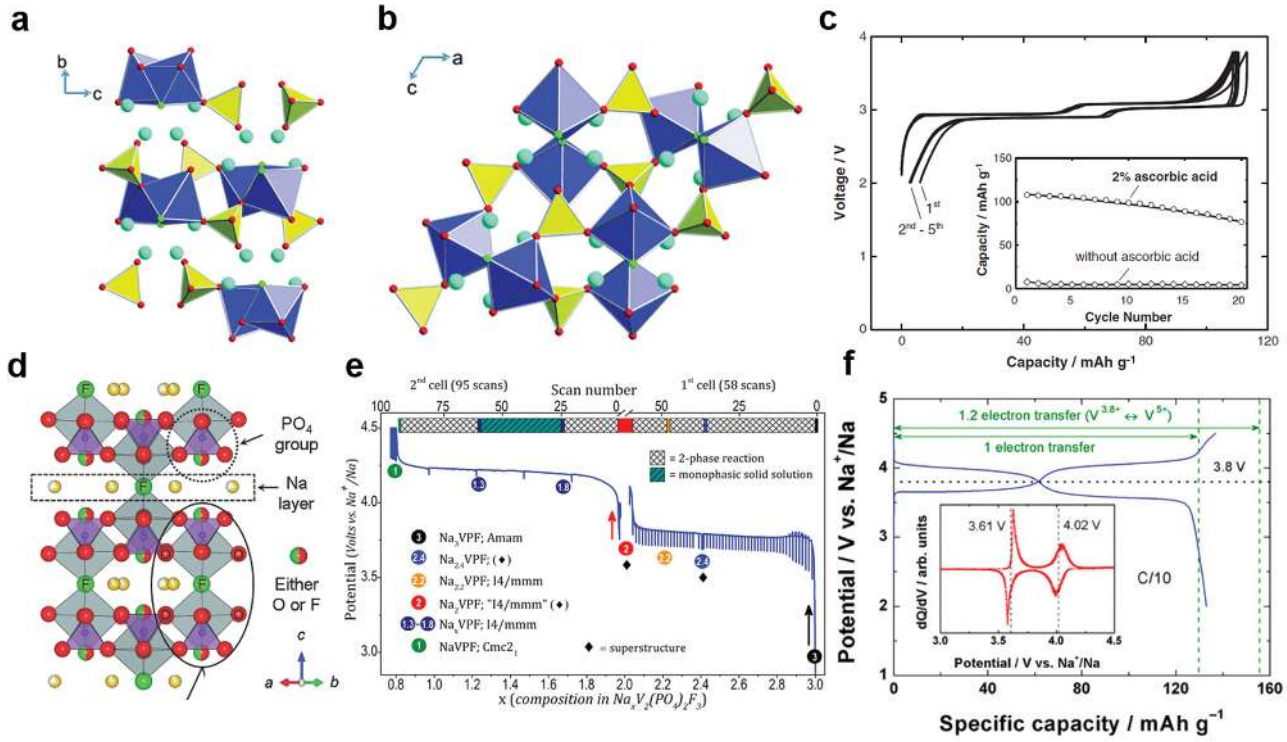

Figure 7. Schematic structure of a) Na_2FePO_4F with space group *Pbcn* and b) Na_2MnPO_4F with space group *P21/n*. Reproduced with permission.[145] Copyright 2011, Royal Society of Chemistry. c) Galvanostatic charge/discharge profiles of the Na_2FePO_4F in a Na-ion cell at a current rate of 6.2 mA g^{-1}. The inset shows the capacity retention of the Na_2FePO_4F synthesized with and without ascorbic acid. Reproduced with permission.[144] Copyright 2011, Elsevier. d) Crystal structure of $Na_3(VO_x)_2(PO_4)_2F_{3-2x}$ ($0 \leq x \leq 1$). Reproduced with permission.[150] Copyright 2014, Wiley-VCH. e) Potential–composition electrochemical profiles upon Na extraction from $Na_3V_2(PO_4)_2F_3$. The GITT measurement was performed at a current rate of C/5, and XRD data were recorded every 5 min. Experimental conditions of a 5-min charge and 5-min relaxation were used in the low-voltage region (3.0–4.2 V), whereas a 10-min relaxation time was used at every 0.25 Na extraction in the high-voltage region (3.8–4.5 V). Reproduced with permission.[151] Copyright 2015, American Chemical Society. f) Charge/discharge profiles of $Na_3(VO_{0.8})_2(PO_4)_2F_{1.4}$ at a current rate of C/10. The inset presents the corresponding d*Q*/d*V* curve. Reproduced with permission.[152] Copyright 2013, American Chemical Society.

cells,[156,162] recent works revealed that two Na (128.2 mA h g^{-1}) can reversibly de/intercalate into the structure with a redox reaction of V^{3+}/V^{4+}, resulting in two distinct voltage plateaus at 3.7 and 4.2 V vs Na^+/Na in Na-ion cells, as observed in Figure 7e.[150,151,163] More recently, Bianchini et al. presented the interesting result based on a high-resolution diffraction study that a subtle distortion in the structure of $Na_3V_2(PO_4)_2F_3$ leads to a new space group of *Amam* instead of *P4₂/mnm*.[164] They revealed that the $Na_xV_2(PO_4)_2F_3$ electrode operates via a complex phase reaction with four intermediate phases (x = 2.4, 2.2, 2, and 1) using in operando high-resolution synchrotron XRD studies.[151] Three biphasic reactions were observed in the low-voltage region (≈3.7 V) involving two intermediate phases (x = 2.4, 2.2), and further Na extraction led to both two-phase and solid-solution reactions until the end of charge (see Figure 7e). In addition, recent work introduced a new Na-rich V-based fluorophosphate compound, $Na_4V_2(PO_4)_2F_3$, as a cathode material for NIBs though mechanical mixing of $Na_3V_2(PO_4)_2F_3$ with 1 M Na_3P.[165]

The electrochemical activity of $Na_3(VO)_2(PO_4)_2F$ in a Na-ion cell was first examined by Sauvage et al.[166] They showed that approximately 1.12 Na can reversibly de/intercalate into the structure involving a V^{4+}/V^{5+} redox reaction with two voltage plateaus at 3.6 and 4.0 V vs Na^+/Na. Later work by Park et al. illustrates that carbon coating significantly enhances the reversible capacity of the electrode up to 120 mA h g^{-1}, which corresponds to ≈2 Na ions per formula unit.[150] In addition, a nanosized $Na_3(VO)_2(PO_4)_2F$ electrode exhibited excellent cycle performances with 90% capacity retention over 1200 cycles at 2C.[167] The reaction mechanism of $Na_3(VO)_2(PO_4)_2F$ during battery operation was investigated by Sharma et al.[168] They revealed that the electrode exhibits complex structural evolution during electrochemical cycling involving at least three intermediate phases similar to the behavior of $Na_3V_2(PO_4)_2F_3$.

A solid-solution phase of $Na_3(VO_{0.8})_2(PO_4)_2F_{1.4}$ was introduced as a high-energy cathode for NIBs by Park et al. and Serras et al.[152,169] It was revealed that this electrode provides one of the highest energy densities ≈600 Wh kg^{-1} among NIB cathodes, which originates from both the multi-electron redox reaction ($V^{3.8+}/V^{5+}$; 1.2e- per formula unit) and the high redox potential (≈3.8 V vs Na^+/Na) (see Figure 7f). Furthermore, promising cycle stability over 500 cycles with the cycle retention of 84% could be achieved, which was attributed to the small volume change (2.9%) upon cycling. Park et al. further reported a series of isostructural $Na_3(VO_x)_2(PO_4)_2F_{3-2x}$ ($0 \le x \le 1$) compounds as cathode materials for NIBs, which exhibited excellent electrochemical performances because of the open framework structure and small volume change (≈2%).[150]

2.2.3. Fluorosulfates and Sulfates

Series of fluorosulfate electrodes were reported by the Tarascon and Nazar groups both for LIBs and NIBs.[170–173] $NaFeSO_4F$, which is isostructural to the mineral tavorite, $LiFe(PO_4)OH$, was evaluated as a cathode for NIBs.[174] Tripathi et al. showed that $NaFeSO_4F$ delivers a capacity of 83 mA h g^{-1} in Li-ion cells,[173] whereas only 0.06 Na can be reversibly intercalated and extracted in Na-ion cells.[174] An atomistic modeling study revealed that only 1D Na hopping is plausible in $NaFeSO_4F$ with a high activation barrier of 0.6 eV in contrast to $LiFeSO_4F$, where 3D Li diffusion pathways with a low activation barrier of 0.35 eV ensure facile diffusion of Li ions.[172] In addition, these authors explained that the large volume change (≈16%) between the end phases of $NaFeSO_4F$ and $FeSO_4F$ is one of the reasons for the poor electrochemical activity. Later, Recham et al. reported K-based fluorosulfate compounds, $KMSO_4F$ (M = Fe, Co, and Ni), which can accommodate various alkali ions including Li^+, Na^+, and K^+.[175,176] They revealed that a desodiated $FeSO_4F$ electrode can uptake 0.85 Na during electrochemical cycling with two distinct voltage plateaus at 3.2 and 3.5 V. Although there have been efforts to find other electrochemically active fluorosulfate-based compounds including $NaMSO_4F$ (M = Co, Ni, Mn, Cu, etc.) and $NaMSO_4F \cdot 2H_2O$ (M = Fe, Co, Ni, and Zn), none of these materials have exhibited electrochemical activities in Na-ion cells thus far.[177–179]

Sulfate compounds are also considered potential candidates for Na intercalation hosts.[108,180–182] Two different hydrated forms of Na metal sulfate minerals, bloedite-type $Na_2M(SO_4)_2 \cdot 4H_2O$ (M = Mg, Fe, Co, and Ni) and Kröhnkite-type $Na_2Fe(SO_4)_2 \cdot 2H_2O$, were investigated as cathode materials for NIBs.[180,181] Reynaud et al. first discovered that approximately 0.7 Na can be reversibly de/intercalated from both $Na_2Fe(SO_4)_2 \cdot 4H_2O$ and dehydrated derivatives of $Na_2Fe(SO_4)_2$ electrodes with an average voltage of 3.3 and 3.4 V, respectively. Kröhnkite-type $Na_2Fe(SO_4)_2 \cdot 2H_2O$ was also introduced as a cathode for NIBs by Barpanda et al. and exhibited a reversible capacity of 70 mA h g^{-1} with a redox activity at 3.25 V.[180] While researchers have recently attempted to enhance the electrochemical properties of these hydrated sulfate compounds,[183,184] issues such as poor electrochemical performances and moisture sensitivity as well as low theoretical capacities below 100 mA h g^{-1} should be addressed.

Recently, Barpanda et al. reported a new alluaudite $Na_2Fe_3(SO_4)_3$ as a cathode material for NIBs.[108] The crystal structure is composed of edge-shared Fe_2O_{10} dimer units that are bridged together by SO_4 units by corner sharing, forming a 3D framework with a large Na diffusion channel along the c axis (see **Figure 8**a). The edge-sharing geometry between FeO_6 octahedra and electron-drawing $(SO_4)^{2-}$ units enables one of the highest Fe^{2+}/Fe^{3+} redox potential at 3.8 V vs Na^+/Na among all the Fe-based intercalation compounds, and the electrode delivers a reversible capacity exceeding 100 mA h g^{-1}, as observed in Figure 8b. The electrode could exhibit high power and cycle performances that originate from the small volume change (≈1.6%) during electrochemical cycling. Further investigations on the electrochemical mechanisms and Na diffusion kinetics of off-stoichiometric phases of $Na_{2+2x}Fe_{2-x}(SO_4)_3$ ($0 \le x \le 0.4$) were performed by the Yamada and Adam groups.[185,186] The Mn-based alluaudite $Na_{2+2x}Mn_{2-x}(SO_4)_3$ and solid-solution phase of $Na_{2.5}(Fe_{1-y}Mn_y)_{1.75}(SO_4)_3$ were also investigated as cathodes for NIBs.[187–189] However, these electrodes exhibited marginal electrochemical activities of Mn^{2+}/Mn^{3+} in Na-ion cells. Recent work introduced the new eldfellite-type $NaFe(SO_4)_2$; however, this electrode exhibited a low energy density with an average voltage of 3 V and specific capacity of 80 mA h g^{-1}.[182]

2.2.4. Pyrophosphates

Since Li metal pyrophosphate, $Li_2MP_2O_7$ (M = Fe, Mn, and Co), cathodes were first reported as promising cathodes for LIBs,[192–194] a series of Na analogues have been extensively studied as cathode materials for NIBs. The first electrochemically active pyrophosphate compound, $Na_2FeP_2O_7$, was introduced by Barpanda et al.[190] They reported that $Na_2FeP_2O_7$ adopts a crystal structure of triclinic *P1* with 3D Na channels and delivers a reversible capacity of 82 mA h g^{-1} with a redox potential of 3.0 V vs Na^+/Na (see Figure 8c). Four redox peaks are observed in the d*Q*/d*V* curves in the inset of Figure 8c, between 2.5V and 3.3V. Later work by Kim et al. revealed that $Na_2FeP_2O_7$ undergoes a single-phase reaction at approximately 2.5 V and a series of two-phase reactions in the voltage range of 3.0 to 3.25 V involving at least three intermediate phases.[195] Off-stoichiometric phases of $Na_{4-x}Fe_{2+x/2}(P_2O_7)_2$ ($2/3 \le x \le 7/8$), which are isostructural to *P1* $Na_2FeP_2O_7$, were also studied by Ha et al.[196] These electrodes exhibit similar electrochemical profiles as $Na_2FeP_2O_7$ but undergo a single-phase reaction upon de/sodiation processes. The high power and good cycle stability were attributed to the off-stoichiometric surface, which prevents the surface oxidation by moisture and CO_2. Recent works have mainly focused on the optimization of the electrochemical properties of $Na_2FeP_2O_7$ by applying carbon coatings and modifying the stoichiometry of the electrode composition.[101,197,198] A stable cycle stability over 1000 times with cycle retention of 91% was achieved by utilizing ionic liquids as electrolytes.[199] The low cost, high thermal stability, and promising electrochemical properties of a series of $Na_{4-x}Fe_{2+x/2}(P_2O_7)_2$ electrodes makes these materials viable competitors for NIB cathodes;[200] however, their low energy density remains a significant challenge.

In the continuous effort to enhance the energy density of pyrophosphate compounds utilizing the Mn^{2+}/Mn^{3+} redox reaction, a new polymorph of β-$Na_2MnP_2O_7$ was investigated as a cathode material for NIBs.[191,201] DFT calculations predicted that the redox potential of this new polymorph lies at approximately 3.65 V vs Na^+/Na, and galvanostatic charge/discharge measurements revealed that the electrode exhibits a reversible capacity approaching 80 mA h g^{-1} along with a Mn^{2+}/Mn^{3+} redox potential at 3.6 V, as shown in Figure 8d. The $Na_2MnP_2O_7$ electrode displayed good electrochemical activity with fast Na kinetics,[191,201,202] whereas the Li counterpart of $Li_2MnP_2O_7$ exhibits no electrochemical activity.[203] Park et al. demonstrated that the improved kinetics of $Na_2MnP_2O_7$ are attributable to the locally flexible accommodation of Jahn–Teller distortions supported by the corner-sharing crystal structure, which efficiently lower the activation barriers for electron conduction and phase boundary migration.[201] Nonetheless, the solid-solution phases of $Na_{2-x}(Fe_{1-y}Mn_y)P_2O_7$ ($0 \le y \le 1$) introduced by Barpanda et al. did not exhibit Mn^{2+}/Mn^{3+} redox activity in Na-ion cells.[204] Co-based orthorhombic $Na_2CoP_2O_7$ was also investigated as a

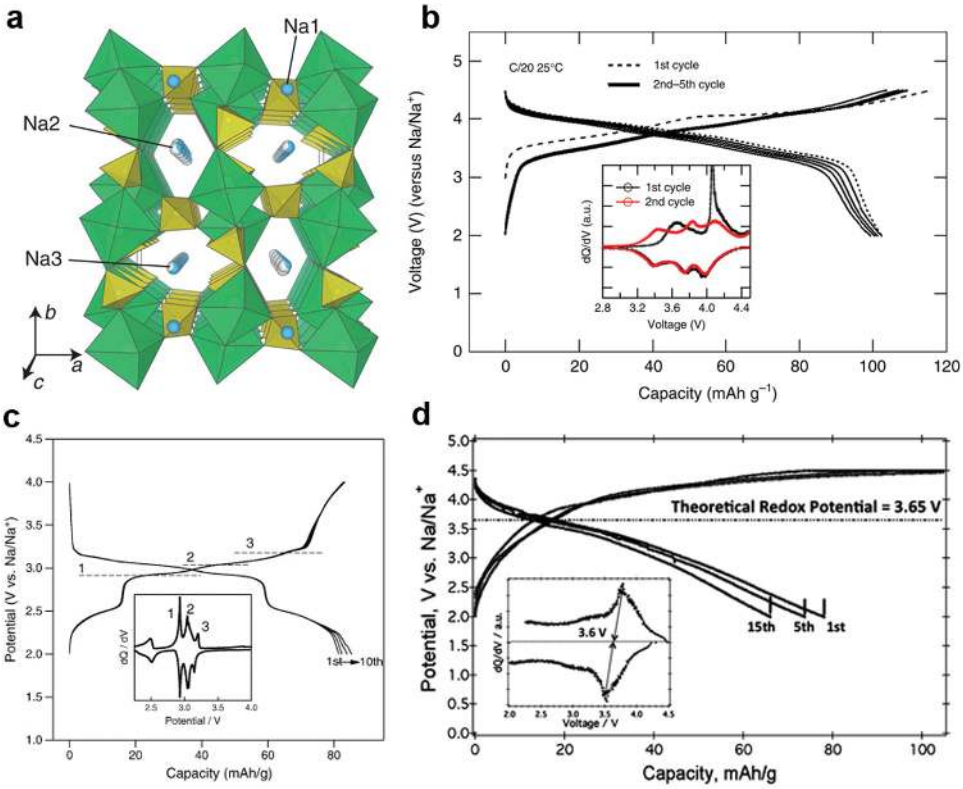

Figure 8. a) Structure representation of alluaudite $Na_2Fe_2(SO_4)_3$ along the *c*-axis. b) Galvanostatic charge/discharge profiles of $Na_2Fe_2(SO_4)_3$ at a current rate of C/20. d*Q*/d*V* curves are shown in the inset. Reproduced with permission.[108] Copyright 2014, Nature Publishing Group. c) Galvanostatic charge/discharge profiles of $Na_2FeP_2O_7$ at C/20. d*Q*/d*V* curves are shown in the inset. Reproduced with permission.[190] Copyright 2012, Elsevier. d) Galvanostatic charge/discharge profiles of $Na_2MnP_2O_7$ at C/20. d*Q*/d*V* curves are shown in the inset. Reproduced with permission.[191] Copyright 2013, Royal Society of Chemistry.

new layered-structured cathode for NIBs. The electrode delivers a reversible capacity approaching 80 mA h g^{-1} involving a redox reaction of Co^{2+}/Co^{3+} at 3.0 V vs Na^+/Na.

V-based pyrophosphate compounds were studied as high-voltage cathodes for NIBs.[205–207] Barpanda et al. first introduced tetragonal $Na_2(VO)P_2O_7$, which yields a reversible capacity of 80 mA h g^{-1} involving the V^{4+}/V^{5+} redox reaction at 3.8 V vs Na^+/Na.[205] More recently, Kim et al. reported a new V-based pyrophosphate compound, $Na_4V_3(P_2O_7)_4$, as a cathode for NIBs.[207] The electrode delivered a capacity of approximately 80 mA h g^{-1} at a current rate of C/10 with an average voltage of 4.13 V vs Na^+/Na. The electrode exhibited the highest V^{3+}/V^{4+} redox potential among all the V-based polyanionic compounds, which is attributed to the unique structural aspect of VO_6 octahedra sharing every corner with a P_2O_7 group, maximizing the inductive effect in the structure. Furthermore, the low volume change (≈1%) was confirmed during electrochemical operation, resulting in stable cycle stability over 600 cycles with 75% retention.

2.2.5. Mixed Polyanionic Compounds

Mixed Phosphates: An interesting approach to design an open framework structure by combining different polyanion groups such as $(PO_4)^{3-}$, $(P_2O_7)^{4-}$, and $(CO_3)^{2-}$ has introduced a new class of mixed polyanion electrode materials for NIBs. Kim et al. first reported a new Fe-based mixed phosphate compound, $Na_4Fe_3(PO_4)_2(P_2O_7)$, as a cathode for NIBs.[107] They synthesized the compound via a simple two-step solid-state method. The crystal framework was observed to be a pseudo-layered framework composed of infinite $[Fe_3P_2O_{13}]_\infty$ layers parallel to the b–c plane, as shown in **Figure 9**a. These layers are connected by P_2O_7 dimers along the a-axis, forming large 3D Na diffusion channels, which enables fast de/sodiation with low activation barriers. Respectable electrochemical properties were observed for the electrode with a reversible capacity of 113 mA h g^{-1} and stable cycle stability over 100 cycles.[208] The electrode operates via a solid-solution reaction and accompanies a volume change of less than 4%.[209] Nevertheless, the significant structural evolution during the last step of charge, which inhibits the full utilization of Na in the structure, and low redox potential of Fe^{2+}/Fe^{3+} (3.2 V vs Na^+/Na) remain challenges for its application for large-scale ESSs.

Recently, new Co- and Mn-based mixed phosphate compounds, $Na_4M_3(PO_4)_2(P_2O_7)$ (M = Co and Mn), which are isostructural with $Na_4Fe_3(PO_4)_2(P_2O_7)$, were reported as a high-voltage cathode for NIBs. Nose et al. discovered that $Na_4Co_3(PO_4)_2(P_2O_7)$ operates at the highest potential of 4.5 V vs Na^+/Na among all reported Na storage materials with a reversible capacity of 95 mA h g^{-1}.[214] This electrode displays high rate performances, where the reversible capacity of 80 mA h g^{-1} can be delivered at a current rate of 25C. They also evaluated the electrochemical properties of $Na_4Co_{2.4}Mn_{0.3}Ni_{0.3}(PO_4)_2P_2O_7$ and demonstrated that it exhibits an improved reversible capacity of 103 mA h g^{-1} based on the concurrent electrochemical activation of Mn^{2+}/Mn^{3+} and Ni^{2+}/Ni^{3+} redox couples.[215] More recently, Kim et al. reported $Na_4Mn_3(PO_4)_2(P_2O_7)$ as a cathode for NIBs.[210] This material exhibits a high Mn^{2+}/Mn^{3+} redox potential of 3.84 V vs Na^+/Na and a reversible capacity of 109 mA h g^{-1} at a rate of C/20, as shown in Figure 9b. $Na_4Mn_3(PO_4)_2(P_2O_7)$ displays a high power and energy density as well as stable cycle performances over 100 cycles in contrast to most other reported Mn-based electrodes, which suffered from Jahn–Teller distortion (Mn^{3+}) and exhibit poor electrochemical activity. DFT calculations indicate that this behavior results from 3D Na diffusion pathways with low activation barriers (0.20 eV) as well as the unique Jahn–Teller distortion of Mn^{3+} that occurs in this material, which opens up Na diffusion channels.[210,216]

A new V-based mixed-phosphate compound, $Na_7V_4(P_2O_7)_4(PO_4)$, was introduced as a NIB cathode. Lim et al. reported that the $Na_7V_4(P_2O_7)_4(PO_4)$ electrode exhibits a single well-defined voltage plateau at 3.88 V vs Na^+/Na with a reversible capacity of 73 mA h g^{-1}, as shown in Figure 9c.[211] A close inspection of the dQ/dV and GITT measurements reveals two separate redox peaks in a very close voltage range at 3.88 and 3.92 V, which is attributed to the intermediate phase between the end phases of charge/discharge. They claimed that the intermediate phase efficiently buffers the lattice mismatch between two end members and yields better Na kinetics, resulting in stable cycle performances over 1000 cycles with a retention of 78%. Recent work by Deng et al. revealed that a 1D nanostructured $Na_7V_4(P_2O_7)_4(PO_4)$ cathode can deliver 80% of the theoretical capacity at 10C rate and 95% of the initial capacity after 200 cycles.[217]

Carbonophosphates: A combination of polyanion groups of $(CO_3)^{2-}$ and $(PO_4)^{3-}$ resulted in the discovery of a new family of inorganic compounds, carbonophosphates, for NIBs. Hautier et al. first proposed that ion-exchanged $Li_3M(CO_3)(PO_4)$ from $Na_3M(CO_3)(PO_4)$ (M = Fe, Mn, Co, Ni, etc.) as a potential cathode for LIBs based on high-throughput ab initio computations, and Chen et al. successfully synthesized stable phases of $Na_3M(CO_3)(PO_4)$ (M = Mg, Fe, Mn, Co, Ni, and Cu) predicted from the previous calculations.[218,219] Later, Chen et al. reported $Na_3Mn(CO_3)(PO_4)$ as a new 3.7-V-class intercalation cathode material for NIBs, delivering a high discharge capacity (≈125 mA h g^{-1}) and specific energy (374 Wh kg^{-1}).[69] They revealed that the electrode adopts a single-phase reaction upon Na de/intercalation, and more than one Na per Mn atom can be deintercalated from the structure, indicating a two-electron intercalation reaction with Mn^{2+}/Mn^{3+} and Mn^{3+}/Mn^{4+} redox couples. Later work by Huang et al. revealed that a similar multi-electron reaction of Fe^{2+}/Fe^{3+} and Fe^{3+}/Fe^{4+} can occur in $Na_3Fe(CO_3)(PO_4)$ nanoplates within the voltage range of 2.0 to 4.55 V.[220] The electrode delivers approximately 120 mA h g^{-1} with an average voltage of 2.7 V. Although Fe- and Mn-based carbonophosphate electrodes exhibit promising electrochemical activities in Na-ion cells, the slow Na kinetics in $Na_3Mn(CO_3)(PO_4)$ and low energy density still hinder their application.

2.2.6. Other Polyanionic Compounds

Various types of polyanionic compounds were evaluated as cathodes for NIBs. The Na de/intercalation behavior in $(MoO_2)_2P_2O_7$ was examined by Uebou et al.[221] They revealed that approximately 3.1 Na, which corresponds to a capacity

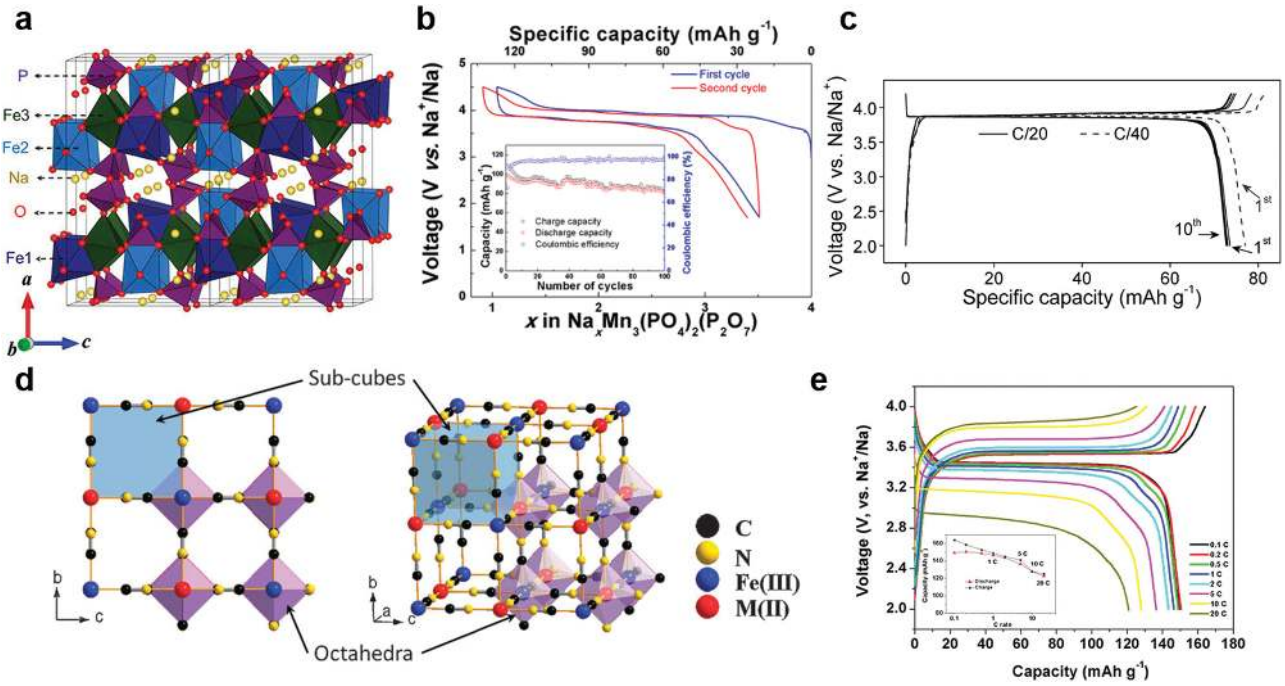

Figure 9. a) Crystal structure of $Na_4Fe_3(PO_4)_2(P_2O_7)$. Reproduced with permission.[107] Copyright 2012, American Chemical Society. b) Galvanostatic charge/discharge profiles of $Na_4Mn_3(PO_4)_2(P_2O_7)$ at a current rate of C/20. The inset shows the cycle performances of the electrode at C/20. Reproduced with permission.[210] Copyright 2015, Royal Society of Chemistry. c) Galvanostatic charge/discharge profiles of $Na_7V_4(P_2O_7)_4PO_4$ at a current rate of C/40 and C/20. Reproduced with permission.[211] Copyright 2014, National Academy of Sciences. d) Schematic representation of PBAs. Reproduced with permission.[212] Copyright 2012, Royal Society of Chemistry. e) Charge/discharge profiles of dehydrated $Na_{1.9}MnFe(CN)_6{\cdot}0.3H_2O$ at various C-rates (0.1C, 0.2C, 0.5C, 1C, 2C, 5C, 10C, and 20 C). Reproduced with permission.[213] Copyright 2015, American Chemical Society.

of 190 mA h g^{-1}, can intercalate into the structure with a concurrent crystalline-to-amorphous phase transformation. Amorphous $NaFe_3(SO_4)_2(OH)_6$ was also examined as a Na intercalation host.[222] This material delivers a reversible capacity of 120 mA h g^{-1} with an average voltage of 2.72 V vs Na^+/Na in Na-ion cells. Recently, the Na de/intercalation behavior in Li_2FeSiO_4 was examined by Zhang et al.[223] They revealed that electrochemical delithiation and subsequent sodiation of the electrode delivers a discharge capacity of 330 mA h g^{-1} at a current density of 10 mA g^{-1}.

Liu et al. reported cubic $Na_3TiP_3O_9N$ as a cathode for NIBs.[224] Approximately 60 mA h g^{-1} was delivered from the electrode with an average voltage of 2.7 V vs Na^+/Na. Experimental and calculation studies indicate that the electrode operation involves a small volume change of 0.5%. Fe-based hydrated polyanionic compounds, including $K_4Na_2[Fe(C_2O_4)_2]_3{\cdot}2H_2O$, $Li_{0.8}Fe(H_2O)_2[BP_2O_8]{\cdot}H_2O$, and $NaFe(H_2O)_2[BP_2O_8]{\cdot}H_2O$, were also reported as NIB cathode materials.[225,226] These electrodes operate via Fe^{2+}/Fe^{3+} redox reaction with an average voltage of approximately 3.0 V but deliver a comparably small capacity below 60 mA h g^{-1}. Recently, Na-containing polyanionic compounds such as $Na_4NiP_2O_7F_2$ and $NaFe(PO_3)_3$ were reported as potential cathodes for NIBs.[227,228] However, these electrodes display insufficient electrochemical activities in Na-ion cells.

2.3. Prussian Blue Analogues

Prussian blue analogues (PBAs) have been investigated as alternative cathode materials to the conventional layered and polyanionic compounds in recent years because of their large alkali-ion channels, which enable fast Na de/intercalation without lattice distortion as well as low element cost, toxicity, and easy synthesis at room temperature.[212,213,229–232] The general formula of PBAs can be described as $A_xP[R(CN)_6]_{1-\gamma}{\cdot}\square_\gamma{\cdot}mH_2O$ (A: alkali metal ion; P: N-coordinated transition metal ion; R: C-coordinated transition metal ion; □: $[R(CN)_6]$ vacancy; $0 \le x \le 2$; $0 \le \gamma \le 1$). PBAs generally adopt a face-centered cubic structure with a space group of *Fm3m*, where transition metal ions are connected by (CN) ligands forming large cage-like interstitial A sites (see Figure 9d). Most of the earlier studies focused on the electrochemical activity of PBAs in aqueous media,[233–235] however, PBAs have attracted significant attention as electrodes for non-aqueous NIBs in the past three years. In this section, we focus on a review of electrode materials for non-aqueous NIBs.

$KM^{II}Fe^{III}(CN)_6$ (M = Mn, Fe, Co, Ni, and Zn) compounds were first examined as cathodes for non-aqueous NIBs.[212] The $KM^{II}Fe^{III}(CN)_6$ (M = Mn, Co, Ni, and Zn) electrodes operate via the Fe^{3+}/Fe^{2+} redox couple with a single voltage plateau at 3.0 V vs Na^+/Na and deliver a reversible capacity of approximately 60 mA h g^{-1}. The $KFe_2(CN)_6$ electrode delivers a reversible capacity of 100 mA h g^{-1} with two potential plateaus at 3.5 and 2.6 V vs Na^+/Na, which are attributed to the high-spin Fe^{3+}/Fe^{2+} redox couple bonded to N and the low-spin Fe^{3+}/Fe^{2+} redox couple bonded to C, respectively. To enhance the electrochemical properties of iron hexacyanoferrate ($AFe_2(CN)_6$ (A = K or Na; $0 \le A \le 1$)), later works introduced various approaches such as carbon coating, nano-sizing, and crystallinity improvements.

Yu et al. reported that nanosized $NaFe_2(CN)_6$ exhibits a high capacity of 118 mA h g^{-1} at a current rate of 5 mA g^{-1},[236] and Wu et al. showed that highly crystalline nanoparticle $Fe_2(CN)_6$ exhibits stable cycle performances over 500 cycles.[237] In addition, the highly crystalline $NaFe_2(CN)_6$/graphene composite delivered a discharge capacity of 150 mA h g^{-1} with an energy density of 280 Wh kg^{-1}.[238] The family of alkali-ion-deficient cubic $AM^{II}Fe^{III}(CN)_6$ (A = Na or K) compounds requires a presodiation process to be combined with conventional Na-free anodes; otherwise, the electrode operation undergoes only one electron transfer with Fe^{3+}/Fe^{2+} redox couples, resulting in a low capacity below 70 mA h g^{-1}.[239–243]

The Na-rich compound, $Na_{1.72}MnFe(CN)_6$, was successfully synthesized by Wang et al.[229] This electrode delivers a capacity of 130 mA h g^{-1} with a high average voltage of 3.4 V involving Mn^{2+}/Mn^{3+} and Fe^{2+}/Fe^{3+} redox reactions. The high Na concentration in the structure induces a structural transition from cubic to rhombohedral symmetry with cooperative Na displacement along the[111] direction. This phase transition was determined to be reversible upon electrochemical cycling. A similar result was also reported for $Na_{2-x}Fe_2(CN)_6$. You et al. showed that $Na_{1.63}Fe_2(CN)_6$ adopts a rhombohedral structure and exhibits a reversible capacity of 150 mA h g^{-1} with stable cycle performances over 200 cycles (90% retention).[241] This electrode also displays a reversible rhombohedral-to-cubic transition during electrochemical cycling. Multicomponent Na-rich PBAs such as $Na_2Ni_xCo_{1-x}Fe(CN)_6$ and $Na_{1.76}Ni_{0.12}Mn_{0.88}[Fe(CN)_6]_{0.98}$ were also introduced as cathode materials for NIBs.[183,244]

The facile synthesis of PBAs at room temperature by the co-precipitation method generally yields low-quality materials, where a large amount of water molecules occupies $[Fe(CN)_6]$ vacancies.[245] In addition, most of the PBA electrodes reported to date contain at least 10 wt% of crystal water in the crystal structure (m in $A_xP[R(CN)_6]_{1-y}\cdot\square_y\cdot mH_2O$; $1 \le m \le 3$).[212,229,236] The water molecules in the PBA structure decompose during electrochemical cycling and lead to deterioration of the cycle performances. To enhance the cycle stability, You et al. synthesized a high-quality Prussian blue nanocrystal of $Na_{0.61}Fe[Fe(CN)_6]_{0.94}$ as a cathode for NIBs.[246] They efficiently reduced the water content in the interstitial sites of the $[Fe(CN)_6]$ using the single Fe-source method, resulting in a high capacity of 170 mA h g^{-1} and the cycle stability for 150 cycles without capacity loss. However, TGA/DTA analyses revealed that 15 wt% crystal water remained in the PBA electrode. Recently, Song et al. reported a dehydrated $Na_{2-\delta}MnFe(CN)_6\cdot mH_2O$ ($\delta \approx 0.1$; $m \approx 0.3$) phase, which exhibits superior electrochemical performances compared with other PBA electrodes for NIBs.[213] The electrode delivered a reversible capacity of 150 mA h g^{-1} with an average voltage of 3.5 V and exhibited 75% capacity retention after 500 cycles. Superior rate performance was obtained from the electrode, where a capacity of 120 mA h g^{-1} was delivered at 20C (see Figure 9e). They revealed that the dehydrated phase of $Na_{1.9}MnFe(CN)_6\cdot 0.3H_2O$ adopts rhombohedral symmetry, and a reversible phase transition occurs from rhombohedral to tetragonal symmetry during electrochemical cycling. In addition, dehydrated $Na_{1.92}Fe_2(CN)_6\cdot 0.08H_2O$ with rhombohedral structure exhibits excellent electrochemical performances in Na-ion cells.[231] A capacity of approximately 160 mA h g^{-1} was delivered with an average voltage of 3.2 V vs Na^+/Na, which corresponds to an energy density of 490 Wh kg^{-1}, and 80% of the initial capacity was retained after 750 cycles. High-quality $Na_2CoFe(CN)_6$ displayed promising electrochemical properties in Na-ion cells as well.[247]

Other types of PBAs including $Na_{1.61}Zn_3[Fe^{II}(CN)_6]_2\cdot 3H_2O$, $Na_4Fe(CN)_6$, and $Na_{1.96}Mn^{II}[Mn^{II}(CN)_6]_{0.99}\cdot 2H_2O$ were also reported as NIB cathodes.[230,248,249] $Na_{1.61}Zn_3[Fe(CN)_6]_2\cdot 3H_2O$ exhibited a electrochemical activity at 3.5 V vs Na^+/Na involving a Fe^{2+}/Fe^{3+} redox reaction with a reversible capacity of 56 mA h g^{-1}.[248] The $Na_4Fe(CN)_6$/C nanocomposite displayed a redox capacity of 90 mA h g^{-1} at a potential of 3.4 V with cycle stability up to 500 cycles and 88% capacity retention.[249] A high-quality Mn hexacyanomanganate compound, $Na_2Mn^{II}[Mn^{II}(CN)_6]\cdot 2H_2O$, was introduced by Lee et al.[230] They showed that this material has a monoclinic structure composed of nonlinear Mn-N≡C-Mn bonds. A surprisingly high reversible capacity of 209 mA h g^{-1} was obtained, which far exceeds its theoretical capacity of 170 mA h g^{-1} based on the Mn^{2+}/Mn^{3+} redox reaction. They explained that the additional capacity arises from the Mn^{2+}/Mn^{1+} redox reaction, forming the stable phase of $Na_3Mn^{II}[Mn^{I}(CN)_6]$.

2.4. Organic Cathodes

Organic-based cathode materials are emerging candidates as alternatives to conventional inorganic electrode materials because of their abundance, safety, environmental friendliness, and high theoretical capacity.[250–253] In this section, we briefly introduce recent investigations on organic cathodes for NIBs.

Disodium rhodizonate ($Na_2C_6O_6$), which is an analogue of the Li version (dilithium rhodizonate),[254] was reported as a Na organic cathode by Chihara et al.[255] $Na_2C_6O_6$ has a layered structure and exhibits n-type properties with conjugated carbonyl groups. They showed that $Na_2C_6O_6$ cathode exhibits a reversible capacity of 170 mA h g^{-1} with a good cycle performance at an average working voltage of 2.18 V vs Na^+/Na; however, the origin of the much lower specific capacity compared with its Li analogue remains unclear.[256–258]

A well-known organic pigment 3, 4, 9, 10-perylene-tetracarboxylicacid-dianhydride (PTCDA), which consists of an aromatic core and two anhydride groups ($C_{24}H_8O_6$), and its derivatives were also investigated as potential cathodes for NIBs.[259,260] Luo et al. measured the electrochemical properties using commercially available PTCDA as a Na organic cathode.[259] The commercial PTCDA delivers a capacity of 145 mA h g^{-1} in the voltage range of 1–3 V vs Na^+/Na, respectable rate performance of 91 mA h g^{-1} at a current density of 1000 mA g^{-1}, and cycle stability over 200 times. Imide groups, which are a type of carbonyl groups with anhydrides, were also recently investigated as Na organic cathodes.[261–263] A 3, 4, 9, 10-perylene-bis(dicarboximide) (PTCDI), which belongs to the perylene diimide group, was reported.[262] The electrode is insoluble in organic electrolytes and has multiple Na ion binding sites. It delivers a reversible capacity of 140 mA h g^{-1} with two Na ion insertions/extractions per molecular unit and exhibits good cyclability with 90% capacity retention over 300 cycles. Similarly, anthraquinone-based polyimide was investigated using a polymerization reaction with pyromellitic dianhydride

(PMDA) and 1, 4, 5, 8-naphthalenetetracarboxylic dianhydride (NTCDA).[263] In the work, two types of polyimides named PI1 and PI2 were presented, which delivered reversible capacities of 165 and 192 mA h g^{-1}, respectively. Despite recent progress on organic cathodes for NIBs, the operation voltage remains far below that of inorganic materials.

Kim et al. very recently proposed a halogen-substituted benzoquinone derivative as a high-voltage cathode for NIBs.[264] They demonstrated the effect of substitution on the redox potential using theoretical DFT calculations and reported that the Na storage potential noticeably increased depending on the substituted halogen atoms. They selected a $C_6Cl_4O_2$ cathode by rational design using theoretical and experimental characterizations, which delivered a reversible capacity of 161 mA h g^{-1} at an average voltage of ≈2.72 V vs Na^+/Na, which is the highest among benzoquinone derivative electrodes.

Zhao et al. reported an aniline/o-nitroaniline copolymer (P(AN-NA)) as a p-type organic cathode.[265] They verified that aniline/o-nitroaniline reacts with anions (PF_6^-), and the cathode exhibits a high redox capacity and stable cyclability. The copolymer electrode exhibits a capacity of 180 mA h g^{-1} at an average potential of ≈3.2 V (vs Na^+/Na) and retains cycle stability after 50 cycles, delivering 173 mA h g^{-1}. Similarly, Deng et al. proposed polytriphenylamine (PTPAn) as a p-type organic cathode for NIBs.[266] This electrode also undergoes a cathodic reversible reaction with p-doping/de-doping of anions (PF_6^-) in the electrolyte, providing a reversible capacity of 96 mA h g^{-1} at an voltage of ≈3.6 V (vs Na^+/Na). Nevertheless, the p-type organic electrodes are less practical because a certain amount of electrolytes participates in the redox reaction, thus, require excess electrolyte in battery configurations. In 2013, Sakaushi et al. reported a bipolar porous honeycomb and polymeric framework composed of benzene rings and a triazine ring in a two-dimensional (2D) structure.[267] The bipolar porous organic electrode (BPOE) exhibited the electrochemical performance with a specific energy density of ≈500 Wh kg^{-1} and specific power density of 10 kW kg^{-1}. More than 80% of its initial capacity was retained after 7,000 cycles in the half-cell configuration.

3. Anode Materials

3.1. Carbon Materials

Carbon materials have been most widely studied as potential anodes for NIBs because of their low cost and environmental benignness as well as the excellent electrochemical stability. For LIBs, graphite has been utilized as a standard anode exhibiting a low operating voltage and high specific capacity based on reversible Li de/intercalation in the graphite structure. Recently, it was also reported that K ions, which have much larger ionic radii (≈1.5 Å) than Li ions (≈0.76 Å), can be reversibly intercalated into graphite in electrochemical cells. Naturally, there have been efforts to utilize graphite as a Na intercalation host.[268,269] However, all the early works consistently resulted in limited reversible capacities of ≈12 mA h g^{-1}, which indicates the failure of forming a stage 1 graphite intercalation compound (GIC), unlike for Li (LiC_6) and K (KC_8). The thermodynamic instability of stage 1 Na-GIC formation has also been observed in theoretical calculations with various structure models (**Figure 10**a).[270–273] For instance, in a comparative study on alkali metal (Li, Na, and K) intercalation into graphite by Okamoto,[272] the formation of LiC_6 and KC_8 showed a positive intercalation potential, whereas the formation of either NaC_6 and NaC_8 was found to be thermodynamically unfavorable. Although the underlying reason of this phenomenon remains unclear to date, the reason for unstable stage 1 Na-GIC is attributed to (i) the high redox potential of Na^+/Na, resulting in the precipitation of metallic Na before Na intercalation;[272] (ii) the large elongation of C–C bond lengths in Na-GICs;[271] and (iii) the low binding energy between the carbon and Na layer.[270] As the utilization of pristine graphite as an anode for NIBs failed, non-graphitic carbon materials (i.e., hard carbon, soft carbon, and amorphous carbon) have been extensively investigated as alternatives. In this section, we discuss the electrochemical properties and mechanistic studies of non-graphitic carbon materials followed by recent investigations that utilize pristine graphite as an active anode material using abnormal Na–solvent co-intercalation.

3.1.1. Non-Graphitic Carbon

Various non-graphitic carbon materials have been experimentally studied as anode materials for NIBs.[138,269,277–324] The storage of Na in carbon materials such as hard carbon, amorphous carbon, defected graphene, and functionalized graphite has been observed to be thermodynamically feasible.[325,326,274,276] In the early works by Doeff et al., they demonstrated that the extent of Na intercalation in carbon materials varies depending on the carbon structure; NaC_{70}, NaC_{30}, and NaC_{15} were formed for graphite, petroleum coke, and Shawinigan black, respectively.[277] The inserted Na ions were also reversibly extracted from the carbon materials. Later, Stevens and Dahn reported that hard carbon (pyrolyzed glucose) can provide a high specific capacity (≈300 mA h g^{-1}), close to that of Li intercalation in graphite, which made hard carbon a promising anode for NIBs.[281] They also proposed a "card-house" model as the Na storage mechanism, in which the Na storage is described as two distinct mechanisms: (i) Na ion intercalation between graphene sheets in the sloping-voltage region and (ii) Na ions filling in the pores between nano-graphitic domains in the plateau region. Since the model was suggested, many researchers have interpreted the electrochemical properties of hard carbon anodes according to the "card-house" model.[269,283–288,299,303,327,328] Nevertheless, there is still a lack of understanding about the Na insertion mechanism in various types of carbon materials, which can explain the observed Na storage potential and capacities.

Recent works by Yun et al. and Bommier et al. attempted to verify the correlation between the atomic structure and Na storage properties of hard carbon.[274,275] Yun et al. fabricated 2D pyroprotein-based carbon nanostructures from a self-assembled silk protein nanoplate that were used as a carbon platform to investigate the Na-ion storage behaviors for various local carbon orderings. Figure 10b presents the typical discharge profiles of carbon materials with different degrees of crystalline ordering. The highly porous and defective carbon structure (A-CNP-800 in Figure 10b) displayed mainly physic/chemisorption-based

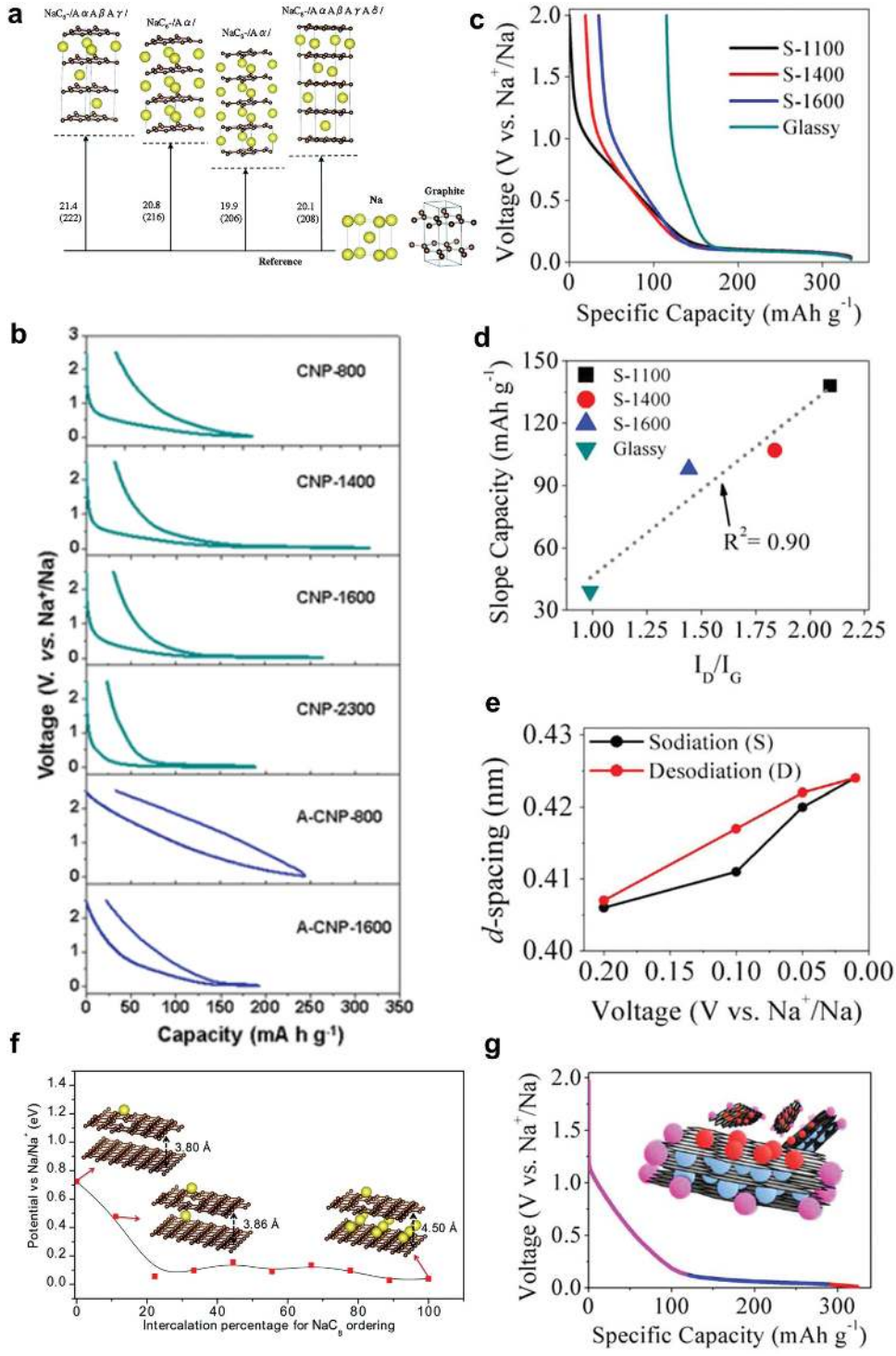

Figure 10. a) Schematic of the enthalpy of formation energy in kJ mol^{-1} (meV f.u.$^{-1}$) of the Na–graphite compounds relative to the reference state of graphite and Na metal. Reproduced with permission.[270] Copyright 2014, Royal Society of Chemistry. b) Discharge profiles of pyroprotein-based carbon nanoplates with different degree of crystalline ordering. Reproduced with permission.[274] Copyright 2015, Wiley-VCH. c) Typical discharge profiles of hard carbons. d) Plot of the sloping capacity vs I_D/I_G ratio. e) Plot of vs*d*-spacing vs voltage. Reproduced with permission.[275] Copyright 2015, American Chemical Society. f) Calculated Na storage potential in disordered carbon. Reproduced with permission.[276] Copyright 2015, Royal Society of Chemistry. g) Schematic of proposed Na storage mechanism. Reproduced with permission.[275] Copyright 2015, American Chemical Society.

Na-ion storage, whereas CNP-800 with numerous pseudographitic crystallites exhibited mixed chemisorption- and insertion-based Na storage below 0.7 V (vs Na/Na$^+$), enabling Na-ion insertion between the graphene layers. The carbon material with a more ordered graphitic structure and nanopores (CNP-2300) showed evidence of the nanoclustering of Na metal.

Bommier et al. also altered the atomic structure of sucrose-derived hard carbon by controlling the annealing temperature. Figure 10c presents typical discharge profiles of hard carbon anodes, where the capacity in the slope region proportionally increases as the defect concentration increases (Figure 10d). This behavior indicates that the number of defect sites in hard carbon is strongly related to the Na storage capacity in the slope-voltage region. They also confirmed that the *d*-spacing between graphene layers is reversibly expanded and contracted upon the de/sodiation based on ex situ XRD analysis, which is indicative of Na intercalation in the hard carbon lattice in the low-voltage plateau region (Figure 10e).[287,302,322] The theoretical study performed by Tsai et al. in Figure 10f suggested that the slope-voltage region is attributable to Na adsorption on the defective carbon surface, and the plateau region is responsible for the Na intercalation in the hard carbon lattice.[276] As a result, the Na storage mechanism can be classified as (i) Na adsorption at defective sites in the slope-voltage region, (ii) Na intercalation in the hard carbon lattice, and (iii) Na-atom adsorption at the pore surface in the plateau region (Figure 10g). Nevertheless, there remains debate concerning the Na storage mechanism, especially in the low-voltage plateau region. For example, Zhang et al. claimed that the mesopore filling is responsible for the low-voltage plateau region and that the Na intercalation or Na plating does not occur at the low-voltage plateau at ≈0.1 V vs Na^+/Na.[279] In addition, an NMR study indicated that Na does not form metallic clusters in nanopores.[301] However, Yun et al. reported that Na metal nanoclusters were formed in the low-voltage plateau region, which was confirmed by ex situ X-ray photoelectron spectroscopy (XPS) and TEM analysis.[276] Therefore, further studies should be conducted to understand the correlation between the microstructures and Na storage properties, which can provide insight into developing high-performance hard carbon anodes. Meanwhile, heteroatom doped-carbon materials have been investigated to improve Na storage properties.[289,294,329–332] For example, Qie et al. investigated sulfur doped carbon as an anode for NIBs.[331] The carbon anode with high level of sulfur atoms provides high specific capacity of ≈400 mA h g^{-1} at 100 mA g^{-1} and delivers cycle stability up to 700 cycles at 500 mA g^{-1}. The improvement in Na storage properties by heteroatom doping was attributed to the enlarged interlayer distance and disordered structure, facilitating the diffusion of the large Na ions and accommodating large volume change during charge/discharge processes. Nevertheless, the large irreversible capacity in the initial discharge is still problematic for its practical utilization.

3.1.2. Graphite

Jache et al. demonstrated that graphite can allow Na intercalation in its galleries in electrochemical cells using ether-based electrolytes.[333] In their work, the graphite anode could provide a reversible capacity of ≈100 mA h g^{-1} and delivered a capacity retention up to 1000 cycles (see **Figure 11**a,b). Kim et al. revealed the precise Na storage mechanism in graphite for the first time.[334,335] They monitored the structural evolution of graphite during de/sodiation using synchrotron-based XRD patterns in operando (Figure 11c). The graphite structure successively transformed into multiple new phases during sodiation, and the structure of the pristine state was completely recovered after charge. It was observed that the repeated distance successively changes by ≈3.4 Å among each phase, indicating a staging phenomenon, and finally, the repeated distance becomes 11.62 Å, which is much larger than stage 1 Li-GIC (≈3.7 Å).[336] It was verified that the graphite significantly expands along the *c*-axis (≈350%) after sodiation by monitoring the expansion of graphite along the *c*-axis (Figure 11d,e), which agreed with a stage 1 compound. The researchers further confirmed that Na ions are co-intercalated in graphite galleries with ether solvent molecules with a composition of Na–ether solvent–C_{21} by monitoring the weight change during de/sodiation combined with Fourier-transform infrared (FTIR) spectroscopy and energy-dispersive X-ray spectroscopy (EDS) analyses. In addition, the structure of the Na–ether solvent co-intercalated graphite compound was proposed based on experimental and theoretical studies (Figure 11f), in which doubly stacked Na–ether solvent complexes are positioned at one-third and two-thirds of the height of the graphite galleries. Nevertheless, it remains unclear why this unique co-intercalation phenomenon is observed only in specific solvents (linear ether solvents). Although Kim et al. proposed a possible explanation that the linear ether solvent molecules can strongly bind Na ions because of the enhanced affinity between solvents and Na ions due to the chelate effect,[335] further experimental and theoretical studies are required.

3.2. Metal Oxides

Metal oxides have also been intensively studied as potential anodes for NIBs. Among various candidates as host materials for Na intercalation, Ti-based oxide compounds have been most widely studied because of their low operation voltage as well as low cost and environmental benignness. The conversion reaction compounds based on metal oxides have also recently attracted much attention because of their high specific capacity utilizing more than one redox reaction per transition metal. In this section, we discuss the electrochemical properties of metal oxide anode materials based on both intercalation and conversion reactions.

3.2.1. Intercalation-Based Materials

TiO_2: The application of TiO_2 anode to NIBs was first investigated by Xiong et al. in 2011.[337] They fabricated amorphous TiO_2 nanotubes for use as anodes in the voltage range between 0.9 and 2.5 V vs Na^+/Na. This work attracted the interest of many researchers in TiO_2 materials; as a result, TiO_2 anodes with various polymorphs (amorphous, anatase, rutile, and bronze) were investigated.[325,338–358] Kim et al. demonstrated that the reversible capacity considerably increases as the discharge cut-off voltage decreases (**Figure 12**a).[343] When the discharge cut-off voltage was 1.0 V vs Na^+/Na, the reversible capacity was limited to ≈8 mA h g^{-1}. However, the reversible capacity became ≈193 mA h g^{-1} when the discharge cut-off voltage decreased to 0.01 V vs Na^+/Na with slope voltage profiles. They argued that the irreversible capacity at relatively high

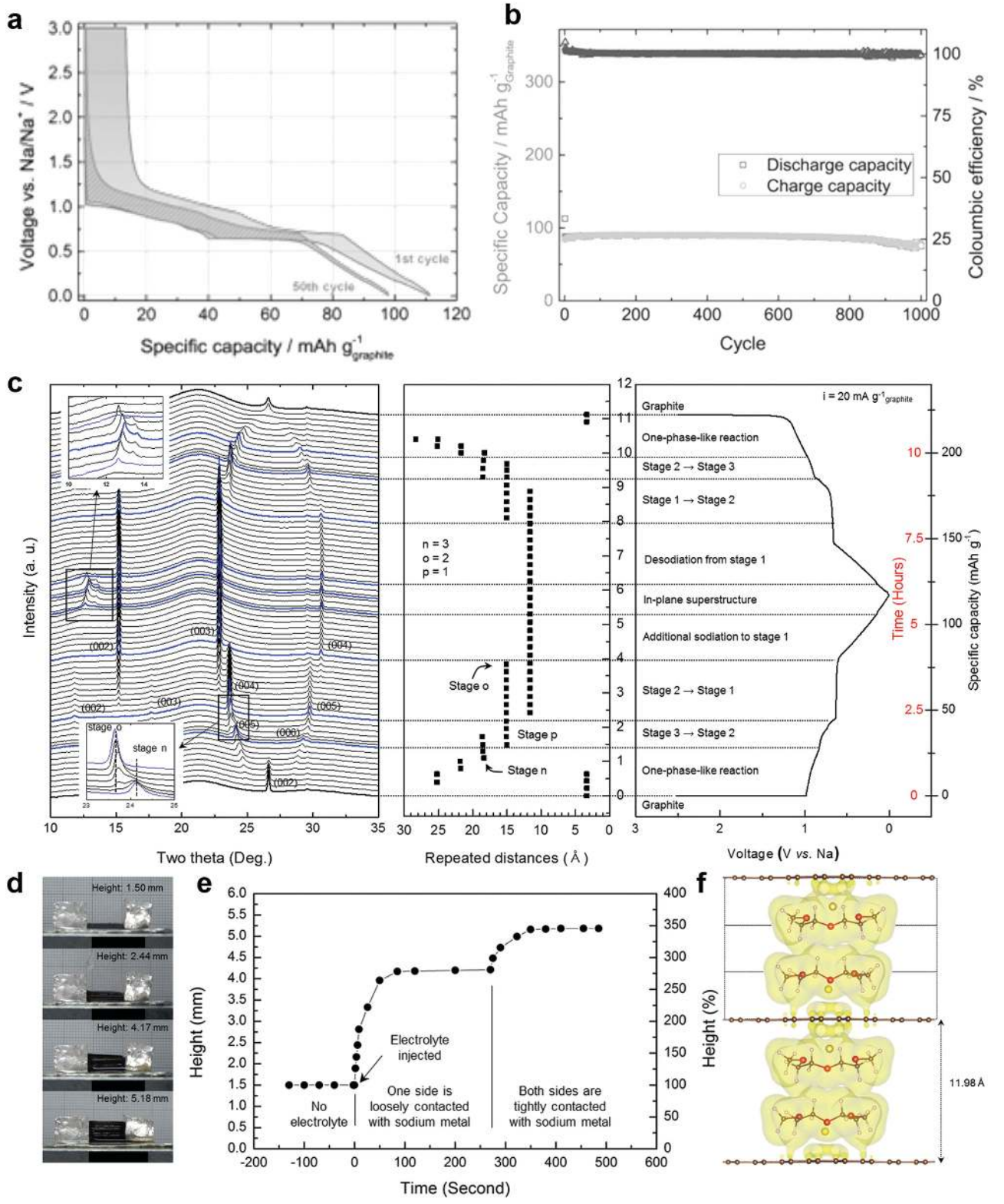

Figure 11. a) Typical charge/discharge profiles and b) cycle stability of graphite anode in ether-based electrolytes. Reproduced with permission.[333] Copyright 2014, Wiley-VCH. c) In operando synchrotron XRD analysis of graphite during sodiation and desodiation. d) Real-time snapshots of graphite under direct contact with Na metal after exposure to 1 M $NaPF_6$ in DEGDME solution. e) Height change of graphite during Na intercalation process. f) Proposed structure of Na-DEGDME co-intercalated graphite. Reproduced with permission.[335] Copyright 2015, Royal Society of Chemistry.

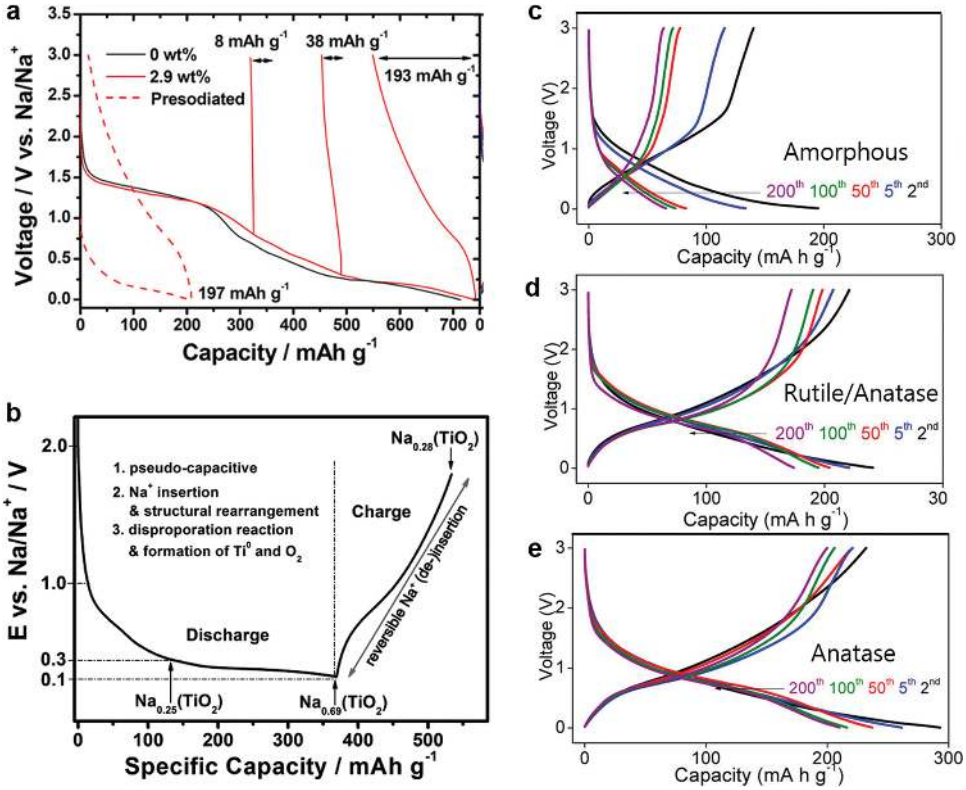

Figure 12. a) Charge/discharge profiles of anatase TiO_2 nanorods with different cutoff voltages. Reproduced with permission.[343] Copyright 2014, American Chemical Society. b) Schematic of the Na storage mechanism in anatase TiO_2 anodes. Reproduced with permission.[347] Copyright 2015, Wiley-VCH. Charge/discharge profiles of c) amorphous, d) rutile/anatase composite, and e) anatase TiO_2 anodes in Na cells. Reproduced with permission.[348] Copyright 2015, American Chemical Society.

voltages is attributable to side reactions with the electrolyte, such as decomposition of the electrolyte and solid-electrolyte interphase (SEI) formation. They also suggested that the Na ions are reversibly de/intercalated in the anatase TiO_2 lattice via the redox activity of Ti^{4+}/Ti^{3+} during charge/discharge. The oxidation state of Ti in the TiO_2 reduces to 3+ after discharge and is then recovered to 4+ after charge, indicative of the reversible redox reaction of Ti^{3+}/Ti^{4+}. In contrast, Gonzalez et al. reported that the lattice of anatase TiO_2 is unchanged even after full discharge up to 0 V vs Na^+/Na.[359] They suggested that Na ions are stored in anatase TiO_2 through pseudo-capacitive reactions.

Recently, Passerini's group conducted more detailed investigations to understand the Na storage mechanism in commercially available TiO_2 nanoparticles using in situ XRD and ex situ XPS.[347] At the initial discharge, the XRD lattice of anatase TiO_2 was slightly shifted to lower angles, indicative of a continuous expansion of the anatase lattice. However, the XRD peaks related to the anatase phase vanished after further discharge below 0.3 V vs Na^+/Na. The XRD peaks were not recovered after the charge process, indicating rearrangement of the TiO_2 anode material to an amorphous structure upon cycling. Based on additional ex situ XPS, scanning electron microscopy (SEM), and Raman analyses, they showed that Na insertion in TiO_2 reduces the oxidation state of Ti^{4+} to Ti^{3+} and partially generates Ti^0 with NaO_2 (irreversible conversion reaction). Based on the investigation on the Ti^{3+}:Ti^{4+} ratio, they determined the amount of the charge that is reversibly stored in the TiO_2. After discharge, the ratio became approximately 2.23, corresponding to 0.69 Na per TiO_2. Upon charge, the ratio decreased to 0.35, which indicates that 0.28 Na per TiO_2 remains in the structure. They also discovered that the reduction of TiO_2 to metallic Ti along with the structural rearrangement is accompanied by O_2 evolution based on in situ gas chromatography and mass spectrometry. It was concluded that Na insertion occurs in TiO_2 through (i) pseudo-capacitive reactions during the initial discharge process, followed by (ii) structural rearrangement, and finally (iii) a disproportionation reaction and formation of Ti^0 and O_2 during further discharge. Then, (iv) reversible Na de/insertion occurs in $Na_x(TiO_2)$ ($0.28 \leq x \leq 0.69$), as illustrated in Figure 12b.

Su et al. conducted a comparative study on the Na storage properties of TiO_2 nanospheres with different crystal structures.[348] They prepared amorphous TiO_2@C nanospheres using a template method and then sintered the materials under different conditions to form anatase and rutile TiO_2 phases. The three different types of TiO_2 materials were characterized as anodes for NIBs (Figure 12c–e). Among them, amorphous TiO_2 provides the lowest specific capacity of ≈196 mA h g^{-1}, which fades rapidly to ≈70 mA h g^{-1} after 50 cycles. The rutile/anatase TiO_2 composite exhibits an improved specific capacity of ≈242 mA h g^{-1}, which was well retained after 200 cycles. The anatase TiO_2 phase alone delivers the highest specific capacity of ≈295 mA h g^{-1} and provides a good cycle life. The specific capacity of ≈210 mA h g^{-1} was obtained after 200 cycles. The

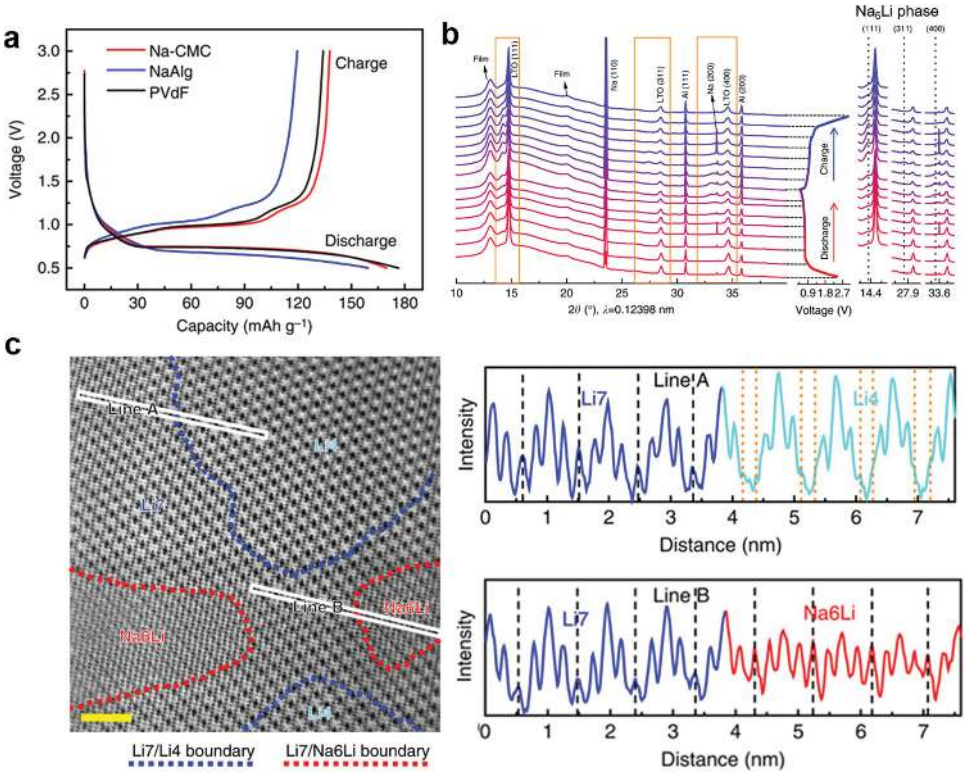

Figure 13. a) Typical charge/discharge profiles of $Li_4Ti_5O_{12}$ anode in Na cells. b) In situ synchrotron XRD analysis of $Li_4Ti_5O_{12}$ anode upon sodiation and desodiation. c) ABF image in the half-discharged $Li_4Ti_5O_{12}$ anode with ABF line profile crossing the Li7/Li4 and Li7/Na6Li boundaries. Reproduced with permission.[361] Copyright 2013, Nature Publishing Group.

theoretical study using DFT calculation demonstrated that the anatase TiO_2 provides a 2D diffusion path to the *a*- and *b*-axes with low energy barriers for Na intercalation, whereas the rutile phase only has one diffusion path along the *c*-axis, suggesting the superior Na diffusivity of the anatase phase over the rutile phase.

$Li_4Ti_5O_{12}$: Hu's group first reported that $Li_4Ti_5O_{12}$ (LTO) can accommodate not only Li but also Na ion de/intercalation reversibly.[360,361] Figure 13a presents typical charge/discharge profiles of LTO in Na half cells, in which the LTO anode delivers a reversible capacity of ≈150 mA h g^{-1}, corresponding to ≈2.6 Na ion utilization, with a redox potential of ≈0.9 V vs Na^+/Na. They observed an interesting three-phase reaction mechanism during Na intercalation in the LTO anode based on in situ XRD analysis (Figure 13b). In LIB systems, the Li storage in the LTO anode occurs through a two-phase reaction between spinel LTO and rock-salt $Li_7Ti_5O_{12}$. However, the in situ XRD characterization confirmed that $LiNa_6Ti_5O_{12}$ and $Li_7Ti_5O_{12}$ phases are formed upon Na intercalation in the LTO anode. This phenomenon was attributed to the different size of Na and Li ions in the LTO lattice, where the large Na ions barely occupy the 8a tetrahedral site, and therefore, Na ions are more likely to occupy the 16c octahedral site. The DFT calculations also indicated that Li/Na solid solution in 16c sites is not energetically favorable, indicative of the phase separation of $Li_7Ti_5O_{12}$ and $LiNa_6Ti_5O_{12}$ phases. To further investigate the three-phase Na intercalation mechanism, they used spherical aberration-corrected STEM analysis to directly visualize the atomic structure. They observed a three-phase coexistence region in the half-discharged product that can distinguish $Li_7Ti_5O_{12}$/LTO and $Li_7Ti_5O_{12}$/$Na_6LiTi_5O_{12}$ phase boundaries (Figure 13c).

Later, Yu et al. discovered the size-dependent Na storage properties in the LTO anode.[362] According to their report, the Na intercalation behavior in the LTO anode strongly depends on the particle size. In 440-nm-sized LTO particles, a small amount of Na ions can be intercalated and provided a specific capacity of ≈16 mA h g^{-1} (corresponding to 0.27 Na per LTO). When the particle size decreased to 44 nm, the reversible capacity increased to ≈150 mA h g^{-1} (corresponding to 2.6 Na ions per LTO). According to their experiments, the Na ion diffusion coefficient of LTO was estimated to be ≈10^{-16} cm^2 s^{-1}, which is 5 orders of magnitude smaller than Li ion diffusion. Because of the slow Na ion diffusion kinetics, nanosizing the LTO was critical to utilize the Na insertion. Consequently, several research groups fabricated nanostructured LTO anode materials to improve their Na storage properties.[363–368] For example, Liu et al. synthesized LTO nanoparticles embedded in carbon nanofibers (LTO/C nanofibers) via electrospinning and annealing.[363] Small LTO nanoparticles (<10 nm) embedded in a conductive carbon matrix could provide a high reversible capacity of ≈165 mA h g^{-1} corresponding to ≈2.83 Na ions transferred per LTO at 35 mA g^{-1}. At increased current rates of 87.5 and 175 mA g^{-1}, specific capacities of ≈133 and 109 mA h g^{-1} could be provided, respectively. The composite nanostructure can supply short transport lengths for Na ions and electrons and low contact resistance. Nevertheless, the low tap density of

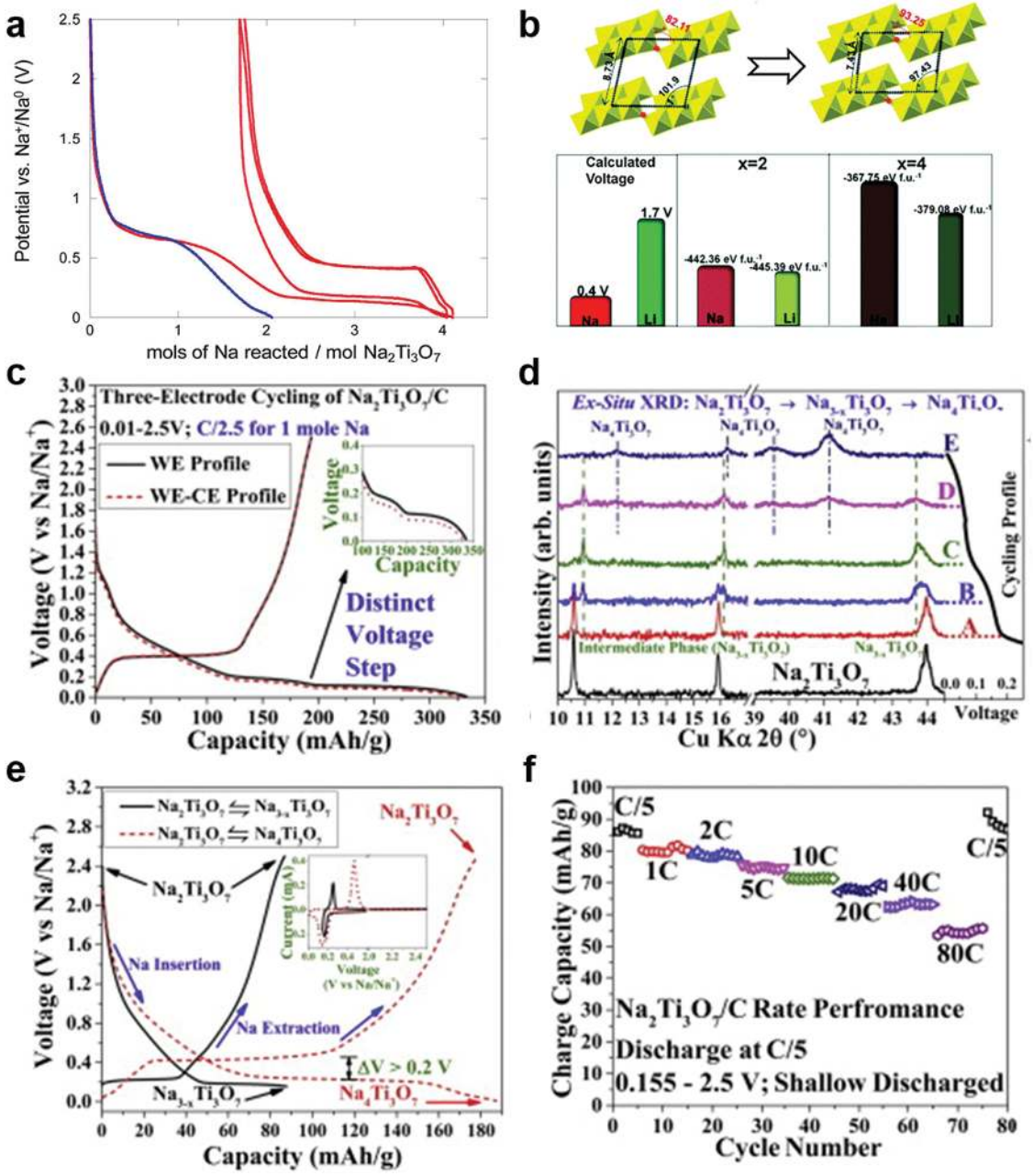

Figure 14. a) Typical charge/discharge profiles of $Na_2Ti_3O_7$ anodes. The blue curve represents the discharge profile of a carbon black anode. Reproduced with permission.[369] Copyright 2011, American Chemical Society. b) Structural change of $Na_2Ti_3O_7$ upon Na intercalation and the calculated voltage and electrostatic energy at $x = 2$ and 4 for $Na_xTi_3O_7$. Reproduced with permission.[370] Copyright 2014, Royal Society of Chemistry. c) Galvanostatic charge/discharge profiles of $Na_2Ti_3O_7$ using the three-electrode configuration (inset: enlarged view of the voltage step). d) Ex situ XRD analysis of $Na_2Ti_3O_7$. e) Galvanostatic charge/discharge profiles of $Na_2Ti_3O_7$ with different cut-off voltages (Black solid line: 0.155 V, Red dotted line: 0.01 V). f) Rate capability of $Na_2Ti_3O_7$ anode in the voltage range between 0.155 and 2.5 V vs Na^+/Na. Reproduced with permission.[371] Copyright 2015, Elsevier.

nanostructured materials remains problematic for practical use, which requires high volumetric energy densities.

Na–Ti–O Compounds: Senguttuvan et al. first reported $Na_2Ti_3O_7$ as a low-voltage oxide anode for NIBs.[369] Typical charge/discharge profiles of the $Na_2Ti_3O_7$/carbon black composite anode are presented in **Figure 14**a, wherein the blue curve is the discharge profile of the carbon black electrode (without $Na_2Ti_3O_7$), and the red curve is that of the composite electrode ($Na_2Ti_3O_7$/carbon black). While the irreversible capacity obtained at ≈0.7 V vs Na^+/Na is attributable to the additive carbon black, the redox reaction of the $Na_2Ti_3O_7$ anode occurs at ≈0.3 V vs Na^+/Na with ≈2 Na ions de/intercalation, corresponding to ≈180 mA h g^{-1}. The plateau voltage of the $Na_2Ti_3O_7$ anode is much lower than its Li analogue ($Li_2Ti_3O_7$), ≈1.7 V vs Li^+/Li.

Xu et al. performed DFT calculations to understand the exceptionally low operating voltage of the $Na_2Ti_3O_7$ anode.[370]

They examined the structural differences between $Na_2Ti_3O_7$ and $Na_4Ti_3O_7$ (Figure 14b) and observed a unique structural flexibility. When 2 Na ions are intercalated in $Na_2Ti_3O_7$ structure, the Na coordination decreases from 9 and 7 in the pristine state to 6 in the fully sodiated phase. In addition, the *c* lattice parameter decreases, which was attributed to the screening effect from the high Na ion concentration in the Na layers. The change of Na site environment results from (i) the shift of Ti–O slab and (ii) modifications within the Ti–O framework. They also observed that the exceptionally low Na storage voltage of $Na_2Ti_3O_7$ is due to the structural instability of the Na intercalated compound from the calculation of the electrostatic interaction in the structure. A larger difference in the electrostatic energy between $Na_2Ti_3O_7$ and $Na_4Ti_3O_7$ compared with that in the Li analogue was observed and suspected to result in structural instability in $Na_4Ti_3O_7$ leading to lower operating voltage. The strong electrostatic repulsion in the discharged state further yielded the self-relaxation phenomenon. When the discharged compound is stored for a few days, the $Na_4Ti_3O_7$ phase gradually transforms into $Na_2Ti_3O_7$.

The poor cycle stability of the $Na_2Ti_3O_7$ anode is one of the important issues to be addressed.[372–375] Munoz–Marquez et al. discovered that the instability of the SEI formed on $Na_2Ti_3O_7$ anodes during the charge process results in a poor cycle stability.[376] The SEI is partially dissolved during the charge process, and the SEI instability involves continuous degradation of the electrolyte upon repeated battery operation. Thus, these authors argued that the exploration of a protective coating on the $Na_2Ti_3O_7$ anode is required to improve its cycle performance.

Recently, Rudola et al. observed an intermediate phase of $Na_{3-x}Ti_3O_7$ between $Na_2Ti_3O_7$ and $Na_4Ti_3O_7$ that considerably affects the electrochemical properties.[371] According to their report, a distinct voltage step is observed in the first discharge profile, indicative of the presence of an intermediate phase between $Na_2Ti_3O_7$ and $Na_4Ti_3O_7$ (Figure 14c). Ex situ XRD analysis in Figure 14d revealed that new XRD peaks evolved at the expense of $Na_2Ti_3O_7$ in the half-discharged state and diminished with the evolution of the XRD peaks of $Na_4Ti_3O_7$ in the fully discharged state indicating the presence of an intermediate phase. It was found that the charge/discharge profile is notably changed depending on whether the intermediate phase appears or not. When the discharge cut-off voltage is limited to ≈0.155 V vs Na^+/Na, the corresponding charge voltage become ≈0.22 V vs Na^+/Na, however, after the deep discharge to 0.01 V, a charge voltage of ≈0.44 V vs Na^+/Na was observed in Figure 14e. The two distinct discharge plateaus were observed in the deep discharge process; however, only one plateau at ≈0.44 V vs Na^+/Na was observed. This finding indicates that an irreversible phase transition occurs upon the deep discharge, and therefore, the path through the intermediate phase is lost in the subsequent cycling. When they cycled the $Na_2Ti_3O_7$ in the upper voltage plateau region, $Na_2Ti_3O_7$ delivered an excellent rate capability up to 80C (1C = ≈85 mA g^{-1}) in Figure 14f.

Other types of Na–Ti–O compounds have also been studied as potential anodes for NIBs,[377–382] including trigonal and monoclinic $Na_4Ti_5O_{12}$ materials.[377,378] $Na_4Ti_5O_{12}$ anodes provided a low specific capacity less than 70 mA h g^{-1}, unlike their Li analogue (LTO), while the monoclinic phase delivered a slightly higher specific capacity than the trigonal polymorph due to the continuous 2D channels for Na ion transfers. Ceder's group recently reported layered $NaTiO_2$ as a potential anode for NIBs.[379] They demonstrated that O3-$NaTiO_2$ can deliver a reversible capacity of ≈150 mA h g^{-1}, corresponding to ≈0.5 Na transfer in the voltage range between 0.6 and 1.6 V vs Na^+/Na, in contrast to a previous report.[383] The widened low voltage window that can be achieved by reducing the water concentration in the electrolyte was speculated to result in the increase in the specific capacity. In addition, they observed an unusual lattice parameter change and Na vacancy orderings upon de/intercalation of Na ions, which lead to a constant interslab distance and small change of the in-plane Ti–Ti distance. It was attributed to the reason for the good cycle stability.

3.2.2. Conversion Reaction Compounds

Iron Oxides: Koo et al. reported iron oxide nanoparticles as anode materials for NIBs for the first time.[384] While the work focused on the Na intercalation in iron oxide host materials, Hariharan et al., later, demonstrated that iron oxides provide a high specific capacity of ≈400 mA h g^{-1} through conversion reactions (**Figure 15**a),[385] forming Fe metal and Na_2O. Nevertheless, the specific capacity is lower than the theoretical value of 926 mA h g^{-1} based on the full conversion reaction. In comparison to the same iron oxide electrode in Li cells that delivers a specific capacity of ≈950 mA h g^{-1}, much less reversible capacity was observed in Na cells than their Li counterparts. Similar observations were made in other conversion reaction compounds and might originate from the (i) sluggish kinetics of Na ion transfer in conversion reaction because of their larger ion size and (ii) different nature of the SEI layer formed in Na cells.[386–393] Recently, Zhang et al. reported a 3D porous Fe_2O_3/C nanocomposite as a high-performance anode for NIBs.[394] The nanocomposite was composed of interconnected nanochannels and Fe_2O_3 nanoparticles that were uniformly incorporated in a conductive porous carbon matrix. The nanocomposite electrode could provide a high specific capacity of ≈1100 mA h g^{-1} in the second cycle and retained a reversible capacity of ≈750 mA h g^{-1} after 200 cycles at 200 mA g^{-1}. It also delivered a high rate capability with a specific capacity of ≈320 mA h g^{-1} at 8000 mA g^{-1}. The excellent electrochemical properties are attributable to the synergistic effect of the nanocomposite, which effectively relieves stress, accommodates large volume expansion/shrinkage, and facilitates the electron and Na ion transport.

Cobalt Oxides: Jiang et al. demonstrated that Co_3O_4 can store Na ions through conversion reactions. The Co_3O_4 anode provided a specific capacity of ≈600 mA h g^{-1} during the initial discharge but exhibited a rapid cycle degradation.[398] Since then, several research groups have investigated cobalt oxides as potential anodes for NIBs and attempted to improve their electrochemical properties.[399–404] Recently, Yang et al. proposed a highly ordered dual porosity mesoporous Co_3O_4 as a stable anode for NIBs.[395] The ordered dual porosity mesoporous Co_3O_4 anode can deliver a high specific capacity of ≈700 mA h g^{-1} during the initial discharge and ≈500 mA h g^{-1} upon extended cycles, which are much higher values than those

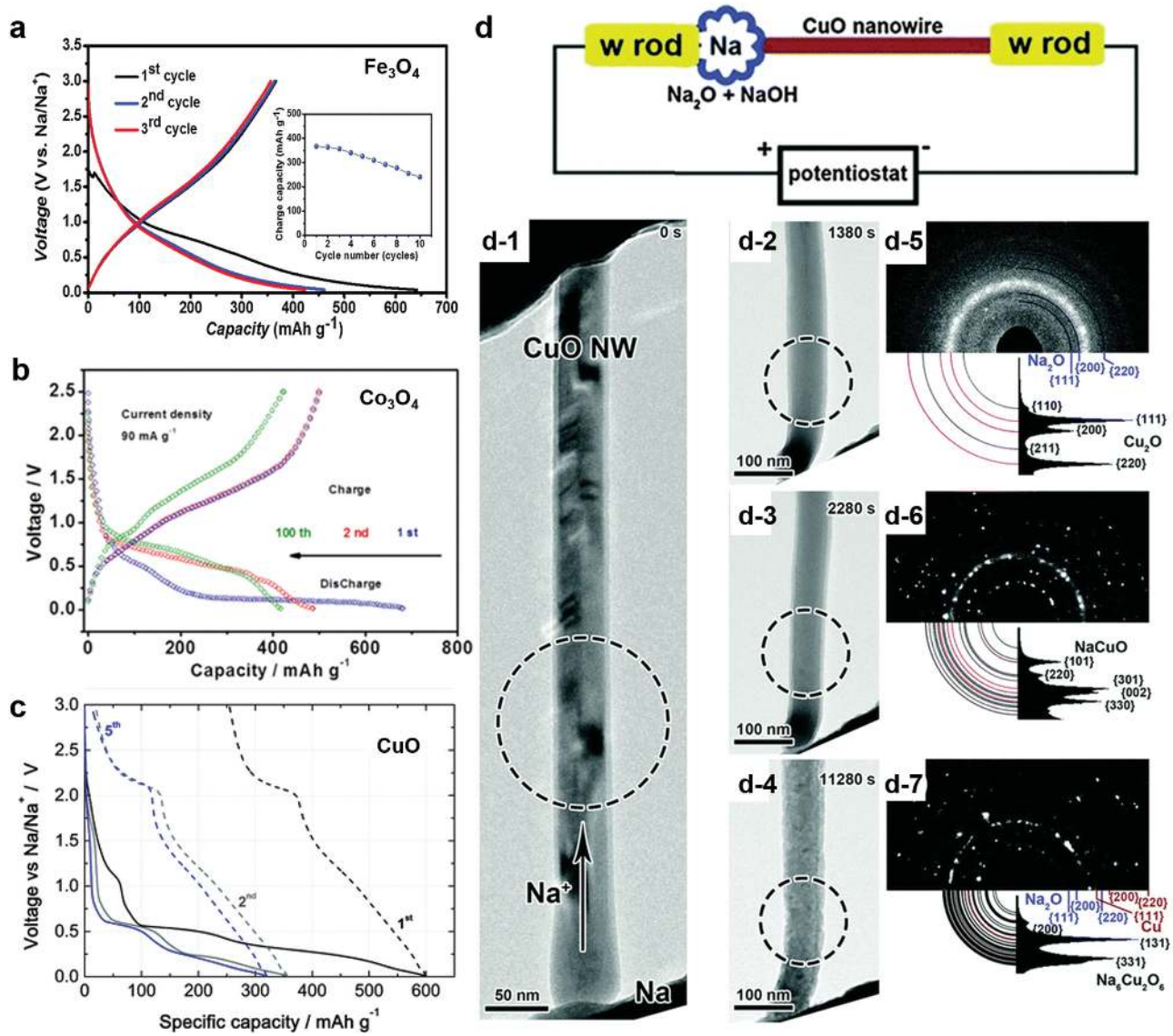

Figure 15. a) Charge/discharge profiles of Fe_3O_4 anodes in the voltage window 0.04–3.0 V vs Na^+/Na (Inset: cycle stability). Reproduced with permission.[385] Copyright 2013, Royal Society of Chemistry. b) Electrochemical charge/discharge profiles of Co_3O_4 anodes in the voltage range between 0.01 and 2.5 V vs Na^+/Na. Reproduced with permission.[395] Copyright 2015, Wiley-VCH. c) Charge/discharge curves of CuO anodes in the voltage window 0.01–3.0 V vs Na^+/Na. Reproduced with permission.[396] Copyright 2013, Royal Society of Chemistry. d) Schematic of in situ experimental setup and TEM images with (d-5), (d-6), and (d-7) electron diffraction patterns of the circled areas in (d-2), (d-3), and (d-4), respectively. Reproduced with permission.[397] Copyright 2015, Royal Society of Chemistry.

for bulk Co_3O_4 particles (Figure 15b). The mesoporous Co_3O_4 anode also exhibits relatively good capacity retention and rate performance, which were attributed to the ordered porous structure that can accommodate a large volume change during charge/discharge and enable the facile supply of electrolyte resulting from the easy penetration to the electrode. It was also shown that the formation of Na_2O occurs after discharge using ex situ XRD, which agreed with previous report by Rahman et al., who observed the sodiation process forming Na_2O and Co using ex situ XRD and TEM analyses.[405]

Copper Oxides: Klein et al. demonstrated that CuO is electrochemically active for Na storage, providing a reversible capacity of ≈300 mA h g^{-1} for cycles (Figure 15c).[396] In principle, CuO can store 2 Na ions and form Cu and $2Na_2O$, delivering a theoretical capacity of ≈674 mA h g^{-1}, similar to that for Li storage. However, the specific capacities obtained in the literature are typically below the theoretical value, and only a few groups have reported a high reversible capacity over 600 mA h g^{-1} (≈90% of the theoretical capacity).[406–410] Zhang's group prepared flexible and porous CuO nanorod arrays by engraving Cu foils and used them as the anode for NIBs.[409] The CuO nanorod arrays exhibited a high specific capacity of ≈640 mA h g^{-1} at 200 mA g^{-1} and showed stable cycle performance. More recently, Chen's group proposed micro-nanostructured CuO/C spheres as a promising anode for NIBs.[410] The micro-nanostructured CuO/C spheres synthesized by aerosol spray pyrolysis delivered a reversible

capacity of ≈660 mA h g^{-1} and maintained 426 mA h g^{-1} after 100 cycles. The improved Na storage properties were attributed to the nanostructure that accommodated a large volume change upon cycling and supplied fast electron and Na ion transport pathways.

More recently, Liu et al. directly observed the Na storage process in CuO nanowires using in situ TEM.[397] In the in situ TEM measurement, CuO nanowires and Na metal were used as the working and counter electrodes, respectively. A mixture of Na_2O and NaOH that was naturally grown on a Na metal surface was used as the solid electrolyte (Figure 15d). The pristine CuO nanowires are shown in Figure 15d-1, and the TEM images were monitored in the circled area during sodiation. Initially, the CuO was converted into Cu_2O and Na_2O, as observed in Figure 15d-5. Then, the products were transformed into NaCuO (Figure 15d-6). Finally, further sodiation formed $Na_6Cu_2O_6$, Na_2O, and Cu, as observed in Figure 15d-7. This result is different from the previous report by Wang et al., which demonstrated that CuO is converted into Cu_2O and Na_2O and then finally became Cu and Na_2O based on their ex situ observation, in which they did not observe NaCuO nor $Na_6Cu_2O_6$ phases.[406] The discrepancy might originate from the different cell configurations between in situ and ex situ measurements. In addition, it was shown that the NaCuO phase is unstable in the air and could be transformed into Cu_2O and Na_2O.

3.3. Intermetallic Compounds

Metals or metalloids, which store Na by forming Na–Me binary intermetallic compounds, have been extensively studied because of the high theoretical capacity and low Na storage potential, as listed in **Table 1**. Most works have focused on Group 14 (Si, Ge, Sn, and Pb) and 15 (P, As, Sb, and Bi) elements. Computational works have predicted their electrode potentials, maximum Na uptake, Na diffusion activation barriers, volumetric change, and mechanical properties (**Figure 16**).[411,412] Although the reversible capacity of intercalation-based electrode materials is limited by their inherent constraint of a heavy framework, metal/metalloid electrodes are able to take multiple Na ions per single atom by an alloying reaction as exemplified in Figure 16a,b, resulting in high reversible capacities of 370–2000 mA h g^{-1} with an average voltage of less than 1 V (Table 1).[122,412] However, the uptake of multiple Na ions naturally causes large volumetric changes upon cycling (Figure 16c,d), leading to detrimental effects on cycle stability. This phenomenon is more serious in NIBs than LIBs because of the large ionic size of Na compared with Li (1.02 Å and 0.76 Å in the 6-coordinated state, respectively). Therefore, studies on metal/metalloid anode materials have mostly focused on enhancing the cycle stability.

3.3.1. Tin

According to the phase diagram of Na–Sn,[420] the maximally sodiated phase is $Na_{15}Sn_4$, indicating that one Sn atom can take a maximum of 3.75 Na atoms. The feasibility of Sn as an anode for NIBs was first theoretically examined using DFT calculations, and it was suggested that the electrochemical alloying reaction between Na and Sn would proceed with the presence of $NaSn_5$, NaSn, Na_9Sn_4, and $Na_{15}Sn_4$ phases, with an average voltage of ≈0.2 V (**Figure 17**a. Red dotted line).[411] Soon after, Komaba et al. succeeded in demonstrating the Sn as an anode material experimentally reporting a final discharged phase of $Na_{15}Sn_4$.[421] Based on these studies, Ellis et al. attempted to investigate the sodiation mechanism using electrochemical tests and in situ XRD.[414] The Na insertion voltage curve consists of four distinct plateaus, which is consistent with the former DFT results, and indicates the existence of four different intermediate phases (Figure 17a). However, these phases were not clearly identified, except for the fully sodiated phase ($Na_{15}Sn_4$), as shown in Figure 17b. They suspected $NaSn_3$, a-NaSn, and Na_9Sn_4 as possible candidates for intermediate phases based on coulometry. In later studies by Wang et al., the sodiation behavior was directly examined using in situ TEM employing a solid-state electrolyte with Na metal as a counter electrode.[413] Sodiation was observed to occur in two steps; the first step is a two-phase reaction to form amorphous $NaSn_2$, and the second step is a single-phase reaction that forms amorphous Na_9Sn_4 and Na_2Sn (Figure 17c). Regarding the inconsistency of the sodiation process revealed by in situ XRD and in situ TEM, the authors explained that it is attributable to different kinetic factors such as the experimental configuration and sample conditions.[413] However, there are still computationally predicted stable intermediate phases such as $NaSn_6$, $NaSn_4$, $NaSn_3$, $NaSn_2$, Na_9Sn_4, and Na_3Sn, which have not appeared in studies thus far. Therefore, further mechanism studies are needed in the future to clarify the electrochemical sodiation behavior of Sn.

The de/sodiation process of Sn inevitably undergoes drastic volume expansion/contraction because of the uptake/release of 3.75 Na atoms. The repetitive structural changes are known to be responsible for capacity fading because a large volume change induces tensile/compressive stress, leading to crack propagation and contact loss. Several strategies such as making

Table 1. Summary of properties of typical metal or metalloid materials for Na-ion batteries.

	Reduction product	Theoretical capacity (mA h g^{-1})	Volume expansion (Na_xX/X) (%)	Average voltage (vs Na^+/Na) (V)
Sn	$Na_{3.75}Sn$	847	520[413]	≈0.2[414]
Sb	Na_3Sb	660	393[415]	≈0.6[123]
P	Na_3P	2596	408 (red)[122]	≈0.4[122]
			≈500 (black)[416]	
Si	NaSi	954	243[415]	≈0.5[417]
Ge	NaGe	369	305[418]	≈0.3[419]

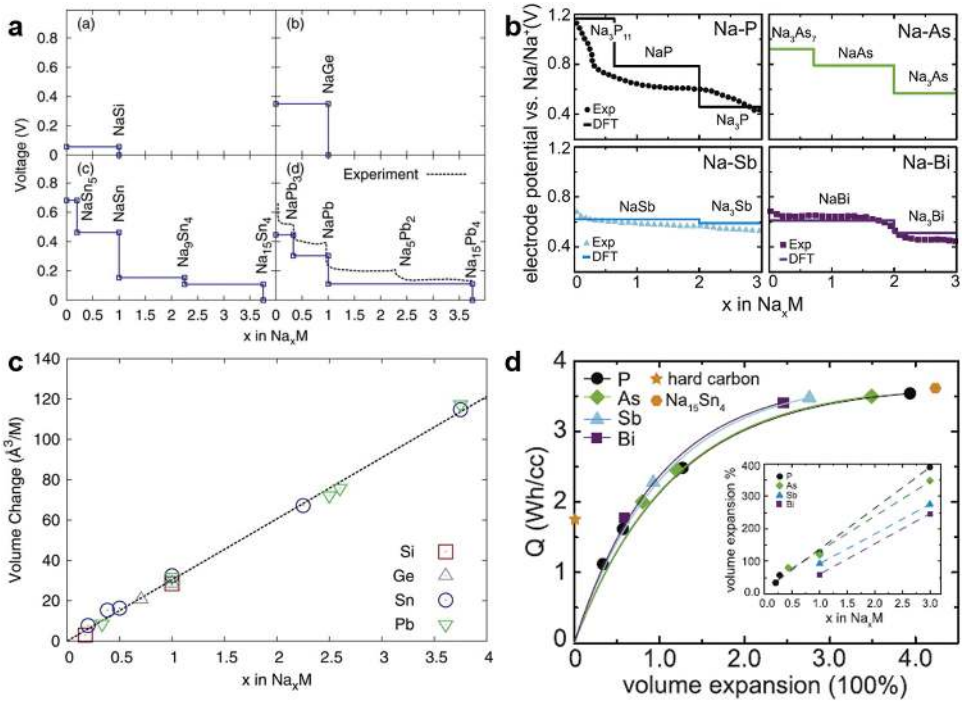

Figure 16. Calculated voltage profiles of Na–M alloys with respect to Na^+/Na for a) group-14 elements and b) group-15 elements and calculated volume changes for c) group-14 elements and d) group-15 elements. Experimental values are also given if available. Reproduced with permission.[411,412] Copyright 2011, The Electrochemical Society. Copyright 2015, Elsevier.

a nanocomposite and modifying the structure have been developed to overcome those problems. Several groups have synthesized Sn nanoparticles uniformly distributed in a porous carbon matrix and claimed that the carbon matrix not only provides an electron-conducting channel but also keeps Sn nanoparticles trapped without segregation.[423–426] The large space between nanoparticles was believed to alleviate stress by volume change, leading to an enhancement of the cycle life. Likewise, a Sn–Cu nanocomposite that exhibits a capacity of 420 mA h g^{-1} for 100 cycles was suggested.[427] In addition, 3D viral nanoforests, which deliver a capacity of 405 mA h g^{-1} at 150 cycles, were introduced, and the stable cycle life was attributed to the nanostructure, which buffers volume expansion and suppresses Sn aggregation.[428]

3.3.2. Antimony

According to Na–Sb phase diagram, there exist two intermetallic phases, NaSb and Na_3Sb.[429] Qian et al. first demonstrated a Sb–carbon nanocomposite with an initial capacity of 610 mA h g^{-1}, corresponding to the storage of nearly three Na atoms.[123] Based on the coulometry and two peaks in the cyclic voltammetry, they claimed that NaSb and Na_3Sb are formed during the sodiation. Darwiche et al. investigated the sodiation mechanism of Sb more precisely by using in situ XRD, as shown in Figure 17d.[422] Unlike the prediction in the previous study, it was observed that Sb forms an amorphous phase during the electrochemical cycling except for the fully sodiated crystalline phase (Na_3Sb). The Na_3Sb phase has a hexagonal structure dissimilar to Li_3Sb, which has a rock salt structure. It partly explains why Sb exhibits better cycling stability in the Na system than in the Li system because the volume expansion problem is less severe in the hexagonal phase (Sb: 181.1 $Å^3$, Na_3Sb: 237 $Å^3$, and Li_3Sb: 283.8 $Å^3$).[422]

Analogous to Sn, making a Sb nanostructure has been extensively carried out to relieve the stress caused by the three Na uptake and to improve the cycle life. Zhu et al. and Wu et al. fabricated 1D carbon nanofibers, which trap Sb nanoparticles via a simple electrospinning process.[430,431] The space between carbon matrices can tolerate volume expansion, and thus, aided in improving the cycle stability (80% capacity retention after 300 cycles and 90% after 400 cycles). Similar approaches were made for Sb-containing nanocomposites such as SiC–Sb–C,[432] Sb–acetylene black,[433] Sb–multiwalled carbon nanotubes,[434] FeSb–TiC–C,[435] and nano Sb–porous carbon.[436]

3.3.3. Phosphorus

P is capable of storing three Na atoms and its small atomic weight (30.97 g mol^{-1}) compared with Sn (118.71 g mol^{-1}) and Sb (121.76 g mol^{-1}) is a great merit in achieving high specific capacity for Na electrode.[437] The use of P as an anode for NIBs was reported by Kim et al. in 2013.[122] In the report, the amorphous red P–carbon composite delivered a reversible capacity of 1890 mA h g^{-1} for 20 cycles (**Figure 18**a), forming crystalline Na_3P. In addition, Qian et al. proposed an amorphous red P–carbon composite (a-P/C) as a potential anode for NIBs,[438] where they noted that a-P/C delivers steadier capacity than red P and black P because of the improved conductivity by carbon and buffering volume change of the carbon matrix. A similar

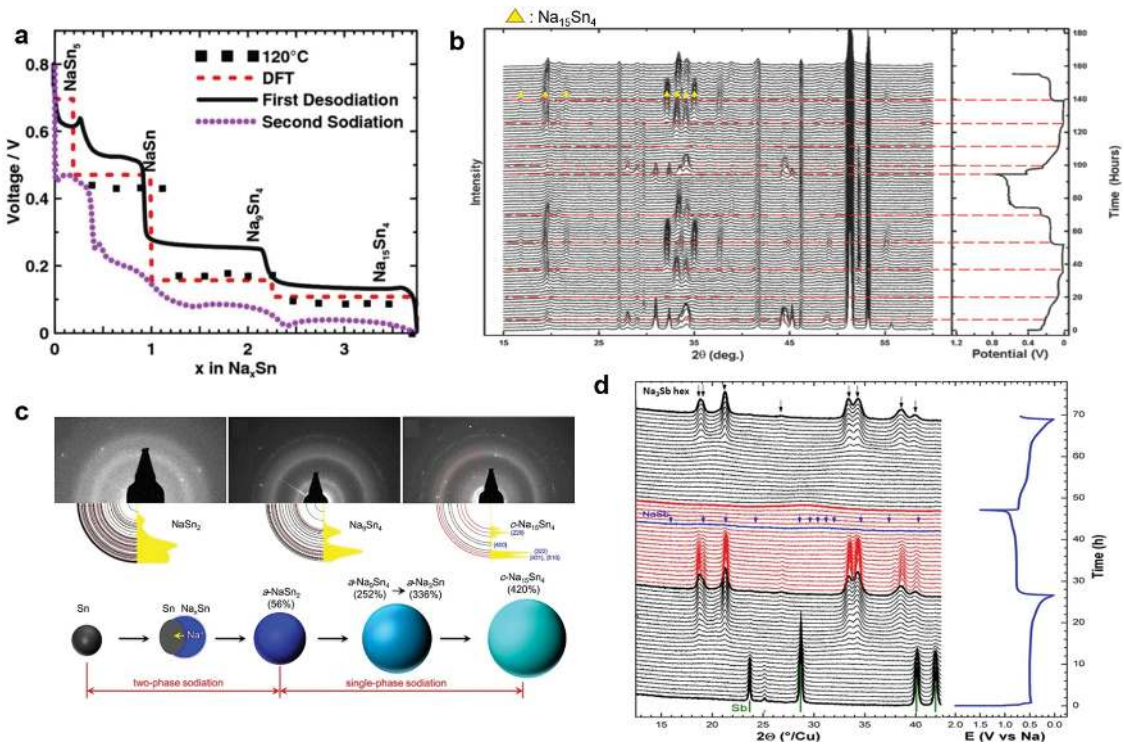

Figure 17. a) Typical charge/discharge profile of Sn anodes. b) In situ XRD patterns of Sn sodiation. Reproduced with permission.[414] Copyright 2012, The Electrochemical Society. c) Microstructural evolution of Sn nanoparticles observed by in situ TEM. Reproduced with permission.[413] Copyright 2012, American Chemical Society. d) In operando XRD patterns of Sb anodes. Reproduced with permission.[422] Copyright 2012, American Chemical Society.

strategy was utilized by Li et al. who mixed red P and CNTs, yielding a reversible capacity of 1675 mA h g^{-1}, with a capacity retention of 76.6% for 10 cycles.[124] The relatively poor cyclability remains to be resolved and is ascribed to the (i) severe volumetric expansion due to the three Na uptake, (ii) electrolyte decomposition by highly reactive Na_3P, and (iii) poor electrical conductivity.[415,416] Very recently, black P with a layered structure was proposed as an anode material for NIBs with merits of the high conductivity (≈0.3 mS m^{-1}) and sufficient interlayer space for facile Na intercalation.[416] The graphene-sandwiched phosphorene delivered a remarkably high specific capacity of 2440 mA h g^{-1} for 100 cycles. The large capacity was explained by the dual mechanism of Na insertion, where the Na ion first intercalates into the *x* (or *a*) axis of the phosphorene layer followed by an alloying process (Figure 18b), as evidenced by ex situ XRD and in situ TEM analyses.[416] These results were supported by theoretical works that black P maintains its layered structure during the initial Na intercalation, followed by the alloying reaction accompanying the P–P bond breaking.[439]

3.3.4. Silicon and Germanium

The phase diagram of Na–Si indicates that the fully sodiated phase of Si is NaSi.[440] Several theoretical works have examined the feasibility of utilizing Si as an anode material for NIBs. However, crystalline Si exhibits poor Na diffusion kinetics, as the activation energy for Na diffusion in bulk Si is calculated to be higher than 1 eV.[441] In addition, the insertion of Na into crystalline Si yields a positive binding energy, indicative of the limited Na uptake in pristine Si.[441–443] Structurally modified Si was predicted to exhibit better electrochemical performance such as in amorphous Si by having more favorable binding between Na and Si.[418,442,444] Reasonable activation barriers for Na diffusion were also predicted, where 0.4 eV was required for Na migration in layered polysilane and amorphous Si.[442,418] The enhanced properties could be attributed to the large interstitial sites provided by structural modification, which enables facile Na intercalation and migration. Based on these studies, Na uptake of Si was realized very recently by Xu et al. They produced Si nanoparticles (≈20 nm in size) partially containing an amorphous part, which delivered a reversible capacity of 248 mA h g^{-1} for 100 cycles (Figure 18c).[417]

Ge has a similar chemistry as Si, taking a maximum of one Na atom.[445] Ge is also theoretically predicted not to be capable of storing Na in its crystalline structure;[419] therefore, most works have focused on amorphous Ge in thin film and nanowire form.[419,446–448] The first report of Ge as a NIB anode material indicated that the amorphous Ge thin film delivered a reversible capacity of 350 mA h g^{-1} for 15 cycles.[448] A recent work by Kohandehghan et al. also experimentally revealed that crystalline Ge exhibits a capacity of less than 20 mA h g^{-1} (Figure 18d, top), whereas amorphorized Ge nanowires exhibited a capacity 370 mA h g^{-1} (Figure 18d, bottom).

3.4. Organic Anodes

Na organic anodes have received considerable attention because of their potentially high capacity, low cost, and sustainability.[252,449]

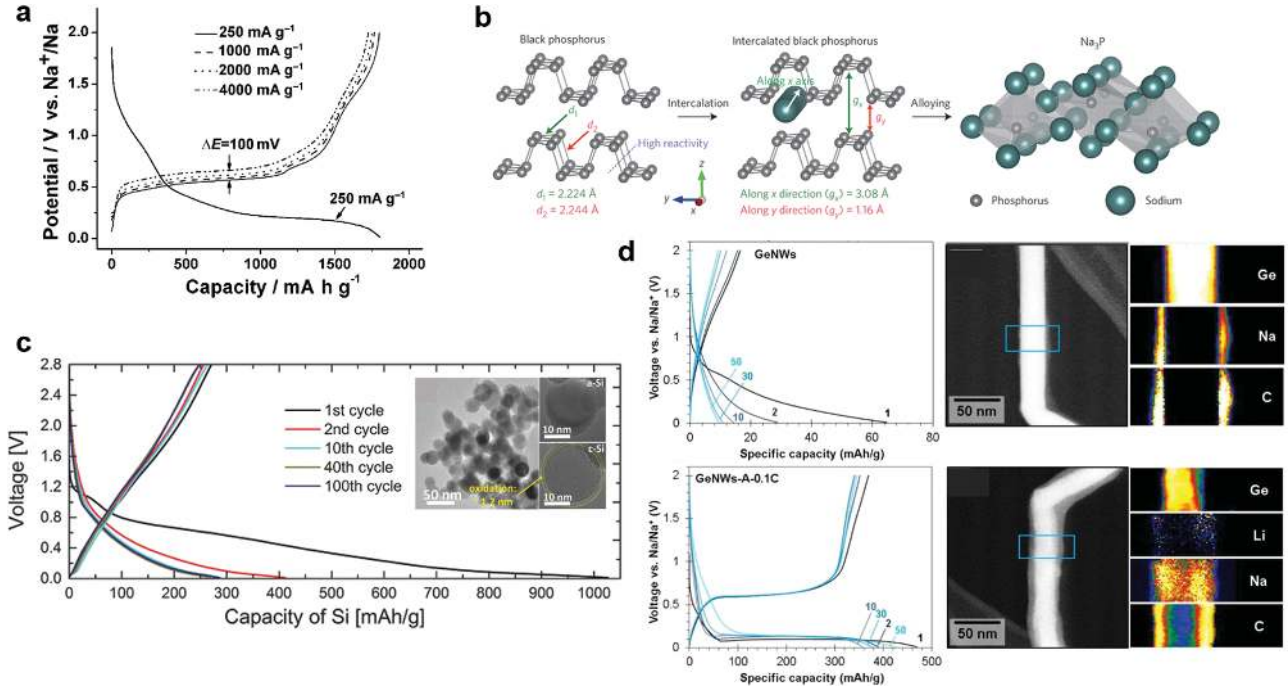

Figure 18. a) Typical voltage profile of amorphous red P/carbon composite. Reproduced with permission.[438] Copyright 2013, Wiley-VCH. b) Schematic of sodiation behavior of black P. Reproduced with permission.[416] Copyright 2015, Nature Publishing Group. c) Charge/discharge profile of Si nanoparticles (inset: TEM image of Si nanoparticles containing amorphous and crystalline parts). Reproduced with permission.[417] Copyright 2016, Wiley-VCH. d) Charge/discharge profile and TEM image of GeNWs before (top) and after (bottom) activation. Reproduced with permission.[419] Copyright 2014. American Chemical Society.

In this section, we briefly introduce recent works on Na organic compounds as anode materials for NIBs, including Na carboxylate-based compounds,[266,389,413,450–458] biomolecular-based compounds,[459–461] and Schiff-based compounds.[462,463]

Conjugated carboxylate organic molecules, such as dilithium terephthalate, have been reported as promising electrode materials for LIBs.[464] Analogous to dilithium terephthalate, disodium terephthalate ($Na_2C_8H_4O_4$) was first introduced by Zhao et al. as a Na organic anode.[450–452] They examined the electrochemical properties of $Na_2C_8H_4O_4$ and reported that two Na ions participate in the redox reaction at 0.29 V vs Na^+/Na and exhibited a reversible capacity of 250 mA h g^{-1}. Although carboxylate organic molecules provide respectable electrochemical properties in terms of capacity and operation voltage, the poor rate and cycle stability remains to be resolved. A few strategies were proposed including molecular tuning of the mother structure, surface coating, and polymerization.[266,389,394,397,454–458,461,465]

Several biomolecule-based organic compounds were also investigated as potential organic anodes for NIBs.[459–461] Luo et al. demonstrated that coroanic acid disodium salt (CADS) is capable of delivering 246.7 mA h g^{-1} of capacity at the voltage range of 0.7 to 2.0 V vs Na^+/Na, however, the capacity of the CADS electrode rapidly faded because of the volume change during phase transformation.[459] Juglone-based organic compounds, which have well-defined quinone carbonyl groups, are another example. Wang et al. prepared a composite of juglone and reduced graphene oxide (RGO) as electrodes, which exhibited a respectable electrochemical performance with a capacity of 305 mA h g^{-1}.[460] Di-sodiated 2, 5-dihydroxy-1, 4-benzoquinone (Na_2DBQ), which is an analogue of the previously reported Li version,[466] was recently proposed as a promising anode for NIBs.[465] Na_2DBQ displayed a capacity of 265 mA h g^{-1} at 0.1 C rate at approximately 1.2 V vs Na^+/Na and a stable cycle life over 300 cycles at 1 C rate. More recently, Wu et al. proposed a new structure of a Na host consisting of repeated inorganic and organic structures in a layered framework using Na salt of 2,5-dihydroxy-1,4-benzoquinon (2,5-DBQ).[467] They suggested a Na storage mechanism, where the inorganic layers play the role in Na ion transfer, and the organic layers are responsible for the electron transfer. The combined structure with inorganic and organic layers was considered as a platform for new Na organic materials.

Schiff-based electrodes were recently investigated as Na organic anodes by Armand's group.[462,463] Polymeric Schiff-based functional (R1HC = NR2) groups were demonstrated as redox centers of the electrode.[462] These researchers observed that –N=CH–Ar–CH=N– (Ar = aromatic group) can work as a redox center for Na storage. The polymeric base has a low discharge voltage below 1 V vs Na^+/Na and delivers a capacity of 350 mA h g^{-1} at a current density of 26 mA g^{-1}. Oligomeric Schiff-based materials were also investigated, which exhibited capacities of over 340 mA h g^{-1} at a current density of 21 mA g^{-1} under 1.2 V vs Na^+/Na.[463]

4. Challenges and Perspectives

NIBs have recently attracted considerable attention from the energy storage community because of the earth abundance of Na resources and their similar electrochemistry compared with well-established LIBs, which are critical merits for large-scale

ESSs. The most important aspects of batteries for such applications are the cost per energy and cost per lifetime cycle. Thus, research on NIBs for large-scale ESSs should proceed in satisfying these cost requirements in terms of the raw materials, parts and processing, energy density, and cycle life. The Na precursors for electrode materials (i.e., Na_2CO_3, NaOH, and Na_2SO_4) and Na-salts (i.e., $NaClO_4$ and $NaPF_6$) for electrolytes are generally cheaper than those for LIBs, and a costly Cu current collector in anode part can be replaced with inexpensive Al current collector because Na metal does not form alloy with Al. Although a large atomic weight and ionic radius of Na sacrifice the energy density of NIBs and require open framework electrodes compared with LIBs, recent studies introduced various electrode materials with high energy density and cycle stability.

Recent studies have led to the development of a few important layered-type cathodes delivering high specific capacities using low cost transition metals such as Fe and Mn. However, sufficient cycle stability has not been achieved, where the fundamental difficulties lie in the additional Na insertion/extraction required for these high-capacity layered-type cathodes, which is related to the larger variation in the slab space and corresponding structural stress that is unavoidable and characteristic of a layered crystal structure. These properties are accompanied by faster capacity degradation, as observed in most previous works. The use of Mn and Fe in high-capacity layered cathodes is typically associated with a low operating voltage, resulting in low gravimetric/volumetric energies that fall short of the requirement for large-scale ESSs. In addition, many Na-containing layered cathodes are easily contaminated by moisture, thus requiring moisture-free processes during the material and battery cell preparation. These moisture sensitivity issues are also somewhat related to the low open-circuit voltage (≈3 V) of the layered cathode (or high Na chemical potential in the layered structure). In this respect, a new layered-type Na ion host material with substantially low Na chemical potential and small volume change with a large amount of Na insertion should be developed. With respect to the operating voltage, polyanion cathodes hold promise. In particular, a few important V-based materials have exhibited operating voltages comparable to those of LIBs. Moreover, the polyanion compounds are generally less susceptible to the volume change associated with Na ion insertion and extraction because of the nature of the open crystal framework. Several examples have already been demonstrated with cycle stabilities of over a few thousand cycles. Nevertheless, the energy densities are hardly satisfactory because of their limited specific capacities. The difficulty lies in the open crystal structure and enhanced voltage attributed to the heavy polyanion frameworks; thus, modification of the polyanion groups to reduce the weight of the material would affect other properties. The development of new light polyanion-based crystal frameworks with numerous Na sites is required. Prussian blue analogues have also attracted much attention because of their excellent electrochemical properties, including their high energy and power densities, which stem from large alkali-ion channels that enable fast Na de/intercalation, combined with their low element cost, low toxicity, and easy synthesis at room temperature. However, their poor thermal and electrochemical stabilities remain problematic.

For practical utilization of NIBs, low-cost anode materials similar to the graphite anodes in LIBs are also needed. While the pristine graphite shows negligible electrochemical activity with Na, other carbon-based materials such as disordered carbon will be the dominant player for the anodes of NIBs. The reduction of processing cost and the increase of the Na storage capacity for such carbon materials would be the important topic for the research. In an effort to utilize graphite anodes, some groups have proposed the co-intercalation of Na and the solvent in graphite, forming ternary Na–solvent–graphite compounds.[333–335,468,469] Nevertheless, the following challenges remain. (i) The low specific capacity and high intercalation voltage will lead to low gravimetric/volumetric energies in full cell systems. (ii) The co-intercalation consumes solvent molecules during discharge, resulting in large resistance. Thus, an excess amount of electrolyte is required to utilize the co-intercalation phenomenon in practical cells. (iii) The large volume expansion/shrinkage (≈350%) resulting from the co-intercalation of Na ions and solvent molecules can lead to the pulverization of graphite particles during repeated battery cycling, which can result in cycle degradation in practical cells. Therefore, the design of micro/nanostructured graphite particles containing large voids that can accommodate large volume change during battery operations is required. TMO materials have also attracted recent interest as potential anode materials for NIBs. In particular, Ti-based oxide materials have been extensively studied as host materials for Na intercalation because of their low operation voltage, low cost, and environmental benignness. However, the catalytic activity of Ti-based oxide materials, which results in the underperformance of binders and electrolytes, can deteriorate cycle performance.[376] Coating of a protective layer would reduce the catalytic activity of Ti-based oxides, thus yielding improved cycle stability. It is also important to search for other metal oxide compounds without catalytic activity as intercalation host materials for NIBs.[470,471] Conversion reaction compounds with high theoretical capacities are worth investigating. The cycle stability and rate capability could be improved by improving the electrode design, such as using a composite with a carbon matrix and nanostructuring. Nevertheless, the factors that affect the intrinsic large-voltage hysteresis between the charge and discharge profiles, which leads to low round-trip efficiency, remain unclear. We expect that the research direction for conversion reaction compounds will lie in understanding and reducing the intrinsic voltage hysteresis as well as in designing better electrode architectures for practical applications. Intermetallic compounds also hold great promise as high-capacity anodes. In particular, P-based materials have exhibited exceptionally high capacity. Although a host metal with larger atomic size can take more Na ions with a higher average voltage and lower Na diffusion activation barrier according to the study by Chou et al.,[472] black P is an exception, which can react with up to 3 Na ions and forms Na_3P in the fully discharged state despite its location in period 3. This behavior of black P results from its layered structure with relatively large available space for Na ions, whereas other metals/metalloids (Si, Ge, Sn, As, Sb, Bi) form the diamond structure in their ground state. Combined with its light weight, P shows great potential in terms of its reversible capacity and rate capability. For further exploration of intermetallic compound

anodes, more systematic works on the properties of metal/metalloid electrodes such as the average voltage, maximum Na uptake, and rate capability should be performed in relation to their structural factors. Recently, growing attention has been focused on organic electrode materials for NIBs, and noticeable progress has been made in sustainable organic electrodes. Nevertheless, the poor cycle stability resulting from the dissolution of organic active molecules in the electrolytes remains a great hurdle for their practical utilization in NIBs. Although there have been several attempts to overcome the aforementioned dissolution problems,[251–253,457] a more convenient, economical, and practical method remains to be developed.

Acknowledgements

This work was supported by (i) Project Code. (IBS-R006-G1) and (ii) Energy Efficiency & Resources of the Korea Institute of Energy Technology Evaluation and Planning (KETEP) grant funded by the Korea government Ministry of Trade, Industry & Energy (MOTIE) (No.20132020000270). H.K. and H.K. contributed equally to this paper.

Received: May 5, 2016
Revised: May 25, 2016
Published online: July 12, 2016

[1] International Energy Agency (IEA), Key World Energy Statistics **2015**, http://www.iea.org/publications/freepublications/publication/KeyWorld_Statistics_2015.pdf (accessed March, 2016).
[2] D. Larcher, J. M. Tarascon, *Nat. Chem.* **2015**, *7*, 19.
[3] Crude Oil and Commodity Prices, http://www.oil-price.net/ (accessed March, 2016).
[4] J. M. Carrasco, L. G. Franquelo, J. T. Bialasiewicz, E. Galvan, R. C. PortilloGuisado, M. A. M. Prats, J. I. Leon, N. Moreno-Alfonso, *IEEE T. Ind. Electron.* **2006**, *53*, 1002.
[5] K. C. Divya, J. Østergaard, *Electr. Power Syst. Res.* **2009**, *79*, 511.
[6] B. Dunn, H. Kamath, J.-M. Tarascon, *Science* **2011**, *334*, 928.
[7] S. Hameer, J. L. van Niekerk, *Int. J. Energy Res.* **2015**, *39*, 1179.
[8] Department of Energy (DOE), Global Energy Storate Database, http://www.energystorageexchange.org/projects (accessed March, 2016).
[9] J. M. Tarascon, M. Armand, *Nature* **2001**, *414*, 359.
[10] M. Armand, J. M. Tarascon, *Nature* **2008**, *451*, 652.
[11] S. Megahed, B. Scrosati, *J. Power Sources* **1994**, *51*, 79.
[12] H. Zhao, Q. Wu, S. Hu, H. Xu, C. N. Rasmussen, *Appl. Energy* **2015**, *137*, 545.
[13] G. Ren, G. Ma, N. Cong, *Renewable Sustainable Energy Rev.* **2015**, *41*, 225.
[14] M. M. Biswas, M. S. Azim, T. K. Saha, U. Zobayer, M. C. Urmi, *Smart Grid and Renewable Energy* **2013**, *4*, 11.
[15] H. Vikström, S. Davidsson, M. Höök, *Appl. Energy* **2013**, *110*, 252.
[16] P. W. Gruber, P. A. Medina, G. A. Keoleian, S. E. Kesler, M. P. Everson, T. J. Wallington, *J. Ind. Ecol.* **2011**, *15*, 760.
[17] The Lithium Market, Fox-Davies Capital, http://www.globalstrategicmetalsnl.com/_content/documents/405.pdf (accessed March, 2016).
[18] S.-W. Kim, D.-H. Seo, X. Ma, G. Ceder, K. Kang, *Adv. Energy Mater.* **2012**, *2*, 710.
[19] S. Y. Hong, Y. Kim, Y. Park, A. Choi, N.-S. Choi, K. T. Lee, *Energy Environ. Sci.* **2013**, *6*, 2067.
[20] H. Pan, Y.-S. Hu, L. Chen, *Energy Environ. Sci.* **2013**, *6*, 2338.
[21] N. Yabuuchi, K. Kubota, M. Dahbi, S. Komaba, *Chem. Rev.* **2014**, *114*, 11636.
[22] X. Lu, B. W. Kirby, W. Xu, G. Li, J. Y. Kim, J. P. Lemmon, V. L. Sprenkle, Z. Yang, *Energy Environ. Sci.* **2013**, *6*, 299.
[23] X. Lu, G. Xia, J. P. Lemmon, Z. Yang, *J. Power Sources* **2010**, *195*, 2431.
[24] B. L. Ellis, L. F. Nazar, *Curr. Opin. Solid State Mater. Sci.* **2012**, *16*, 168.
[25] C. Delmas, J.-J. Braconnier, C. Fouassier, P. Hagenmuller, *Solid State Ionics* **1981**, *3–4*, 165.
[26] C. Delmas, C. Fouassier, P. Hagenmuller, *Physica B+C* **1980**, *99*, 81.
[27] J. J. Braconnier, C. Delmas, P. Hagenmuller, *Mater. Res. Bull.* **1982**, *17*, 993.
[28] M. H. Han, E. Gonzalo, G. Singh, T. Rojo, *Energy Environ. Sci.* **2015**, *8*, 81.
[29] J.-P. Parant, R. Olazcuaga, M. Devalette, C. Fouassier, P. Hagenmuller, *J. Solid State Chem.* **1971**, *3*, 1.
[30] C. Delmas, A. Maazaz, C. Fouassier, J.-M. Réau, P. Hagenmuller, *Mater. Res. Bull.* **1979**, *14*, 329.
[31] Y. Lei, X. Li, L. Liu, G. Ceder, *Chem. Mater.* **2014**, *26*, 5288.
[32] R. Berthelot, D. Carlier, C. Delmas, *Nat. Mater.* **2011**, *10*, 74.
[33] L. W. Shacklette, T. R. Jow, M. Maxfield, R. Hatami, *Synth. Met.* **1989**, *28*, 655.
[34] T. Shibata, Y. Fukuzumi, W. Kobayashi, Y. Moritomo, *Sci. Rep.* **2015**, *5*, 9006.
[35] Y. Mo, S. P. Ong, G. Ceder, *Chem. Mater.* **2014**, *26*, 5208.
[36] J. J. Ding, Y. N. Zhou, Q. Sun, X. Q. Yu, X. Q. Yang, Z. W. Fu, *Electrochim. Acta* **2013**, *87*, 388.
[37] S. C. Han, H. Lim, J. Jeong, D. Ahn, W. B. Park, K.-S. Sohn, M. Pyo, *J. Power Sources* **2015**, *277*, 9.
[38] A. Mendiboure, C. Delmas, P. Hagenmuller, *J. Solid State Chem.* **1985**, *57*, 323.
[39] J. M. Paulsen, J. R. Dahn, *Solid State Ionics* **1999**, *126*, 3.
[40] J. Billaud, G. Singh, A. R. Armstrong, E. Gonzalo, V. Roddatis, M. Armand, T. Rojo, P. G. Bruce, *Energy Environ. Sci.* **2014**, *7*, 1387.
[41] N. Yabuuchi, R. Hara, M. Kajiyama, K. Kubota, T. Ishigaki, A. Hoshikawa, S. Komaba, *Adv. Energy Mater.* **2014**, *4*, 1301453.
[42] N. Yabuuchi, R. Hara, K. Kubota, J. Paulsen, S. Kumakura, S. Komaba, *J. Mater. Chem. A* **2014**, *2*, 16851.
[43] K. Hemalatha, M. Jayakumar, P. Bera, A. S. Prakash, *J. Mater. Chem. A* **2015**, *3*, 20908.
[44] W. Kang, Z. Zhang, P.-K. Lee, T.-W. Ng, W. Li, Y. Tang, W. Zhang, C.-S. Lee, D. Y. Wai Yu, *J. Mater. Chem. A* **2015**, *3*, 22846.
[45] Z. Lu, J. R. Dahn, *J. Electrochem. Soc.* **2001**, *148*, A1225.
[46] D. H. Lee, J. Xu, Y. S. Meng, *Phys. Chem. Chem. Phys.* **2013**, *15*, 3304.
[47] H. Wang, B. Yang, X.-Z. Liao, J. Xu, D. Yang, Y.-S. He, Z.-F. Ma, *Electrochim. Acta* **2013**, *113*, 200.
[48] D. Kim, S.-H. Kang, M. Slater, S. Rood, J. T. Vaughey, N. Karan, M. Balasubramanian, C. S. Johnson, *Adv. Energy Mater.* **2011**, *1*, 333.
[49] W. Zhao, A. Tanaka, K. Momosaki, S. Yamamoto, F. Zhang, Q. Guo, H. Noguchi, *Electrochim. Acta* **2015**, *170*, 171.
[50] I. Hasa, D. Buchholz, S. Passerini, B. Scrosati, J. Hassoun, *Adv. Energy Mater.* **2014**, *4*, 1400083.
[51] J. Xu, D. H. Lee, R. J. Clément, X. Yu, M. Leskes, A. J. Pell, G. Pintacuda, X.-Q. Yang, C. P. Grey, Y. S. Meng, *Chem. Mater.* **2014**, *26*, 1260.
[52] R. Shanmugam, W. Lai, *J. Electrochem. Soc.* **2015**, *162*, A8.
[53] D. Yuan, W. He, F. Pei, F. Wu, Y. Wu, J. Qian, Y. Cao, X. Ai, H. Yang, *J. Mater. Chem. A* **2013**, *1*, 3895.
[54] N. K. Karan, M. D. Slater, F. Dogan, D. Kim, C. S. Johnson, M. Balasubramanian, *J. Electrochem. Soc.* **2014**, *161*, A1107.

[55] N. Yabuuchi, H. Yoshida, S. Komaba, *Electrochemistry* **2012**, *80*, 716.
[56] E. Lee, D. E. Brown, E. E. Alp, Y. Ren, J. Lu, J.-J. Woo, C. S. Johnson, *Chem. Mater.* **2015**, *27*, 6755.
[57] N. Yabuuchi, M. Kajiyama, J. Iwatate, H. Nishikawa, S. Hitomi, R. Okuyama, R. Usui, Y. Yamada, S. Komaba, *Nat. Mater.* **2012**, *11*, 512.
[58] W. K. Pang, S. Kalluri, V. K. Peterson, N. Sharma, J. Kimpton, B. Johannessen, H. K. Liu, S. X. Dou, Z. Guo, *Chem. Mater.* **2015**, *27*, 3150.
[59] E. Talaie, V. Duffort, H. L. Smith, B. Fultz, L. F. Nazar, *Energy Environ. Sci.* **2015**, *8*, 2512.
[60] Y. H. Jung, A. S. Christiansen, R. E. Johnsen, P. Norby, D. K. Kim, *Adv. Funct. Mater.* **2015**, *25*, 3227.
[61] L. Liu, X. Li, S.-H. Bo, Y. Wang, H. Chen, N. Twu, D. Wu, G. Ceder, *Adv. Energy Mater.* **2015**, *5*, 1500944.
[62] J. S. Thorne, R. A. Dunlap, M. N. Obrovac, *J. Electrochem. Soc.* **2014**, *161*, A2232.
[63] E. Lee, J. Lu, Y. Ren, X. Luo, X. Zhang, J. Wen, D. Miller, A. DeWahl, S. Hackney, B. Key, D. Kim, M. D. Slater, C. S. Johnson, *Adv. Energy Mater.* **2014**, *4*, 1400458.
[64] S. Guo, P. Liu, H. Yu, Y. Zhu, M. Chen, M. Ishida, H. Zhou, *Angew. Chem. Int. Ed.* **2015**, *54*, 5894.
[65] Y. Wang, R. Xiao, Y.-S. Hu, M. Avdeev, L. Chen, *Nat. Commun.* **2015**, *6*, 6954.
[66] R. Shanmugam, W. Lai, *ECS Electrochem. Lett.* **2014**, *3*, A23.
[67] X. Chen, X. Zhou, M. Hu, J. Liang, D. Wu, J. Wei, Z. Zhou, *J. Mater. Chem. A* **2015**, *3*, 20708.
[68] X. Ma, H. Chen, G. Ceder, *J. Electrochem. Soc.* **2011**, *158*, A1307.
[69] C.-Y. Chen, K. Matsumoto, T. Nohira, R. Hagiwara, A. Fukunaga, S. Sakai, K. Nitta, S. Inazawa, *J. Power Sources* **2013**, *237*, 52.
[70] S. Komaba, C. Takei, T. Nakayama, A. Ogata, N. Yabuuchi, *Electrochem. Commun.* **2010**, *12*, 355.
[71] S.-T. Myung, S. Komaba, N. Hirosaki, N. Kumagai, K. Arai, R. Kodama, I. Nakai, *J. Electrochem. Soc.* **2003**, *150*, A1560.
[72] C.-Y. Yu, J.-S. Park, H.-G. Jung, K.-Y. Chung, D. Aurbach, Y.-K. Sun, S.-T. Myung, *Energy Environ. Sci.* **2015**, *8*, 2019.
[73] M. H. Han, E. Gonzalo, M. Casas-Cabanas, T. Rojo, *J. Power Sources* **2014**, *258*, 266.
[74] S. Komaba, N. Yabuuchi, T. Nakayama, A. Ogata, T. Ishikawa, I. Nakai, *Inorg. Chem.* **2012**, *51*, 6211.
[75] K. Kang, Y. S. Meng, J. Bréger, C. P. Grey, G. Ceder, *Science* **2006**, *311*, 977.
[76] D. D. Yuan, Y. X. Wang, Y. L. Cao, X. P. Ai, H. X. Yang, *ACS Appl. Mater. Interfaces* **2015**, *7*, 8585.
[77] X. Wang, G. Liu, T. Iwao, M. Okubo, A. Yamada, *J. Phys. Chem. C* **2014**, *118*, 2970.
[78] M. Sathiya, K. Hemalatha, K. Ramesha, J. M. Tarascon, A. S. Prakash, *Chem. Mater.* **2012**, *24*, 1846.
[79] X. Li, D. Wu, Y.-N. Zhou, L. Liu, X.-Q. Yang, G. Ceder, *Electrochem. Commun.* **2014**, *49*, 51.
[80] L. Mu, S. Xu, Y. Li, Y.-S. Hu, H. Li, L. Chen, X. Huang, *Adv. Mater.* **2015**, *27*, 6928.
[81] J.-Y. Hwang, S.-M. Oh, S.-T. Myung, K. Y. Chung, I. Belharouak, Y.-K. Sun, *Nat. Commun.* **2015**, *6*, 6865.
[82] N. Yabuuchi, M. Yano, S. Kuze, S. Komaba, *Electrochim. Acta* **2012**, *82*, 296.
[83] R. Kataoka, T. Mukai, A. Yoshizawa, T. Sakai, *J. Electrochem. Soc.* **2013**, *160*, A933.
[84] H. Liu, J. Xu, C. Ma, Y. S. Meng, *Chem. Commun.* **2015**, *51*, 4693.
[85] S.-M. Oh, S.-T. Myung, C. S. Yoon, J. Lu, J. Hassoun, B. Scrosati, K. Amine, Y.-K. Sun, *Nano Lett.* **2014**, *14*, 1620.
[86] P. Vassilaras, A. J. Toumar, G. Ceder, *Electrochem. Commun.* **2014**, *38*, 79.
[87] S. Guo, H. Yu, P. Liu, Y. Ren, T. Zhang, M. Chen, M. Ishida, H. Zhou, *Energy Environ. Sci.* **2015**, *8*, 1237.
[88] N. Sharma, E. Gonzalo, J. C. Pramudita, M. H. Han, H. E. A. Brand, J. N. Hart, W. K. Pang, Z. Guo, T. Rojo, *Adv. Funct. Mater.* **2015**, *25*, 4994.
[89] D. Buchholz, L. G. Chagas, C. Vaalma, L. Wu, S. Passerini, *J. Mater. Chem. A* **2014**, *2*, 13415.
[90] V. Duffort, E. Talaie, R. Black, L. F. Nazar, *Chem. Mater.* **2015**, *27*, 2515.
[91] M. M. Doeff, M. Y. Peng, Y. Ma, L. C. De Jonghe, *J. Electrochem. Soc.* **1994**, *141*, L145.
[92] F. Sauvage, L. Laffont, J. M. Tarascon, E. Baudrin, *Inorg. Chem.* **2007**, *46*, 3289.
[93] H. Kim, D. J. Kim, D.-H. Seo, M. S. Yeom, K. Kang, D. K. Kim, Y. Jung, *Chem. Mater.* **2012**, *24*, 1205.
[94] J. F. Whitacre, A. Tevar, S. Sharma, *Electrochem. Commun.* **2010**, *12*, 463.
[95] E. Hosono, T. Saito, J. Hoshino, M. Okubo, Y. Saito, D. Nishio-Hamane, T. Kudo, H. Zhou, *J. Power Sources* **2012**, *217*, 43.
[96] X. Zhou, R. K. Guduru, P. Mohanty, *J. Mater. Chem. A* **2013**, *1*, 2757.
[97] M. Xu, Y. Niu, C. Chen, J. Song, S. Bao, C. M. Li, *RSC Adv.* **2014**, *4*, 38140.
[98] K. Dai, J. Mao, X. Song, V. Battaglia, G. Liu, *J. Power Sources* **2015**, *285*, 161.
[99] P. Zhan, S. Wang, Y. Yuan, K. Jiao, S. Jiao, *J. Electrochem. Soc.* **2015**, *162*, A1028.
[100] P. Zhan, K. Jiao, J. Wang, Z. Hu, R. Ma, H. Zhu, S. Jiao, *J. Electrochem. Soc.* **2015**, *162*, A2296.
[101] Y. Niu, M. Xu, C. Cheng, S. Bao, J. Hou, S. Liu, F. Yi, H. He, C. M. Li, *J. Mater. Chem. A* **2015**, *3*, 17224.
[102] D. Hamani, M. Ati, J.-M. Tarascon, P. Rozier, *Electrochem. Commun.* **2011**, *13*, 938.
[103] C. Didier, M. Guignard, J. Darriet, C. Delmas, *Inorg. Chem.* **2012**, *51*, 11007.
[104] D. Chao, C. Zhu, X. Xia, J. Liu, X. Zhang, J. Wang, P. Liang, J. Lin, H. Zhang, Z. X. Shen, H. J. Fan, *Nano Lett.* **2015**, *15*, 565.
[105] Q. Wei, J. Liu, W. Feng, J. Sheng, X. Tian, L. He, Q. An, L. Mai, *J. Mater. Chem. A* **2015**, *3*, 8070.
[106] C. Masquelier, L. Croguennec, *Chem. Rev.* **2013**, *113*, 6552.
[107] H. Kim, I. Park, D.-H. Seo, S. Lee, S.-W. Kim, W. J. Kwon, Y.-U. Park, C. S. Kim, S. Jeon, K. Kang, *J. Am. Chem. Soc.* **2012**, *134*, 10369.
[108] P. Barpanda, G. Oyama, S.-i. Nishimura, S.-C. Chung, A. Yamada, *Nat. Commun.* **2014**, *5*, 4358.
[109] P. Moreau, D. Guyomard, J. Gaubicher, F. Boucher, *Chem. Mater.* **2010**, *22*, 4126.
[110] K. T. Lee, T. N. Ramesh, F. Nan, G. Botton, L. F. Nazar, *Chem. Mater.* **2011**, *23*, 3593.
[111] J. Lu, S. C. Chung, S.-i. Nishimura, A. Yamada, *Chem. Mater.* **2013**, *25*, 4557.
[112] F. Boucher, J. Gaubicher, M. Cuisinier, D. Guyomard, P. Moreau, *J. Am. Chem. Soc.* **2014**, *136*, 9144.
[113] M. Galceran, V. Roddatis, F. J. Zúñiga, J. M. Pérez-Mato, B. Acebedo, R. Arenal, I. Peral, T. Rojo, M. Casas-Cabanas, *Chem. Mater.* **2014**, *26*, 3289.
[114] M. Galceran, D. Saurel, B. Acebedo, V. V. Roddatis, E. Martin, T. Rojo, M. Casas-Cabanas, *Phys. Chem. Chem. Phys.* **2014**, *16*, 8837.
[115] J. Kim, D.-H. Seo, H. Kim, I. Park, J.-K. Yoo, S.-K. Jung, Y.-U. Park, W. A. Goddard Iii, K. Kang, *Energy Environ. Sci.* **2015**, *8*, 540.
[116] S.-M. Oh, S.-T. Myung, J. Hassoun, B. Scrosati, Y.-K. Sun, *Electrochem. Commun.* **2012**, *22*, 149.
[117] R. Tripathi, S. M. Wood, M. S. Islam, L. F. Nazar, *Energy Environ. Sci.* **2013**, *6*, 2257.

[118] Y. Zhu, Y. Xu, Y. Liu, C. Luo, C. Wang, *Nanoscale* **2013**, *5*, 780.
[119] T. Shiratsuchi, S. Okada, J. Yamaki, T. Nishida, *J. Power Sources* **2006**, *159*, 268.
[120] C. Li, X. Miao, W. Chu, P. Wu, D. G. Tong, *J. Mater. Chem. A* **2015**, *3*, 8265.
[121] Y. Fang, L. Xiao, J. Qian, X. Ai, H. Yang, Y. Cao, *Nano Lett.* **2014**, *14*, 3539.
[122] Y. Kim, Y. Park, A. Choi, N.-S. Choi, J. Kim, J. Lee, J. H. Ryu, S. M. Oh, K. T. Lee, *Adv. Mater.* **2013**, *25*, 3045.
[123] J. Qian, Y. Chen, L. Wu, Y. Cao, X. Ai, H. Yang, *Chem. Commun.* **2012**, *48*, 7070.
[124] W.-J. Li, S.-L. Chou, J.-Z. Wang, H.-K. Liu, S.-X. Dou, *Nano Lett.* **2013**, *13*, 5480.
[125] J. B. Goodenough, H. Y. P. Hong, J. A. Kafalas, *Mater. Res. Bull.* **1976**, *11*, 203.
[126] L. S. Plashnitsa, E. Kobayashi, Y. Noguchi, S. Okada, J.-i. Yamaki, *J. Electrochem. Soc.* **2010**, *157*, A536.
[127] Z. Jian, W. Han, X. Lu, H. Yang, Y.-S. Hu, J. Zhou, Z. Zhou, J. Li, W. Chen, D. Chen, L. Chen, *Adv. Energy Mater.* **2013**, *3*, 156.
[128] Y. Fang, L. Xiao, X. Ai, Y. Cao, H. Yang, *Adv. Mater.* **2015**, *27*, 5895.
[129] Z. Jian, L. Zhao, H. Pan, Y.-S. Hu, H. Li, W. Chen, L. Chen, *Electrochem. Commun.* **2012**, *14*, 86.
[130] Y. Uebou, T. Kiyabu, S. Okada, J.-i. Yamaki, *Rep. Inst. Adv. Mater. Study, Kyushu Univ.* **2002**, *16*, 1.
[131] K. Saravanan, C. W. Mason, A. Rudola, K. H. Wong, P. Balaya, *Adv. Energy Mater.* **2013**, *3*, 444.
[132] X. Rui, W. Sun, C. Wu, Y. Yu, Q. Yan, *Adv. Mater.* **2015**, *27*, 6670.
[133] K. Trad, D. Carlier, L. Croguennec, A. Wattiaux, B. Lajmi, M. Ben Amara, C. Delmas, *J. Phys. Chem. C* **2010**, *114*, 10034.
[134] K. Trad, D. Carlier, L. Croguennec, A. Wattiaux, M. Ben Amara, C. Delmas, *Chem. Mater.* **2010**, *22*, 5554.
[135] W. Huang, B. Li, M. F. Saleem, X. Wu, J. Li, J. Lin, D. Xia, W. Chu, Z. Wu, *Chem. – Eur. J.* **2015**, *21*, 851.
[136] J. Song, M. Xu, L. Wang, J. B. Goodenough, *Chem. Commun.* **2013**, *49*, 5280.
[137] W. Huang, J. Zhou, B. Li, L. An, P. Cui, W. Xia, L. Song, D. Xia, W. Chu, Z. Wu, *Small* **2015**, *11*, 2170.
[138] W. Li, M. Zhou, H. Li, K. Wang, S. Cheng, K. Jiang, *Energy Environ. Sci.* **2015**, *8*, 2916.
[139] F. Sanz, C. Parada, C. Ruiz-Valero, *J. Mater. Chem.* **2001**, *11*, 208.
[140] O. V. Yakubovich, O. V. Karimova, O. K. Mel'nikov, *Acta Cryst. C* **1997**, *53*, 395.
[141] B. L. Ellis, W. R. M. Makahnouk, Y. Makimura, K. Toghill, L. F. Nazar, *Nat. Mater.* **2007**, *6*, 749.
[142] N. Recham, J.-N. Chotard, L. Dupont, K. Djellab, M. Armand, J.-M. Tarascon, *J. Electrochem. Soc.* **2009**, *156*, A993.
[143] B. L. Ellis, W. R. M. Makahnouk, W. N. Rowan-Weetaluktuk, D. H. Ryan, L. F. Nazar, *Chem. Mater.* **2010**, *22*, 1059.
[144] Y. Kawabe, N. Yabuuchi, M. Kajiyama, N. Fukuhara, T. Inamasu, R. Okuyama, I. Nakai, S. Komaba, *Electrochem. Commun.* **2011**, *13*, 1225.
[145] X. Wu, J. Zheng, Z. Gong, Y. Yang, *J. Mater. Chem.* **2011**, *21*, 18630.
[146] S.-W. Kim, D.-H. Seo, H. Kim, K.-Y. Park, K. Kang, *Phys. Chem. Chem. Phys.* **2012**, *14*, 3299.
[147] Y. Zhong, Z. Wu, Y. Tang, W. Xiang, X. Guo, B. Zhong, *Mater. Lett.* **2015**, *145*, 269.
[148] H. Zou, S. Li, X. Wu, M. J. McDonald, Y. Yang, *ECS Electrochem. Lett.* **2015**, *4*, A53.
[149] K. Kubota, K. Yokoh, N. Yabuuchi, S. Komaba, *Electrochemistry* **2014**, *82*, 909.
[150] Y.-U. Park, D.-H. Seo, H. Kim, J. Kim, S. Lee, B. Kim, K. Kang, *Adv. Funct. Mater.* **2014**, *24*, 4603.
[151] M. Bianchini, F. Fauth, N. Brisset, F. Weill, E. Suard, C. Masquelier, L. Croguennec, *Chem. Mater.* **2015**, *27*, 3009.
[152] Y.-U. Park, D.-H. Seo, H.-S. Kwon, B. Kim, J. Kim, H. Kim, I. Kim, H.-I. Yoo, K. Kang, *J. Am. Chem. Soc.* **2013**, *135*, 13870.
[153] X. Lin, X. Hou, X. Wu, S. Wang, M. Gao, Y. Yang, *RSC Adv.* **2014**, *4*, 40985.
[154] Y. Kawabe, N. Yabuuchi, M. Kajiyama, N. Fukuhara, T. Inamasu, R. Okuyama, I. Nakai, S. Komaba, *Electrochemistry* **2012**, *80*, 80.
[155] J. Barker, M. Y. Saidi, J. L. Swoyer, *Electrochem. Solid-State Lett.* **2003**, *6*, A1.
[156] T. Jiang, G. Chen, A. Li, C. Wang, Y. Wei, *J. Alloys Compd.* **2009**, *478*, 604.
[157] J. Zhao, J. He, X. Ding, J. Zhou, Y. o. Ma, S. Wu, R. Huang, *J. Power Sources* **2010**, *195*, 6854.
[158] H. Zhuo, X. Wang, A. Tang, Z. Liu, S. Gamboa, P. J. Sebastian, *J. Power Sources* **2006**, *160*, 698.
[159] Z.-m. Liu, X.-y. Wang, Y. Wang, A.-p. Tang, S.-y. Yang, L.-f. He, *Trans. Nonferrous Met. Soc. China* **2008**, *18*, 346.
[160] Y.-L. Ruan, K. Wang, S.-D. Song, X. Han, B.-W. Cheng, *Electrochim. Acta* **2015**, *160*, 330.
[161] J. M. Le Meins, M. P. Crosnier-Lopez, A. Hemon-Ribaud, G. Courbion, *J. Solid State Chem.* **1999**, *148*, 260.
[162] R. K. B. Gover, A. Bryan, P. Burns, J. Barker, *Solid State Ionics* **2006**, *177*, 1495.
[163] R. A. Shakoor, D.-H. Seo, H. Kim, Y.-U. Park, J. Kim, S.-W. Kim, H. Gwon, S. Lee, K. Kang, *J. Mater. Chem.* **2012**, *22*, 20535.
[164] M. Bianchini, N. Brisset, F. Fauth, F. Weill, E. Elkaim, E. Suard, C. Masquelier, L. Croguennec, *Chem. Mater.* **2014**, *26*, 4238.
[165] B. Zhang, R. Dugas, G. Rousse, P. Rozier, A. M. Abakumov, J.-M. Tarascon, *Nat. Commun.* **2016**, *7*, 10308.
[166] F. Sauvage, E. Quarez, J. M. Tarascon, E. Baudrin, *Solid State Sci.* **2006**, *8*, 1215.
[167] Y. Qi, L. Mu, J. Zhao, Y.-S. Hu, H. Liu, S. Dai, *Angew. Chem.* **2015**, *127*, 10049.
[168] N. Sharma, P. Serras, V. Palomares, H. E. A. Brand, J. Alonso, P. Kubiak, M. L. Fdez-Gubieda, T. Rojo, *Chem. Mater.* **2014**, *26*, 3391.
[169] P. Serras, V. Palomares, J. Alonso, N. Sharma, J. M. L. del Amo, P. Kubiak, M. L. Fdez-Gubieda, T. Rojo, *Chem. Mater.* **2013**, *25*, 4917.
[170] P. Barpanda, M. Ati, B. C. Melot, G. Rousse, J. N. Chotard, M. L. Doublet, M. T. Sougrati, S. A. Corr, J. C. Jumas, J. M. Tarascon, *Nat. Mater.* **2011**, *10*, 772.
[171] N. Recham, J. N. Chotard, L. Dupont, C. Delacourt, W. Walker, M. Armand, J. M. Tarascon, *Nat. Mater.* **2010**, *9*, 68.
[172] R. Tripathi, G. R. Gardiner, M. S. Islam, L. F. Nazar, *Chem. Mater.* **2011**, *23*, 2278.
[173] R. Tripathi, T. N. Ramesh, B. L. Ellis, L. F. Nazar, *Angew. Chem.* **2010**, *122*, 8920.
[174] P. Barpanda, J.-N. Chotard, N. Recham, C. Delacourt, M. Ati, L. Dupont, M. Armand, J.-M. Tarascon, *Inorg. Chem.* **2010**, *49*, 7401.
[175] N. Recham, G. Rousse, M. T. Sougrati, J.-N. Chotard, C. Frayret, S. Mariyappan, B. C. Melot, J.-C. Jumas, J.-M. Tarascon, *Chem. Mater.* **2012**, *24*, 4363.
[176] G. Rousse, J. M. Tarascon, *Chem. Mater.* **2014**, *26*, 394.
[177] M. Reynaud, P. Barpanda, G. Rousse, J.-N. Chotard, B. C. Melot, N. Recham, J.-M. Tarascon, *Solid State Sci.* **2012**, *14*, 15.
[178] M. Ati, L. Dupont, N. Recham, J. N. Chotard, W. T. Walker, C. Davoisne, P. Barpanda, V. Sarou-Kanian, M. Armand, J. M. Tarascon, *Chem. Mater.* **2010**, *22*, 4062.
[179] B. C. Melot, J. N. Chotard, G. Rousse, M. Ati, M. Reynaud, J. M. Tarascon, *Inorg. Chem.* **2011**, *50*, 7662.
[180] P. Barpanda, G. Oyama, C. D. Ling, A. Yamada, *Chem. Mater.* **2014**, *26*, 1297.

[181] M. Reynaud, G. Rousse, A. M. Abakumov, M. T. Sougrati, G. Van Tendeloo, J.-N. Chotard, J.-M. Tarascon, *J. Mater. Chem. A* **2014**, *2*, 2671.
[182] P. Singh, K. Shiva, H. Celio, J. B. Goodenough, *Energy Environ. Sci.* **2015**, *8*, 3000.
[183] M. Xie, M. Xu, Y. Huang, R. Chen, X. Zhang, L. Li, F. Wu, *Electrochem. Commun.* **2015**, *59*, 91.
[184] Y. Meng, Q. Li, T. Yu, S. Zhang, C. Deng, *CrystEngComm* **2016**, *18*, 1645.
[185] G. Oyama, S.-i. Nishimura, Y. Suzuki, M. Okubo, A. Yamada, *ChemElectroChem* **2015**, *2*, 1019.
[186] L. L. Wong, H. M. Chen, S. Adams, *Phys. Chem. Chem. Phys.* **2015**, *17*, 9186.
[187] D. Dwibedi, R. B. Araujo, S. Chakraborty, P. P. Shanbogh, N. G. Sundaram, R. Ahuja, P. Barpanda, *J. Mater. Chem. A* **2015**, *3*, 18564.
[188] R. B. Araujo, M. S.-u. Islam, S. Chakraborty, R. Ahuja, *J. Mater. Chem. A* **2016**, *4*, 451.
[189] S. Wei, B. M. de Boisse, G. Oyama, S.-i. Nishimura, A. Yamada, *ChemElectroChem* **2015**, *3*, 209.
[190] P. Barpanda, T. Ye, S.-i. Nishimura, S.-C. Chung, Y. Yamada, M. Okubo, H. Zhou, A. Yamada, *Electrochem. Commun.* **2012**, *24*, 116.
[191] P. Barpanda, T. Ye, M. Avdeev, S.-C. Chung, A. Yamada, *J. Mater. Chem. A* **2013**, *1*, 4194.
[192] S.-i. Nishimura, M. Nakamura, R. Natsui, A. Yamada, *J. Am. Chem. Soc.* **2010**, *132*, 13596.
[193] H. Kim, S. Lee, Y.-U. Park, H. Kim, J. Kim, S. Jeon, K. Kang, *Chem. Mater.* **2011**, *23*, 3930.
[194] P. Barpanda, S.-i. Nishimura, A. Yamada, *Adv. Energy Mater.* **2012**, *2*, 841.
[195] H. Kim, R. A. Shakoor, C. Park, S. Y. Lim, J.-S. Kim, Y. N. Jo, W. Cho, K. Miyasaka, R. Kahraman, Y. Jung, J. W. Choi, *Adv. Funct. Mater.* **2013**, *23*, 1147.
[196] K.-H. Ha, S. H. Woo, D. Mok, N.-S. Choi, Y. Park, S. M. Oh, Y. Kim, J. Kim, J. Lee, L. F. Nazar, K. T. Lee, *Adv. Energy Mater.* **2013**, *3*, 770.
[197] G. Longoni, J. E. Wang, Y. H. Jung, D. K. Kim, C. M. Mari, R. Ruffo, *J. Power Sources* **2016**, *302*, 61.
[198] Y. Niu, M. Xu, S.-J. Bao, C. M. Li, *Chem. Commun.* **2015**, *51*, 13120.
[199] C.-Y. Chen, K. Matsumoto, T. Nohira, R. Hagiwara, Y. Orikasa, Y. Uchimoto, *J. Power Sources* **2014**, *246*, 783.
[200] P. Barpanda, G. Liu, C. D. Ling, M. Tamaru, M. Avdeev, S.-C. Chung, Y. Yamada, A. Yamada, *Chem. Mater.* **2013**, *25*, 3480.
[201] C. S. Park, H. Kim,R. A. Shakoor, E. Yang, S. Y. Lim, R. Kahraman, Y. Jung, J. W. Choi,*J. Am. Chem. Soc.* **2013**, *135*, 2787.
[202] J. M. Clark, P. Barpanda, A. Yamada, M. S. Islam, *J. Mater. Chem. A* **2014**, *2*, 11807.
[203] N. Furuta, S.-i. Nishimura, P. Barpanda, A. Yamada, *Chem. Mater.* **2012**, *24*, 1055.
[204] P. Barpanda, G. Liu, Z. Mohamed, C. D. Ling, A. Yamada, *Solid State Ionics* **2014**, *268, Part B*, 305.
[205] P. Barpanda, G. Liu, M. Avdeev, A. Yamada, *ChemElectroChem* **2014**, *1*, 1488.
[206] Y. Kee, N. Dimov, A. Staikov, P. Barpanda, Y.-C. Lu, K. Minami, S. Okada, *RSC Adv.* **2015**, *5*, 64991.
[207] J. Kim, I. Park, H. Kim, K.-Y. Park, Y.-U. Park, K. Kang, *Adv. Energy Mater.* **2016**, 1502147.
[208] J. Y. Jang, H. Kim, Y. Lee, K. T. Lee, K. Kang, N.-S. Choi, *Electrochem. Commun.* **2014**, *44*, 74.
[209] H. Kim, I. Park, S. Lee, H. Kim, K.-Y. Park, Y.-U. Park, H. Kim, J. Kim, H.-D. Lim, W.-S. Yoon, K. Kang, *Chem. Mater.* **2013**, *25*, 3614.
[210] H. Kim, G. Yoon, I. Park, K.-Y. Park, B. Lee, J. Kim, Y.-U. Park, S.-K. Jung, H.-D. Lim, D. Ahn, S. Lee, K. Kang, *Energy Environ. Sci.* **2015**, *8*, 3325.
[211] S. Y. Lim, H. Kim, J. Chung, J. H. Lee, B. G. Kim, J.-J. Choi, K. Y. Chung, W. Cho, S.-J. Kim, W. A. Goddard, Y. Jung, J. W. Choi, *Proc. Natl. Acad. Sci. USA* **2014**, *111*, 599.
[212] Y. Lu, L. Wang, J. Cheng, J. B. Goodenough, *Chem. Commun.* **2012**, *48*, 6544.
[213] J. Song, L. Wang, Y. Lu, J. Liu, B. Guo, P. Xiao, J.-J. Lee, X.-Q. Yang, G. Henkelman, J. B. Goodenough, *J. Am. Chem. Soc.* **2015**, *137*, 2658.
[214] M. Nose, H. Nakayama, K. Nobuhara, H. Yamaguchi, S. Nakanishi, H. Iba, *J. Power Sources* **2013**, *234*, 175.
[215] M. Nose, S. Shiotani, H. Nakayama, K. Nobuhara, S. Nakanishi, H. Iba, *Electrochem. Commun.* **2013**, *34*, 266.
[216] S. M. Wood, C. Eames, E. Kendrick, M. S. Islam, *J. Phys. Chem. C* **2015**, *119*, 15935.
[217] C. Deng, S. Zhang, *ACS Appl. Mater. Interfaces* **2014**, *6*, 9111.
[218] G. Hautier, A. Jain, H. Chen, C. Moore, S. P. Ong, G. Ceder, *J. Mater. Chem.* **2011**, *21*, 17147.
[219] H. Chen, G. Hautier, G. Ceder, *J. Am. Chem. Soc.* **2012**, *134*, 19619.
[220] W. Huang, J. Zhou, B. Li, J. Ma, S. Tao, D. Xia, W. Chu, Z. Wu, *Sci. Rep.* **2014**, *4*, 4188.
[221] Y. Uebou, S. Okada, J.-i. Yamaki, *J. Power Sources* **2003**, *115*, 119.
[222] M. Gnanavel, O. I. Lebedev, P. Bazin, B. Raveau, V. Pralong, *Solid State Ionics* **2015**, *278*, 38.
[223] Y. Zhang, H. Yu, H. Zhou, *J. Mater. Chem. A* **2014**, *2*, 11574.
[224] J. Liu, D. Chang, P. Whitfield, Y. Janssen, X. Yu, Y. Zhou, J. Bai, J. Ko, K.-W. Nam, L. Wu, Y. Zhu, M. Feygenson, G. Amatucci, A. Van der Ven, X.-Q. Yang, P. Khalifah, *Chem. Mater.* **2014**, *26*, 3295.
[225] S. Wang, J. Zhao, L. Wang, X. Liu, Y. Wu, J. Xu, *Ionics* **2015**, *21*, 2633.
[226] H. Yaghoobnejad Asl, P. Stanley, K. Ghosh, A. Choudhury, *Chem. Mater.* **2015**, *27*, 7058.
[227] X. Lin, Y. Zhao, Y. Dong, Q. Kuang, Z. Liang, D. Yan, X. Liu, *Mater. Sci. Eng. B* **2015**, *197*, 58.
[228] D. Kundu, R. Tripathi, G. Popov, W. R. M. Makahnouk, L. F. Nazar, *Chem. Mater.* **2015**, *27*, 885.
[229] L. Wang, Y. Lu, J. Liu, M. Xu, J. Cheng, D. Zhang, J. B. Goodenough, *Angew. Chem. Int. Ed.* **2013**, *52*, 1964.
[230] H.-W. Lee, R. Y. Wang, M. Pasta, S. W. Lee, N. Liu, Y. Cui, *Nat. Commun.* **2014**, *5*, 5280.
[231] L. Wang, J. Song, R. Qiao, L. A. Wray, M. A. Hossain, Y.-D. Chuang, W. Yang, Y. Lu, D. Evans, J.-J. Lee, S. Vail, X. Zhao, M. Nishijima, S. Kakimoto, J. B. Goodenough, *J. Am. Chem. Soc.* **2015**, *137*, 2548.
[232] D. Yang, J. Xu, X.-Z. Liao, H. Wang, Y.-S. He, Z.-F. Ma, *Chem. Commun.* **2015**, *51*, 8181.
[233] H. Kim, J. Hong, K.-Y. Park, H. Kim, S.-W. Kim, K. Kang, *Chem. Rev.* **2014**, *114*, 11788.
[234] C. D. Wessells, S. V. Peddada, R. A. Huggins, Y. Cui, *Nano Lett.* **2011**, *11*, 5421.
[235] C. D. Wessells, R. A. Huggins, Y. Cui, *Nat. Commun.* **2011**, *2*, 550.
[236] S.-H. Yu, M. Shokouhimehr, T. Hyeon, Y.-E. Sung, *ECS Electrochem. Lett.* **2013**, *2*, A39.
[237] X. Wu, W. Deng, J. Qian, Y. Cao, X. Ai, H. Yang, *J. Mater. Chem. A* **2013**, *1*, 10130.
[238] S. J. R. Prabakar, J. Jeong, M. Pyo, *RSC Adv.* **2015**, *5*, 37545.
[239] T. Matsuda, M. Takachi, Y. Moritomo, *Chem. Commun.* **2013**, *49*, 2750.
[240] M. Okubo, C. H. Li, D. R. Talham, *Chem. Commun.* **2014**, *50*, 1353.
[241] Y. You, X. Yu, Y. Yin, K.-W. Nam, Y.-G. Guo, *Nano Res.* **2015**, *8*, 117.
[242] Y. Yue, A. J. Binder, B. Guo, Z. Zhang, Z.-A. Qiao, C. Tian, S. Dai, *Angew. Chem.* **2014**, *126*, 3198.
[243] M. Xie, Y. Huang, M. Xu, R. Chen, X. Zhang, L. Li, F. Wu, *J. Power Sources* **2016**, *302*, 7.

[244] D. Yang, J. Xu, X.-Z. Liao, Y.-S. He, H. Liu, Z.-F. Ma, *Chem. Commun.* **2014**, *50*, 13377.
[245] D. Asakura, C. H. Li, Y. Mizuno, M. Okubo, H. Zhou, D. R. Talham, *J. Am. Chem. Soc.* **2013**, *135*, 2793.
[246] Y. You, X.-L. Wu, Y.-X. Yin, Y.-G. Guo, *Energy Environ. Sci.* **2014**, *7*, 1643.
[247] X. Wu, C. Wu, C. Wei, L. Hu, J. Qian, Y. Cao, X. Ai, J. Wang, H. Yang, *ACS Appl. Mater. Interfaces* **2016**, *8*, 5393.
[248] H. Lee, Y.-I. Kim, J.-K. Park, J. W. Choi, *Chem. Commun.* **2012**, *48*, 8416.
[249] J. Qian, M. Zhou, Y. Cao, X. Ai, H. Yang, *Adv. Energy Mater.* **2012**, *2*, 410.
[250] B. Häupler, A. Wild, U. S. Schubert, *Adv. Energy Mater.* **2015**, *5*, 1402034.
[251] Y. Liang, Z. Tao, J. Chen, *Adv. Energy Mater.* **2012**, *2*, 742.
[252] Z. Song, H. Zhou, *Energy Environ. Sci.* **2013**, *6*, 2280.
[253] Z. Zhu, J. Chen, *J. Electrochem. Soc.* **2015**, *162*, A2393.
[254] H. Chen, M. Armand, G. Demailly, F. Dolhem, P. Poizot, J.-M. Tarascon, *ChemSusChem* **2008**, *1*, 348.
[255] K. Chihara, N. Chujo, A. Kitajou, S. Okada, *Electrochim. Acta* **2013**, *110*, 240.
[256] C. Wang, Y. Fang, Y. Xu, L. Liang, M. Zhou, H. Zhao, Y. Lei, *Adv. Funct. Mater.* **2016**, *26*, 1777.
[257] H. Kim, D.-H. Seo, G. Yoon, W. A. Goddard, Y. S. Lee, W.-S. Yoon, K. Kang, *J. Phys. Chem. Lett.* **2014**, *5*, 3086.
[258] D.-H. Seo, H. Kim, H. Kim, W. A. Goddard, K. Kang, *Energy Environ. Sci.* **2011**, *4*, 4938.
[259] W. Luo, M. Allen, V. Raju, X. Ji, *Adv. Energy Mater.* **2014**, *4*, 1400554.
[260] H.-g. Wang, S. Yuan, D.-l. Ma, X.-l. Huang, F.-l. Meng, X.-b. Zhang, *Adv. Energy Mater.* **2014**, *4*, 1301651.
[261] H. Banda, D. Damien, K. Nagarajan, M. Hariharan, M. M. Shaijumon, *J. Mater. Chem. A* **2015**, *3*, 10453.
[262] W. Deng, Y. Shen, J. Qian, Y. Cao, H. Yang, *ACS Appl. Mater. Interfaces* **2015**, *7*, 21095.
[263] F. Xu, J. Xia, W. Shi, *Electrochem. Commun.* **2015**, *60*, 117.
[264] H. Kim, J. E. Kwon, B. Lee, J. Hong, M. Lee, S. Y. Park, K. Kang, *Chem. Mater.* **2015**, *27*, 7258.
[265] R. Zhao, L. Zhu, Y. Cao, X. Ai, H. X. Yang, *Electrochem. Commun.* **2012**, *21*, 36.
[266] W. Deng, X. Liang, X. Wu, J. Qian, Y. Cao, X. Ai, J. Feng, H. Yang, *Sci. Rep.* **2013**, *3*, 2671.
[267] K. Sakaushi, E. Hosono, G. Nickerl, T. Gemming, H. Zhou, S. Kaskel, J. Eckert, *Nat. Commun.* **2013**, *4*, 1485.
[268] P. Ge, M. Fouletier, *Solid State Ionics* **1988**, *28*, 1172.
[269] D. A. Stevens, J. R. Dahn, *J. Electrochem. Soc.* **2001**, *148*, A803.
[270] Z. Wang, S. M. Selbach, T. Grande, *RSC Adv.* **2014**, *4*, 4069.
[271] K. Nobuhara, H. Nakayama, M. Nose, S. Nakanishi, H. Iba, *J. Power Sources* **2013**, *243*, 585.
[272] Y. Okamoto, *J. Phys. Chem. C* **2014**, *118*, 16.
[273] G. Yoon, D.-H. Seo, K. Ku, J. Kim, S. Jeon, K. Kang, *Chem. Mater.* **2015**, *27*, 2067.
[274] Y. S. Yun, K.-Y. Park, B. Lee, S. Y. Cho, Y.-U. Park, S. J. Hong, B. H. Kim, H. Gwon, H. Kim, S. Lee, Y. W. Park, H.-J. Jin, K. Kang, *Adv. Mater.* **2015**, *27*, 6914.
[275] C. Bommier, T. W. Surta, M. Dolgos, X. Ji, *Nano Lett.* **2015**, *15*, 5888.
[276] P.-c. Tsai, S.-C. Chung, S.-k. Lin, A. Yamada, *J. Mater. Chem. A* **2015**, *3*, 9763.
[277] M. M. Doeff, Y. Ma, S. J. Visco, L. C. De Jonghe, *J. Electrochem. Soc.* **1993**, *140*, L169.
[278] X. Zhou, Y.-G. Guo, *ChemElectroChem* **2014**, *1*, 83.
[279] H.-G. Wang, S. Yuan, D.-L. Ma, X.-B. Zhang, J.-M. Yan, *Energy Environ. Sci.* **2015**, *8*, 1660.
[280] D. A. Stevens, J. R. Dahn, *J. Electrochem. Soc.* **2000**, *147*, 4428.
[281] D. A. Stevens, J. R. Dahn, *J. Electrochem. Soc.* **2000**, *147*, 1271.
[282] R. Alcántara, J. M. Jiménez-Mateos, P. Lavela, J. L. Tirado, *Electrochem. Commun.* **2001**, *3*, 639.
[283] P. Thomas, D. Billaud, *Electrochim. Acta* **2002**, *47*, 3303.
[284] R. Alcántara, P. Lavela, G. F. Ortiz, J. L. Tirado, *Electrochem. Solid-State Lett.* **2005**, *8*, A222.
[285] S. Wenzel, T. Hara, J. Janek, P. Adelhelm, *Energy Environ. Sci.* **2011**, *4*, 3342.
[286] Y. Cao, L. Xiao, M. L. Sushko, W. Wang, B. Schwenzer, J. Xiao, Z. Nie, L. V. Saraf, Z. Yang, J. Liu, *Nano Lett.* **2012**, *12*, 3783.
[287] J. Ding, H. Wang, Z. Li, A. Kohandehghan, K. Cui, Z. Xu, B. Zahiri, X. Tan, E. M. Lotfabad, B. C. Olsen, D. Mitlin, *ACS Nano* **2013**, *7*, 11004.
[288] K.-l. Hong, L. Qie, R. Zeng, Z.-q. Yi, W. Zhang, D. Wang, W. Yin, C. Wu, Q.-j. Fan, W.-x. Zhang, Y.-h. Huang, *J. Mater. Chem. A* **2014**, *2*, 12733.
[289] L. Fu, K. Tang, K. Song, P. A. van Aken, Y. Yu, J. Maier, *Nanoscale* **2014**, *6*, 1384.
[290] H. Liu, M. Jia, N. Sun, B. Cao, R. Chen, Q. Zhu, F. Wu, N. Qiao, B. Xu, *ACS Appl. Mater. Interfaces* **2015**, *7*, 27124.
[291] T. Yang, T. Qian, M. Wang, X. Shen, N. Xu, Z. Sun, C. Yan, *Adv. Mater.* **2016**, *28*, 539.
[292] Z. Jian, Z. Xing, C. Bommier, Z. Li, X. Ji, *Adv. Energy Mater.* **2015**, 1501874.
[293] L. Wu, D. Buchholz, C. Vaalma, G. A. Giffin, S. Passerini, *ChemElectroChem* **2015**, n/a.
[294] H.-g. Wang, Z. Wu, F.-l. Meng, D.-l. Ma, X.-l. Huang, L.-m. Wang, X.-b. Zhang, *ChemSusChem* **2013**, *6*, 56.
[295] K. Kuratani, M. Yao, H. Senoh, N. Takeichi, T. Sakai, T. Kiyobayashi, *Electrochim. Acta* **2012**, *76*, 320.
[296] X. Xia, J. R. Dahn, *J. Electrochem. Soc.* **2012**, *159*, A515.
[297] Z. Wang, L. Qie, L. Yuan, W. Zhang, X. Hu, Y. Huang, *Carbon* **2013**, *55*, 328.
[298] Y.-X. Wang, S.-L. Chou, H.-K. Liu, S.-X. Dou, *Carbon* **2013**, *57*, 202.
[299] A. Ponrouch, A. R. Goñi, M. R. Palacín, *Electrochem. Commun.* **2013**, *27*, 85.
[300] J. Zhao, L. Zhao, K. Chihara, S. Okada, J.-i. Yamaki, S. Matsumoto, S. Kuze, K. Nakane, *J. Power Sources* **2013**, *244*, 752.
[301] K. Gotoh, T. Ishikawa, S. Shimadzu, N. Yabuuchi, S. Komaba, K. Takeda, A. Goto, K. Deguchi, S. Ohki, K. Hashi, T. Shimizu, H. Ishida, *J. Power Sources* **2013**, *225*, 137.
[302] E. M. Lotfabad, J. Ding, K. Cui, A. Kohandehghan, W. P. Kalisvaart, M. Hazelton, D. Mitlin, *ACS Nano* **2014**, *8*, 7115.
[303] C. Bommier, W. Luo, W.-Y. Gao, A. Greaney, S. Ma, X. Ji, *Carbon* **2014**, *76*, 165.
[304] J. Liu, H. Liu, T. Yang, G. Wang, M. Tade, *Chin. Sci. Bull.* **2014**, *59*, 2186.
[305] A. Suryawanshi, D. Mhamane, S. Nagane, S. Patil, V. Aravindan, S. Ogale, M. Srinivasan, *Electrochim. Acta* **2014**, *146*, 218.
[306] V. G. Pol, E. Lee, D. Zhou, F. Dogan, J. M. Calderon-Moreno, C. S. Johnson, *Electrochim. Acta* **2014**, *127*, 61.
[307] A. Fukunaga, T. Nohira, R. Hagiwara, K. Numata, E. Itani, S. Sakai, K. Nitta, S. Inazawa, *J. Power Sources* **2014**, *246*, 387.
[308] Y. Matsuo, K. Ueda, *J. Power Sources* **2014**, *263*, 158.
[309] L. Zeng, W. Li, J. Cheng, J. Wang, X. Liu, Y. Yu, *RSC Adv.* **2014**, *4*, 16920.
[310] W. Li, L. Zeng, Z. Yang, L. Gu, J. Wang, X. Liu, J. Cheng, Y. Yu, *Nanoscale* **2014**, *6*, 693.
[311] Y. Bai, Z. Wang, C. Wu, R. Xu, F. Wu, Y. Liu, H. Li, Y. Li, J. Lu, K. Amine, *ACS Appl. Mater. Interfaces* **2015**, *7*, 5598.
[312] W. Luo, Z. Jian, Z. Xing, W. Wang, C. Bommier, M. M. Lerner, X. Ji, *ACS Cent. Sci.* **2015**, *1*, 516.
[313] H. Hou, C. E. Banks, M. Jing, Y. Zhang, X. Ji, *Adv. Mater.* **2015**, *27*, 7861.

[314] F. Yang, Z. Zhang, K. Du, X. Zhao, W. Chen, Y. Lai, J. Li, *Carbon* **2015**, *91*, 88.
[315] A. Ponrouch, M. R. Palacín, *Electrochem. Commun.* **2015**, *54*, 51.
[316] K. R. Saravanan, V. Mullaivananathan, N. Kalaiselvi, *Electrochim. Acta* **2015**, *176*, 670.
[317] L.-J. Song, S.-S. Liu, B.-J. Yu, C.-Y. Wang, M.-W. Li, *Carbon* **2015**, *95*, 972.
[318] A. Ramos, I. Cameán, N. Cuesta, A. B. García, *Electrochim. Acta* **2015**, *178*, 392.
[319] S. Li, J. Qiu, C. Lai, M. Ling, H. Zhao, S. Zhang, *Nano Energy* **2015**, *12*, 224.
[320] E. Irisarri, A. Ponrouch, M. R. Palacin, *J. Electrochem. Soc.* **2015**, *162*, A2476.
[321] L. Xiao, Y. Cao, W. A. Henderson, M. L. Sushko, Y. Shao, J. Xiao, W. Wang, M. H. Engelhard, Z. Nie, J. Liu, *Nano Energy* **2016**, *19*, 279.
[322] J. Ding, H. Wang, Z. Li, K. Cui, D. Karpuzov, X. Tan, A. Kohandehghan, D. Mitlin, *Energy Environ. Sci.* **2015**, *8*, 941.
[323] Y. Li, Y.-S. Hu, H. Li, L. Chen, X. Huang, *J. Mater. Chem. A* **2016**, *4*, 96.
[324] C. Jo, Y. Park, J. Jeong, K. T. Lee, J. Lee, *ACS Appl. Mater. Interfaces* **2015**, *7*, 11748.
[325] H. Liu, K. Cao, X. Xu, L. Jiao, Y. Wang, H. Yuan, *ACS Appl. Mater. Interfaces* **2015**, *7*, 11239.
[326] F. Legrain, J. Sottmann, K. Kotsis, S. Gorantla, S. Sartori, S. Manzhos, *J. Phys. Chem. C* **2015**, *119*, 13496.
[327] A. Ramos, I. Cameán, N. Cuesta, C. Antuña, A. B. García, *Electrochim. Acta* **2016**, *187*, 496.
[328] C. Ding, T. Nohira, R. Hagiwara, A. Fukunaga, S. Sakai, K. Nitta, *Electrochim. Acta* **2015**, *176*, 344.
[329] J. Xu, M. Wang, N. P. Wickramaratne, M. Jaroniec, S. Dou, L. Dai, *Adv. Mater.* **2015**, *27*, 2042.
[330] Y. Li, Z. Wang, L. Li, S. Peng, L. Zhang, M. Srinivasan, S. Ramakrishna, *Carbon* **2016**, *99*, 556.
[331] L. Qie, W. Chen, X. Xiong, C. Hu, F. Zou, P. Hu, Y. Huang, *Adv. Sci.* **2015**, *2*, 1500195.
[332] P. Wang, B. Qiao, Y. Du, Y. Li, X. Zhou, Z. Dai, J. Bao, *J. Phys. Chem. C* **2015**, *119*, 21336.
[333] B. Jache, P. Adelhelm, *Angew. Chem. Int. Ed.* **2014**, *53*, 10169.
[334] H. Kim, J. Hong, Y.-U. Park, J. Kim, I. Hwang, K. Kang, *Adv. Funct. Mater.* **2015**, *25*, 534.
[335] H. Kim, J. Hong, G. Yoon, H. Kim, K.-Y. Park, M.-S. Park, W.-S. Yoon, K. Kang, *Energy Environ. Sci.* **2015**, *8*, 2963.
[336] F. Wang, J. Graetz, M. S. Moreno, C. Ma, L. Wu, V. Volkov, Y. Zhu, *ACS Nano* **2011**, *5*, 1190.
[337] H. Xiong, M. D. Slater, M. Balasubramanian, C. S. Johnson, T. Rajh, *J. Phys. Chem. Lett.* **2011**, *2*, 2560.
[338] Z. Bi, M. P. Paranthaman, P. A. Menchhofer, R. R. Dehoff, C. A. Bridges, M. Chi, B. Guo, X.-G. Sun, S. Dai, *J. Power Sources* **2013**, *222*, 461.
[339] J. P. Huang, D. D. Yuan, H. Z. Zhang, Y. L. Cao, G. R. Li, H. X. Yang, X. P. Gao, *RSC Adv.* **2013**, *3*, 12593.
[340] J. Lee, Y.-M. Chen, Y. Zhu, B. D. Vogt, *ACS Appl. Mater. Interfaces* **2014**, *6*, 21011.
[341] S.-M. Oh, J.-Y. Hwang, C. S. Yoon, J. Lu, K. Amine, I. Belharouak, Y.-K. Sun, *ACS Appl. Mater. Interfaces* **2014**, *6*, 11295.
[342] H. A. Cha, H. M. Jeong, J. K. Kang, *J. Mater. Chem. A* **2014**, *2*, 5182.
[343] K.-T. Kim, G. Ali, K. Y. Chung, C. S. Yoon, H. Yashiro, Y.-K. Sun, J. Lu, K. Amine, S.-T. Myung, *Nano Lett.* **2014**, *14*, 416.
[344] C. Chen, Y. Wen, X. Hu, X. Ji, M. Yan, L. Mai, P. Hu, B. Shan, Y. Huang, *Nat. Commun.* **2015**, *6*, 6929.
[345] H. Usui, S. Yoshioka, K. Wasada, M. Shimizu, H. Sakaguchi, *ACS Appl. Mater. Interfaces* **2015**, *7*, 6567.
[346] M. N. Tahir, B. Oschmann, D. Buchholz, X. Dou, I. Lieberwirth, M. Panthöfer, W. Tremel, R. Zentel, S. Passerini, *Adv. Energy Mater.* **2015**, *6*, 1501489.
[347] L. Wu, D. Bresser, D. Buchholz, G. A. Giffin, C. R. Castro, A. Ochel, S. Passerini, *Adv. Energy Mater.* **2015**, *5*, 1401142.
[348] D. Su, S. Dou, G. Wang, *Chem. Mater.* **2015**, *27*, 6022.
[349] Y. Xu, M. Zhou, L. Wen, C. Wang, H. Zhao, Y. Mi, L. Liang, Q. Fu, M. Wu, Y. Lei, *Chem. Mater.* **2015**, *27*, 4274.
[350] J.-M. Feng, L. Dong, Y. Han, X.-F. Li, D.-J. Li, *Int. J. Hydrogen Energy* **2016**, *41*, 355.
[351] C. Fu, T. Chen, W. Qin, T. Lu, Z. Sun, X. Xie, L. Pan, *Ionics* **2015**, *22*, 555.
[352] L. Wu, D. Bresser, D. Buchholz, S. Passerini, *J. Electrochem. Soc.* **2015**, *162*, A3052.
[353] D. Yan, C. Yu, Y. Bai, W. Zhang, T. Chen, B. Hu, Z. Sun, L. Pan, *Chem. Commun.* **2015**, *51*, 8261.
[354] Y. Yang, X. Ji, M. Jing, H. Hou, Y. Zhu, L. Fang, X. Yang, Q. Chen, C. E. Banks, *J. Mater. Chem. A* **2015**, *3*, 5648.
[355] S. K. Das, B. Jache, H. Lahon, C. L. Bender, J. Janek, P. Adelhelm, *Chem. Commun.* **2016**.
[356] Y. Yeo, J.-W. Jung, K. Park, I.-D. Kim, *Sci. Rep.* **2015**, *5*, 13862.
[357] Y. Zhang, Y. Yang, H. Hou, X. Yang, J. Chen, M. Jing, X. Jia, X. Ji, *J. Mater. Chem. A* **2015**, *3*, 18944.
[358] Z. Hong, K. Zhou, Z. Huang, M. Wei, *Sci. Rep.* **2015**, *5*, 11960.
[359] J. R. Gonzalez, R. Alcantara, F. Nacimiento, G. F. Ortiz, J. L. Tirado, *CrystEngComm* **2014**, *16*, 4602.
[360] L. Zhao, H.-L. Pan, Y.-S. Hu, H. Li, L.-Q. Chen, *Chi. Phys. B* **2012**, *21*, 028201.
[361] Y. Sun, L. Zhao, H. Pan, X. Lu, L. Gu, Y.-S. Hu, H. Li, M. Armand, Y. Ikuhara, L. Chen, X. Huang, *Nat. Commun.* **2013**, *4*, 1870.
[362] X. Yu, H. Pan, W. Wan, C. Ma, J. Bai, Q. Meng, S. N. Ehrlich, Y.-S. Hu, X.-Q. Yang, *Nano Lett.* **2013**, *13*, 4721.
[363] J. Liu, K. Tang, K. Song, P. A. van Aken, Y. Yu, J. Maier, *Phys. Chem. Chem. Phys.* **2013**, *15*, 20813.
[364] J. Wang, W. Li, Z. Yang, L. Gu, Y. Yu, *RSC Adv.* **2014**, *4*, 25220.
[365] L. Y. Yang, H. Z. Li, J. Liu, S. S. Tang, Y. K. Lu, S. T. Li, J. Min, N. Yan, M. Lei, *J. Mater. Chem. A* **2015**, *3*, 24446.
[366] Y. Ge, H. Jiang, K. Fu, C. Zhang, J. Zhu, C. Chen, Y. Lu, Y. Qiu, X. Zhang, *J. Power Sources* **2014**, *272*, 860.
[367] G. Hasegawa, K. Kanamori, T. Kiyomura, H. Kurata, K. Nakanishi, T. Abe, *Adv. Energy Mater.* **2015**, *5*, 1400730.
[368] M. Kitta, K. Kuratani, M. Tabuchi, R. Kataoka, T. Kiyobayashi, M. Kohyama, *Electrochemistry* **2015**, *83*, 989.
[369] P. Senguttuvan, G. Rousse, V. Seznec, J.-M. Tarascon, M. R. Palacín, *Chem. Mater.* **2011**, *23*, 4109.
[370] J. Xu, C. Ma, M. Balasubramanian, Y. S. Meng, *Chem. Commun.* **2014**, *50*, 12564.
[371] A. Rudola, N. Sharma, P. Balaya, *Electrochem. Commun.* **2015**, *61*, 10.
[372] H. Pan, X. Lu, X. Yu, Y.-S. Hu, H. Li, X.-Q. Yang, L. Chen, *Adv. Energy Mater.* **2013**, *3*, 1186.
[373] W. Zou, J. Li, Q. Deng, J. Xue, X. Dai, A. Zhou, J. Li, *Solid State Ionics* **2014**, *262*, 192.
[374] A. Rudola, K. Saravanan, C. W. Mason, P. Balaya, *J. Mater. Chem. A* **2013**, *1*, 2653.
[375] W. Wang, C. Yu, Y. Liu, J. Hou, H. Zhu, S. Jiao, *RSC Adv.* **2013**, *3*, 1041.
[376] M. A. Muñoz-Márquez, M. Zarrabeitia, E. Castillo-Martínez, A. Eguía-Barrio, T. Rojo, M. Casas-Cabanas, *ACS Appl. Mater. Interfaces* **2015**, *7*, 7801.
[377] S. H. Woo, Y. Park, W. Y. Choi, N.-S. Choi, S. Nam, B. Park, K. T. Lee, *J. Electrochem. Soc.* **2012**, *159*, A2016.
[378] P. J. P. Naeyaert, M. Avdeev, N. Sharma, H. B. Yahia, C. D. Ling, *Chem. Mater.* **2014**, *26*, 7067.

[379] D. Wu, X. Li, B. Xu, N. Twu, L. Liu, G. Ceder, *Energy Environ. Sci.* **2015**, *8*, 195.
[380] J.-Y. Liao, A. Manthiram, *Nano Energy* **2015**, *18*, 20.
[381] A. Rudola, K. Saravanan, S. Devaraj, H. Gong, P. Balaya, *Chem. Commun.* **2013**, *49*, 7451.
[382] H. Li, H. Fei, X. Liu, J. Yang, M. Wei, *Chem. Commun.* **2015**, *51*, 9298.
[383] A. Maazaz, C. Delmas, P. Hagenmuller, *J. Inclusion Phenom.* **1983**, *1*, 45.
[384] B. Koo, S. Chattopadhyay, T. Shibata, V. B. Prakapenka, C. S. Johnson, T. Rajh, E. V. Shevchenko, *Chem. Mater.* **2013**, *25*, 245.
[385] S. Hariharan, K. Saravanan, V. Ramar, P. Balaya, *Phys. Chem. Chem. Phys.* **2013**, *15*, 2945.
[386] D.-Y. Park, S.-T. Myung, *ACS Appl. Mater. Interfaces* **2014**, *6*, 11749.
[387] B. Huang, K. Tai, M. Zhang, Y. Xiao, S. J. Dillon, *Electrochim. Acta* **2014**, *118*, 143.
[388] P. R. Kumar, Y. H. Jung, K. K. Bharathi, C. H. Lim, D. K. Kim, *Electrochim. Acta* **2014**, *146*, 503.
[389] H. Zhu, J. Yin, X. Zhao, C. Wang, X. Yang, *Chem. Commun.* **2015**, *51*, 14708.
[390] S. Liu, Y. Wang, Y. Dong, Z. Zhao, Z. Wang, J. Qiu, *ChemElectroChem* **2016**, *3*, 38.
[391] X. Liu, T. Chen, H. Chu, L. Niu, Z. Sun, L. Pan, C. Q. Sun, *Electrochim. Acta* **2015**, *166*, 12.
[392] M. Valvo, F. Lindgren, U. Lafont, F. Björefors, K. Edström, *J. Power Sources* **2014**, *245*, 967.
[393] B. Philippe, M. Valvo, F. Lindgren, H. Rensmo, K. Edström, *Chem. Mater.* **2014**, *26*, 5028.
[394] S. Zhang, W. Huang, P. Hu, C. Huang, C. Shang, C. Zhang, R. Yang, G. Cui, *J. Mater. Chem. A* **2015**, *3*, 1896.
[395] J. Yang, T. Zhou, R. Zhu, X. Chen, Z. Guo, J. Fan, H. K. Liu, W.-X. Zhang, *Adv. Mater. Interfaces* **2015**, 1500464.
[396] F. Klein, B. Jache, A. Bhide, P. Adelhelm, *Phys. Chem. Chem. Phys.* **2013**, *15*, 15876.
[397] H. Liu, F. Cao, H. Zheng, H. Sheng, L. Li, S. Wu, C. Liu, J. Wang, *Chem. Commun.* **2015**, *51*, 10443.
[398] Y. Jiang, M. Hu, D. Zhang, T. Yuan, W. Sun, B. Xu, M. Yan, *Nano Energy* **2014**, *5*, 60.
[399] J.-W. Wen, D.-W. Zhang, Y. Zang, X. Sun, B. Cheng, C.-X. Ding, Y. Yu, C.-H. Chen, *Electrochim. Acta* **2014**, *132*, 193.
[400] Q. Deng, L. Wang, J. Li, *J. Mater. Sci.* **2015**, *50*, 4142.
[401] P. Han, X. Han, J. Yao, Z. Liu, X. Cao, G. Cui, *Electrochem. Commun.* **2015**, *61*, 84.
[402] M. M. Rahman, A. M. Glushenkov, T. Ramireddy, Y. Chen, *Chem. Commun.* **2014**, *50*, 5057.
[403] Z. Jian, P. Liu, F. Li, M. Chen, H. Zhou, *J. Mater. Chem. A* **2014**, *2*, 13805.
[404] K. C. Klavetter, S. Garcia, N. Dahal, J. L. Snider, J. Pedro de Souza, T. H. Cell, M. A. Cassara, A. Heller, S. M. Humphrey, C. B. Mullins, *J. Mater. Chem. A* **2014**, *2*, 14209.
[405] M. M. Rahman, I. Sultana, Z. Chen, M. Srikanth, L. H. Li, X. J. Dai, Y. Chen, *Nanoscale* **2015**, *7*, 13088.
[406] L. Wang, K. Zhang, Z. Hu, W. Duan, F. Cheng, J. Chen, *Nano Res.* **2013**, *7*, 199.
[407] I. Hasa, R. Verrelli, J. Hassoun, *Electrochim. Acta* **2015**, *173*, 613.
[408] X. Zhang, W. Qin, D. Li, D. Yan, B. Hu, Z. Sun, L. Pan, *Chem. Commun.* **2015**, *51*, 16413.
[409] S. Yuan, X.-l. Huang, D.-l. Ma, H.-g. Wang, F.-z. Meng, X.-b. Zhang, *Adv. Mater.* **2014**, *26*, 2273.
[410] Y. Lu, N. Zhang, Q. Zhao, J. Liang, J. Chen, *Nanoscale* **2015**, *7*, 2770.
[411] V. L. Chevrier, G. Ceder, *J. Electrochem. Soc.* **2011**, *158*, A1011.
[412] M. Mortazavi, Q. Ye, N. Birbilis, N. V. Medhekar, *J. Power Sources* **2015**, *285*, 29.
[413] J. W. Wang, X. H. Liu, S. X. Mao, J. Y. Huang, *Nano Lett.* **2012**, *12*, 5897.
[414] L. D. Ellis, T. D. Hatchard, M. N. Obrovac, *J. Electrochem. Soc.* **2012**, *159*, A1801.
[415] N. Yabuuchi, Y. Matsuura, T. Ishikawa, S. Kuze, J.-Y. Son, Y.-T. Cui, H. Oji, S. Komaba, *ChemElectroChem* **2014**, *1*, 580.
[416] J. Sun, H.-W. Lee, M. Pasta, H. Yuan, G. Zheng, Y. Sun, Y. Li, Y. Cui, *Nat. Nanotechnol.* **2015**, *10*, 980.
[417] Y. Xu, E. Swaans, S. Basak, H. W. Zandbergen, D. M. Borsa, F. M. Mulder, *Adv. Energy Mater.* **2016**, *6*, 1501436.
[418] S. C. Jung, D. S. Jung, J. W. Choi, Y.-K. Han, *J. Phys. Chem. Lett.* **2014**, *5*, 1283.
[419] A. Kohandehghan, K. Cui, M. Kupsta, J. Ding, E. Memarzadeh Lotfabad, W. P. Kalisvaart, D. Mitlin, *Nano Lett.* **2014**, *14*, 5873.
[420] J. Sangster, C. W. Bale, *J. Phase Equilib. Diffus.* **2014**, *19*, 76.
[421] S. Komaba, Y. Matsuura, T. Ishikawa, N. Yabuuchi, W. Murata, S. Kuze, *Electrochem. Commun.* **2012**, *21*, 65.
[422] A. Darwiche, C. Marino, M. T. Sougrati, B. Fraisse, L. Stievano, L. Monconduit, *J. Am. Chem. Soc.* **2012**, *134*, 20805.
[423] Y. Xu, Y. Zhu, Y. Liu, C. Wang, *Adv. Energy Mater.* **2013**, *3*, 128.
[424] S.-M. Oh, S.-T. Myung, M.-W. Jang, B. Scrosati, J. Hassoun, Y.-K. Sun, *Phys. Chem. Chem. Phys.* **2013**, *15*, 3827.
[425] D. Bresser, F. Mueller, D. Buchholz, E. Paillard, S. Passerini, *Electrochim. Acta* **2014**, *128*, 163.
[426] W. Chen, D. Deng, *ACS Sust. Chem. Eng.* **2015**, *3*, 63.
[427] Y.-M. Lin, P. R. Abel, A. Gupta, J. B. Goodenough, A. Heller, C. B. Mullins, *ACS Appl. Mater. Interfaces* **2013**, *5*, 8273.
[428] Y. Liu, Y. Xu, Y. Zhu, J. N. Culver, C. A. Lundgren, K. Xu, C. Wang, *ACS Nano* **2013**, *7*, 3627.
[429] J. Songster, A. D. Pelton, *J. Phase Equilib.* **1993**, *14*, 250.
[430] Y. Zhu, X. Han, Y. Xu, Y. Liu, S. Zheng, K. Xu, L. Hu, C. Wang, *ACS Nano* **2013**, *7*, 6378.
[431] L. Wu, X. Hu, J. Qian, F. Pei, F. Wu, R. Mao, X. Ai, H. Yang, Y. Cao, *Energy Environ. Sci.* **2014**, *7*, 323.
[432] L. Wu, F. Pei, R. Mao, F. Wu, Y. Wu, J. Qian, Y. Cao, X. Ai, H. Yang, *Electrochim. Acta* **2013**, *87*, 41.
[433] H. Hou, Y. Yang, Y. Zhu, M. Jing, C. Pan, L. Fang, W. Song, X. Yang, X. Ji, *Electrochim. Acta* **2014**, *146*, 328.
[434] X. Zhou, Z. Dai, J. Bao, Y.-G. Guo, *J. Mater. Chem. A* **2013**, *1*, 13727.
[435] I. T. Kim, E. Allcorn, A. Manthiram, *Phys. Chem. Chem. Phys.* **2014**, *16*, 12884.
[436] N. Zhang, Y. Liu, Y. Lu, X. Han, F. Cheng, J. Chen, *Nano Res.* **2015**, *8*, 3384.
[437] J. M. Sangster, *J. Phase Equilib. Diffus.* **2009**, *31*, 62.
[438] J. Qian, X. Wu, Y. Cao, X. Ai, H. Yang, *Angew. Chem.* **2013**, *125*, 4731.
[439] K. P. S. S. Hembram, H. Jung, B. C. Yeo, S. J. Pai, S. Kim, K.-R. Lee, S. S. Han, *J. Phys. Chem. C* **2015**, *119*, 15041.
[440] H. Morito, T. Yamada, T. Ikeda, H. Yamane, *J. Alloys Compd.* **2009**, *480*, 723.
[441] O. I. Malyi, T. L. Tan, S. Manzhos, *Appl. Phys. Express* **2013**, *6*, 027301.
[442] V. V. Kulish, O. I. Malyi, M.-F. Ng, Z. Chen, S. Manzhos, P. Wu, *Phys. Chem. Chem. Phys.* **2014**, *16*, 4260.
[443] F. Legrain, O. I. Malyi, S. Manzhos, *Comp. Mater. Sci.* **2014**, *94*, 214.
[444] O. Malyi, V. V. Kulish, T. L. Tan, S. Manzhos, *Nano Energy* **2013**, *2*, 1149.
[445] J. Sangster, A. D. Pelton, *J. Phase Equilib.* **1997**, *18*, 295.
[446] L. Baggetto, J. K. Keum, J. F. Browning, G. M. Veith, *Electrochem. Commun.* **2013**, *34*, 41.

[447] C. Yue, Y. Yu, S. Sun, X. He, B. Chen, W. Lin, B. Xu, M. Zheng, S. Wu, J. Li, J. Kang, L. Lin, *Adv. Funct. Mater.* **2015**, *25*, 1386.
[448] P. R. Abel, Y.-M. Lin, T. de Souza, C.-Y. Chou, A. Gupta, J. B. Goodenough, G. S. Hwang, A. Heller, C. B. Mullins, *J. Phys. Chem. C* **2013**, *117*, 18885.
[449] M. Dahbi, N. Yabuuchi, K. Kubota, K. Tokiwa, S. Komaba, *Phys. Chem. Chem. Phys.* **2014**, *16*, 15007.
[450] A. Abouimrane, W. Weng, H. Eltayeb, Y. Cui, J. Niklas, O. Poluektov, K. Amine, *Energy Environ. Sci.* **2012**, *5*, 9632.
[451] Y. Park, D.-S. Shin, S. H. Woo, N. S. Choi, K. H. Shin, S. M. Oh, K. T. Lee, S. Y. Hong, *Adv. Mater.* **2012**, *24*, 3562.
[452] L. Zhao, J. Zhao, Y.-S. Hu, H. Li, Z. Zhou, M. Armand, L. Chen, *Adv. Energy Mater.* **2012**, *2*, 962.
[453] R. R. Zhao, Y. L. Cao, X. P. Ai, H. X. Yang, *J. Electroanal. Chem.* **2013**, *688*, 93.
[454] L. Chen, W. Li, Y. Wang, C. Wang, Y. Xia, *RSC Adv.* **2014**, *4*, 25369.
[455] A. Choi, Y. K. Kim, T. K. Kim, M.-S. Kwon, K. T. Lee, H. R. Moon, *J. Mater. Chem. A* **2014**, *2*, 14986.
[456] V. A. Mihali, S. Renault, L. Nyholm, D. Brandell, *RSC Adv.* **2014**, *4*, 38004.
[457] S. Renault, V. A. Mihali, K. Edström, D. Brandell, *Electrochem. Commun.* **2014**, *45*, 52.
[458] H.-g. Wang, S. Yuan, Z. Si, X.-b. Zhang, *Energy Environ. Sci.* **2015**, *8*, 3160.
[459] C. Luo, Y. Zhu, Y. Xu, Y. Liu, T. Gao, J. Wang, C. Wang, *J. Power Sources* **2014**, *250*, 372.
[460] H. Wang, P. Hu, J. Yang, G. Gong, L. Guo, X. Chen, *Adv. Mater.* **2015**, *27*, 2348.
[461] C. Luo, J. Wang, X. Fan, Y. Zhu, F. Han, L. Suo, C. Wang, *Nano Energy* **2015**, *13*, 537.
[462] E. Castillo-Martínez, J. Carretero-González, M. Armand, *Angew. Chem. Int. Ed.* **2014**, *53*, 5341.
[463] M. Lopez-Herraiz, E. Castillo-Martinez, J. Carretero-Gonzalez, J. Carrasco, T. Rojo, M. Armand, *Energy Environ. Sci.* **2015**, *8*, 3233.
[464] M. Armand, S. Grugeon, H. Vezin, S. Laruelle, P. Ribiere, P. Poizot, J. M. Tarascon, *Nat. Mater.* **2009**, *8*, 120.
[465] Z. Zhu, H. Li, J. Liang, Z. Tao, J. Chen, *Chem. Commun.* **2015**, *51*, 1446.
[466] J. Xiang, C. Chang, M. Li, S. Wu, L. Yuan, J. Sun, *Cryst. Growth Des.* **2008**, *8*, 280.
[467] X. Wu, S. Jin, Z. Zhang, L. Jiang, L. Mu, Y.-S. Hu, H. Li, X. Chen, M. Armand, L. Chen, X. Huang,*Sci. Adv.* **2015**, *1*, 1500330.
[468] P. Han, X. Han, J. Yao, L. Zhang, X. Cao, C. Huang, G. Cui, *J. Power Sources* **2015**, *297*, 457.
[469] A. P. Cohn, K. Share, R. Carter, L. Oakes, C. L. Pint, *Nano Lett.* **2016**, *16*, 543.
[470] K. Zhu, S. Guo, J. Yi, S. Bai, Y. Wei, G. Chen, H. Zhou, *J. Mater. Chem. A* **2015**, *3*, 22012.
[471] H. Kim, E. Lim, C. Jo, G. Yoon, J. Hwang, S. Jeong, J. Lee, K. Kang, *Nano Energy* **2015**, *16*, 62.
[472] C.-Y. Chou, M. Lee, G. S. Hwang, *J. Phys. Chem. C* **2015**, *119*, 14843.